Université catholique de Louvain
Earth and Life Institute - Environmental Sciences

Linking soil hydraulic properties to structure indicators

Experiments and modelling

Mélanie Weynants

Avril 2011

Thèse présentée en vue de l'obtention
du grade de docteur en sciences agronomiques
et ingénierie biologique

Composition du jury:

Président:	Pr Jacques Mahillon (UCL, Belgique)
Promoteur:	Pr Mathieu Javaux (UCL, Belgique)
Lecteurs:	Pr Patrick Bogaert (UCL, Belgique)
	Dr Hugues Titeux (UCL, Belgique)
	Pr Harry Vereecken (FZJuelich, Allemagne)
	Pr Wolfgang Durner (TU Braunschweig, Allemagne)

And the day came when the risk to remain tight in a bud
was more painful than the risk it took to blossom.
Anais Nin

Remerciements

Cette thèse de doctorat est l'aboutissement de quatre années de travail. Je n'aurais cependant pas pu la produire sans l'aide de nombreuses personnes qu'il me tient à coeur de remercier.

Avant tout, je remercie Mathieu Javaux, qui m'a encouragée, stimulée et sans qui je n'en mènerais probablement pas bien large. Sa motivation, son cerveau en ébullition constante et ses idées nouvelles de chaque jour ont été autant de stimulants tout au long de notre collaboration.

Je remercie également les membres de mon jury qui m'ont fait l'honneur de consacrer une part de leur temps à mon travail et qui m'ont permis d'améliorer ce document grâce à leurs remarques et commentaires.

Je me dois aussi de remercier le Fonds pour la Formation à la Recherche dans l'Industrie et dans l'Agriculture (F.R.I.A.), qui m'a financée durant près de quatre ans et grâce auquel j'ai pu me consacrer entièrement à ma recherche.

Mes recherches ont été largement basées sur des mesures de MSO. Merci à Guido pour son développement technique et au FNRS pour son financement.

Ensuite, je voudrais remercier tous les mémorants qui ont contribué à mes travaux. Le temps que je leur ai consacré en valait la peine et j'espère qu'ils ont apprécié mon aide autant que j'ai apprécié la leur. Maxime Poncelet, Michael Servais, Jérémy Pouglio et Edith Maroy ont grandement contribué au développement du MSO et à la construction de la base de données belge. Nicolas Feltz et Martin Germeau ont traversé l'Atlantique pour récolter les données de Guadeloupe. Je les aurais bien imités, mais je n'en ai malheureusement pas eu l'occasion. Le MSO ne serait pas ce qu'il est sans les talents de nos stagiaires informaticiens Samuel Rogé et Benjamin Melebeck.

La motivation de chaque jour n'est pas toujours facile à trouver. Mais il n'y a rien de tel pour vous motiver qu'un agréable cadre de travail. Avec une grande baie vitrée qui permet de faire serre en été et congélateur en hiver, mon petit bureau m'a vue progresser au fil des années. Mais bien plus encore que le local, mes collègues ont su m'offrir une ambiance de travail agréable. Plus particulièrement, je tiens à remercier Quentin et Samuel pour les échanges divers et leur amitié. Merci aussi à Eric, pour les échanges scientifiques que nous avons eu. Le GERU ne tournerait pas sans Carine, son dévouement et son efficacité, merci à elle pour son soutien logistique.

La persévérance est un atout indispensable pour mener à bien un doctorat. Cette volonté d'aller jusqu'au bout de ce que j'entreprends, c'est mon papa qui me l'a transmise. Il m'a toujours soutenue dans mes choix d'études et m'a toujours fourni toutes les clés pour les accomplir. Merci papa pour tout cela et le reste. Merci aussi à ma maman, mon frère, mes soeurs, mes beaux-frères, ma belles-soeur et leur progéniture pour la belle famille que nous formons et sur laquelle j'ai toujours pu compter. Merci également à mes beaux-parents et ma belle-soeur pour leur soutien et leurs encouragements.

Merci à Grégory, pour son soutien de chaque instant, sa présence à mes côtés et son amour qui donne sens à ma vie. Et merci à ma petite Danaé, certes parfois frein à ma progression, mais aussi stimulant tellement puissant...

Ispra, 4 avril 2011

Contents

List of Figures ix
List of Tables xi
List of Acronyms xiii

Introduction **1**
Objectives 4
Outline of this thesis 6

1 Revisiting Vereecken PTF: introducing a closed-form hydraulic model* **9**
1.1 Introduction 9
1.2 Material and methods 10
1.2.1 Datasets 10
1.2.2 Models 12
1.2.3 Pedotransfer functions 14
1.3 Results and discussion 18
1.3.1 Water retention and hydraulic conductivity models . . . 18
1.3.2 Coefficients of PTF 19
1.3.3 Performances of PTF 20
1.4 Conclusion 29

2 Development of a Multistep Outflow device **31**
2.1 Development 32
2.2 Sources of errors 34
2.2.1 Errors affecting the outflow 34
2.2.2 Errors affecting the boundary conditions 35
2.2.3 Errors affecting the measured suction head 35
2.3 Sensitivity analysis 35
2.3.1 Saturation and retention water content - θ_s and θ_r . . . 38
2.3.2 Parameter α 39
2.3.3 Parameter n 39
2.3.4 Saturated hydraulic conductvity - K_s 39
2.3.5 Parameter λ 40
2.4 Conclusion 40

*Adapted from Weynants, M., Vereecken, H. and Javaux, M. Revisiting Vereecken Pedotransfer Functions: Introducing a Closed-Form Hydraulic Model. Vadose Zone Journal, 2009, 8, 86-95

3 Tackling the sources of uncertainty in multistep outflow experiments[†] 41
3.1 Introduction . . . 41
3.2 Material and methods . . . 43
3.2.1 Field sampling and laboratory measurements . . . 43
3.2.2 Methodology . . . 45
3.2.3 Statistical analyses . . . 50
3.3 Results and discussion . . . 52
3.3.1 Experimental results: inter-horizon differences . . . 52
3.3.2 Goodness of fit: protocol and model effects . . . 55
3.3.3 Comparison of optimised hydraulic curves . . . 57
3.3.4 Extrapolation experiments . . . 62
3.4 Conclusion . . . 64

4 Impact of land cover and horizon depth on hydraulic properties of silt loam soils[‡] 67
4.1 Introduction . . . 67
4.2 Materials and methods . . . 68
4.2.1 Field sampling and pedological measurements . . . 68
4.2.2 Soil hydraulic properties . . . 69
4.2.3 Macroporosity indicators . . . 70
4.2.4 Statistical analysis . . . 70
4.2.5 Soil hydraulic models . . . 71
4.2.6 Inverse modelling . . . 73
4.3 Results . . . 73
4.3.1 Database . . . 73
4.3.2 Moisture retention curves . . . 77
4.3.3 Multistep outflow and hydraulic conductivity . . . 84
4.4 Conclusion . . . 93

5 Hydraulic behaviour of volcanic soils linked to structure indicators[§] 95
5.1 Introduction . . . 95
5.2 Material and methods . . . 97
5.2.1 Selection of sites . . . 97
5.2.2 Sampling and infiltrometer measurements . . . 98
5.2.3 Structural indices . . . 99
5.2.4 Chemical characterisation . . . 99
5.2.5 Hydraulic characterisation . . . 101
5.2.6 Statistical analysis . . . 101
5.3 Results and discussion . . . 102

[†]Adapted from Weynants, M., Laloy, E. and Javaux, M. Soil hydraulic properties obtained from multistep outflow: impact of model choice, protocol and spatial variability on the uncertainty at the horizon scale, *submitted to Journal of Hydrology*

[‡]Adapted from Weynants, M. and Javaux, M. (in preparation). Impact of land cover and horizon depth on close to saturation hydraulic properties of silt loam soils, *To be submitted to European Journal of Soil Science*

[§]In collaboration with P. Cattan, CIRAD, Guadeloupe, France.

5.3.1 Data description 102
5.3.2 Correlations between soil hydraulic properties and structure indicators 105
5.4 Conclusion 108

Conclusion and perspectives **111**
General conclusions 111
Measuring hydraulic properties: Sensitivity to soil structure . . 111
Tackling the uncertainty of soil hydraulic properties 112
Structure indicators 113
Perspectives 113
Technical perspectives 114
The bigger picture 114

Appendices **117**

A Sensitivity analysis **119**

B Profile descriptions **123**

References **135**

List of publications **143**

List of Figures

1 Hypotheses of this thesis 5

1.1 Belgian textural classes of the sampled soil horizons 11
1.2 Differences between VG1 and VG2 models 19
1.3 MRC PTF accuracy and reliability 22
1.4 HCC PTF accuracy 23
1.5 PCA of K_{sat} and its potential predictors 25
1.6 Boxplot of $\ln(K_{sat})/\ln(K_o)$ 26
1.7 $\ln(K_{sat})/\ln(K_o)$ versus sand and clay contents 28

2.1 MSO in pressure mode 33
2.2 MSO in suction mode 34

3.1 Illustration of the sampled profiles 44
3.2 Illustrations of the models concepts 48
3.3 Initial conditions of the three simulation protocols 49
3.4 Infiltration front depth calculation 52
3.5 MSO measurements: cumulative outflow and pressure head . . 53
3.6 Observed variation in cumulative outflow, pressure head and water retention measurements 54
3.7 Observed and simulated cumulative outflow and pressure head 56
3.8 MRC obtained from inversion of MSO experiments 58
3.9 HCC obtained from inversion of MSO experiments 59
3.10 95 % confidence intervals on hydraulic curves 61
3.11 Infiltration front depth distributions 63

4.1 Illustration of the sampled soil profiles 72
4.2 USDA soil texture triangle with sampled horizons 74
4.3 Moisture retention data 75
4.4 Moisture retention data compared to PTF 76
4.5 Moisture retention data of three profiles 78
4.6 Moisture retention data of A and B horizons 79
4.7 Histograms of the macroporosity indicators of Silt Loam samples. 80
4.8 Boxplots of the macroporosity indicators 81
4.9 Boxplots of inflection suctions 83
4.10 Boxplots of $h_{2,\mathsf{DR}}$ 84
4.11 Boxplots of measured MSO variables 85

4.12 Scatter plots of $K_{sat,\mathsf{DR}}$ and $K_{sat,\mathsf{MV}}$, showing also $K_{sat,obs}$. . . 87
4.13 MRC and HCC obtained from MSO inversions with MV and DR 88
4.14 MRC and HCC obtained from MSO inversions with MV and DR 89
4.15 Boxplots of hydraulic conductivity 92

5.1 Soil transect of Basse-Terre island 97
5.2 Soil structure quantification 100
5.3 Average MRC by soil type and horizon 103
5.4 Suction infiltrometer results averaged by soil type 104
5.5 HCC obtained from inversion of MSO experiments for surface horizons 105
5.6 Regressions of the infiltration fluxes 106

A.1 Response surfaces of the OF. 120
A.2 Response surfaces of the OF. 121
A.3 Response surfaces of the OF. 122

List of Tables

1 Hydraulic properties, their modelisation and PTF 2

1.1 Ranges of soil basic properties 12
1.2 Models of water retention and hydraulic conductivity 13
1.3 Empirical relationships 15
1.4 Statistics for evaluating the PTF accuracy 17
1.5 Averaged RMSE of coupled models 18
1.6 PTFs coefficients 20
1.7 MRC PTF performance indicators 21
1.8 HCC PTF performance indicators 24
1.9 Global PTF performance 24
1.10 Correlation matrix of the training set parameters 26
1.11 Correlation matrix of the PTF coefficients 27

2.1 Bottom BC of MSO experiment 36
2.2 Variation ranges of the parameters 37
2.3 Quality of MV parameters identification 38

3.1 Basic properties of the analysed horizons 44
3.2 Optimised and fixed parameters 47
3.3 Adjusted RMSE of the three terms of the objective function . . 55
3.4 Variation of HCC in different pore categories 60
3.5 Estimated standard deviations of distributions of infiltration front depths Δz, merged according to the replicates and to the models. Units are in cm and the maximum infiltration depth is 10 cm. 64

4.1 Basic properties of the sampled soils 74
4.2 Basic properties of the sampled soil horizons 74
4.3 adjusted RMSE obtained with different models on MRC data . 82
4.4 Inflection suctions distributions 83

5.1 Chemical properties of the four soil types 102
5.2 Explaining variables included in the stepwise procedure 107
5.3 Regression coefficients of variables explaining infiltration rates . 107

Acronyms

AN	andosol.
AP	andosol perhydraté.
BA	andic brown soil (sol brun andique) as defined by Colmet-Daage and Lagache (1965).
BR	rust-brown soil (sol brun rouille) as defined by Colmet-Daage and Lagache (1965).
CEC	cation exchange capacity.
C	cropland.
DREAM	DiffeRential Evolution Adaptive Metropolis.
DR	Durner (1994) bimodal model (Eq. 3.3, 3.4).
DUAL	Gerke and van Genuchten (1993a) dual porosity model (Eq. 3.5, 3.6).
DX	Dexter *et al.* (2008a) model (Eq. 4.2).
F	forest.
G	grassland.
HCC	hydraulic conductivity curves.
MRC	moisture retention curves.
MSO	multistep outflow.
MV	Mualem-van Genuchten (van Genuchten, 1980) model (Eq. 3.1, 3.2).
OF	objective function.
PTF	pedotransfer functions.
RD	root density.
SC	continuous structure.
SD	less easily discernible clod.
SF	easily discernible clod.
TF	fine earth.
VG0	van Genuchten (1980) model (Eq. 3.1), with fitted m.
VG1	van Genuchten (1980) model (Eq. 3.1), with $m = 1$.
VG2	van Genuchten (1980) model (Eq. 3.1), with $m = 1 - 1/n$.

Introduction

World population is prospected to surpass nine billion people by 2050 (United Nations, Department of Economic and Social Affairs, Population Division, 2009). Forty percent of the agricultural production comes from irrigated croplands, which represent 16% of cultivated areas. FAO says that in 2025, 1.8 billion people will live in conditions of water scarcity. Today, already one third of humanity is dependent on groundwater. In the next decades, humanity's growing needs for food, fiber, and bioenergy will substantially increase. Soils, which are already today under pressure, will have to be managed increasingly more efficiently in order to produce more in a more sustainable way. Climate change will generate additional negative impacts on soil fertility and mineral nutrition of crops in particular in developing countries (St. Clair and Lynch, 2010). Soil-water interaction occurring in the root zone is a key interface between the biotic and the abiotic and thus a key determinant of the state of the earth system (Lin *et al.*, 2005). An adequate management of the near-surface environment of the Earth, otherwise known as the "critical zone", is therefore urgently needed (Richter and Mobley, 2009).

A full understanding of the processes undergoing in the below-ground critical zone encompasses the knowledge of the soil hydraulic properties and their spatial and temporal distributions. These properties control water flow and solute transport in the variably saturated zone. Richards equation represents the movement of water in non-swelling unsaturated soils (Richards, 1931). However, it is a non-linear partial differential equation, which can be difficult to approximate due to the non existence of a closed-form analytical solution. Assuming that Richards equation is valid, hydraulic properties are the hydraulic conductivity, K, and the moisture retention, θ. Both are functions of the soil hydraulic pressure head, h. These three state variables are interdependent. Functions $K(h)$ and $\theta(h)$ depend on the soil particles size (texture) but also on how these particles are organised (structure). Many mathematical models exist for approximating these functions (e.g. Brooks and Corey, 1964; Mualem, 1976; van Genuchten, 1980; Durner, 1994; Kosugi, 1996; Assouline *et al.*, 1998; Iden and Durner, 2007). The models are generally based on sets of physical or experimental parameters that are to be calibrated for each soil (Table 1).

These characteristic functions are known to be very variable in space and time, but also across scales. Their direct estimation remains expensive and time-consuming, even if techniques of measurement have been developed over years. Soil heterogeneity has long been recognised to influence the soil physical

and hydrological properties (Nielsen *et al.*, 1973). Especially for large-scale applications, tools are needed to assess the soil hydraulic behaviour from more readily available data. Therefore researchers have developed pedotransfer functions (PTF) for hydraulic properties (Bouma, 1989). Most PTF are based on soil texture. Some include organic matter content or bulk density, or both. A number of PTF also use points of the moisture retention curves (MRC), typically at field capacity (pF 2.5) and wilting point (pF 4.2).

Lin *et al.* (2005) recently defined hydropedology as an interwined branch of soil science and hydrology that encompasses multiscale basic and applied research of interactive pedological and hydrological processes and their properties in the unsaturated zone. Advancing hydropedology includes enhancing PTF and developing soil inference systems and hydropedoinformatics (Lin *et al.*, 2005). Although PTF are a powerful mean for assessing MRC and hydraulic conductivity curves (HCC), they are subject to reliability problems, in particular close to saturation, due to the fact that they do not encompass structural or morphological properties.

Soil structure can implicitly be characterised in PTF by *texture*. Soil mineral particles are classified according to their size and the gravimetric proportion of each class gives an overall picture of the soil texture. As a first approximation it seems logical that particles sizes would directly be linked to pores sizes. Texture has indeed a significant impact on soil hydraulic properties. However, it can certainly not explain the entire porous network architecture. Indeed, soils with the same texture may differ in structure. Structure may result from long term pedogenetic processes controlling the horizons and the aggregates formations. Aggregation of soil particles also depends on the *nature of clay minerals* and their interaction with the *organic matter*. On the one hand, soils originating from similar parent materials and exposed to similar climatic conditions will develop the same secondary minerals. On the other hand, organic matter

Table 1: Hydraulic functions, their mathematical formalisation and pedotransfer functions. K: hydraulic conductivity, θ: water content, h: hydraulic potential, t: texture and $\hat{t}$ its approximation, s: structure and $\hat{s}$ its approximation, F and G: natural functions, $\mathbf{p}$: vector of parameters, f and g: mathematical functions, f' and g': pedotransfer functions.

Hydraulic properties	Mathematical models	Pedotransfer functions	
		Continuous PTF	Class PTF
$K = F(h,t,s)$	$K \approx f(h, \mathbf{p}_K(t,s))$	$\mathbf{p}_K \approx f'(\hat{t},\hat{s})$	for $h_i \in [h_1, \cdots, h_n]$ $K(h_i) \approx f'_i(\hat{t},\hat{s})$
$\theta = G(h,t,s)$	$\theta \approx g(h, \mathbf{p}_\theta(t,s))$	$\mathbf{p}_\theta \approx g'(\hat{t},\hat{s})$	$\theta(h_i) \approx g'_i(\hat{t},\hat{s})$

content is highly variable and depends, among other factors, on the vegetation and the soil management practices. Hence, structure formation can also be a short-term process affected by very recent anthropogenic practices, like in agricultural surface horizons. *Land cover* can therefore be a valuable indicator of soil structure.

Besides the organic matter content itself, other elements present in the soil can structure it. The network formed by *roots* can play a significant role. They stabilise the soil structure and when decaying they leave behind a porous network. The *soil fauna* also creates pores of various sizes. The roots and the biological features are generally mostly active in the surface horizons. The *horizon position* in the profile can hence also be an indicator of the soil structure. The soil *bulk density* gives an overall picture of the soil porosity and can therefore be a valuable structure indicator. More detailed information such as the *peds shape, size and grade* can also give indications on the soil structure. Figure 1 summarises the effects of the different factors determining the soil structure and hydraulic properties.
Several authors studied the effect of various variables related to the soil structure on hydraulic properties. McKeague *et al.* (1982) predicted saturated hydraulic conductivity from soil morphology. Lin *et al.* (1999 a,b) quantified soil morphology descriptors and used them in PTF. Lilly (2000) developed class PTF to predict saturated hydraulic conductivity based on ped size. Zhou *et al.* (2008) studied the impact of land use and seasonality on hydraulic properties from four soil series. They found that the sesonality had the main effect on the close to saturation hydraulic conductivity, followed by the land use and the soil series. Vanwalleghem *et al.* (2010) studied the horizontal and vertical variability of loess-derived soils from central Belgium and tried to link it with surface characteristics and soil map units.

Whatever the structure-generating process (long or short-term), morphological or topological indices are expected to always be good indicators for predicting close-to-saturation hydraulic properties (Vogel and Roth, 1998). However, today, topological indices can only be obtained on small samples, often through expensive noninvasive techniques: X-ray tomography, spectral induced polarization, nuclear magnetic resonance, electromagnetic signals. They currently cannot be brought to the field for assessing spatial variability of structure. In addition, no consensus exists on what are these indices and how to deduce them from measurements. Proxies or auxiliary information could then be a good way of getting structure information.

When long-term processes affect the structure, it is expected that soil pedogenetic factors may suffice to characterise its development. This type of information is typically found in pedological databases and characterised in soil survey: horizons, soil classification or texture could then be used as structure indicators. When short-term processes drive structure formation, then management practices or land cover may become good proxies. When both short and long term processes come into play, this is a matter of controversy to know which indicators are necessary to characterise soil structure. However, Vereecken *et al.* (2010) gave a definition on what should be a relevant predictor for developing PTF, also valid for structure indicators. These should

ideally be determined on the exact same sample as the hydraulic properties. They also "need to be easily identified and bring relevant information". Soil structure, clay mineralogy and taxonomic information showed their potential as predictors of soil hydraulic properties (e.g. Pachepsky and Schaap, 2004).

Other problems also affect PTF development. Vereecken *et al.* (2010) recently reviewed the use of Mualem-van Genuchten (van Genuchten, 1980) model (Eq. 3.1, 3.2) (MV) to parametrise soil hydraulic properties and for developping PTF. They identified four reasons for which PTF could not reproduce exactly the soil hydraulic properties: (i) spatial and temporal variability affect the results when the predictors and soil hydraulic properties are not measured on exactly the same sample; (ii) databases are not always large enough (Wösten *et al.*, 2001; Pachepsky and Schaap, 2004) and often lack relevant information on the soil structure, mineralogy, support scale or other data; (iii) the functional relationships are not appropriate and accurate; (iv) measurement methods are not accurate enough.

Vereecken *et al.* (2010) therefore recommended several axes of research for future development of PTF. They first insisted on the reliability of hydraulic measurements. They stress that, "to be predicted accurately, measurements must be repeatable, scale consistent, and associated with the lowest possible experimental error". They advocate the development of "databases with harmonised support scales and experimental protocols". Second, they highlighted the need of databases covering more soil classes so that PTF can be more universal. Third, they suggest the use of new exploration techniques for developing PTF based on sparse or unevenly distributed datasets. Fourth, they call on including metadata to databases, so that sampling and measurement conditions could be considered when developing PTF. Finally, they advocate the development of temporal PTF that could explicitly consider agricultural management practices. This would naturally require prior understanding of temporal evolution of soil hydraulic properties.

Objectives

The general objective of this thesis is to consolidate the understanding of the links between soil hydraulic properties and structure indicators. Bearing in mind the determining factors of soil hydraulic properties (Figure 1), the following three overarching research question are addressed:

Are hydraulic properties measurement methods sensitive to soil structure? Knowledge of soil hydraulic properties requires measurements. In situ or laboratory measurements of soil hydraulic properties remain a challenge due to their extreme spatial variability and the fragility of the soil structure. Indeed, the measurement itself can deteriorate the structure: the spatial organisation of soil constituents. The architecture of smallest pores is mostly controlled by the soil texture. The largest pores affect the soil properties under saturated and close to saturation conditions. Their presence and their organisation is conditioned by structuring elements. Detecting their effect on the

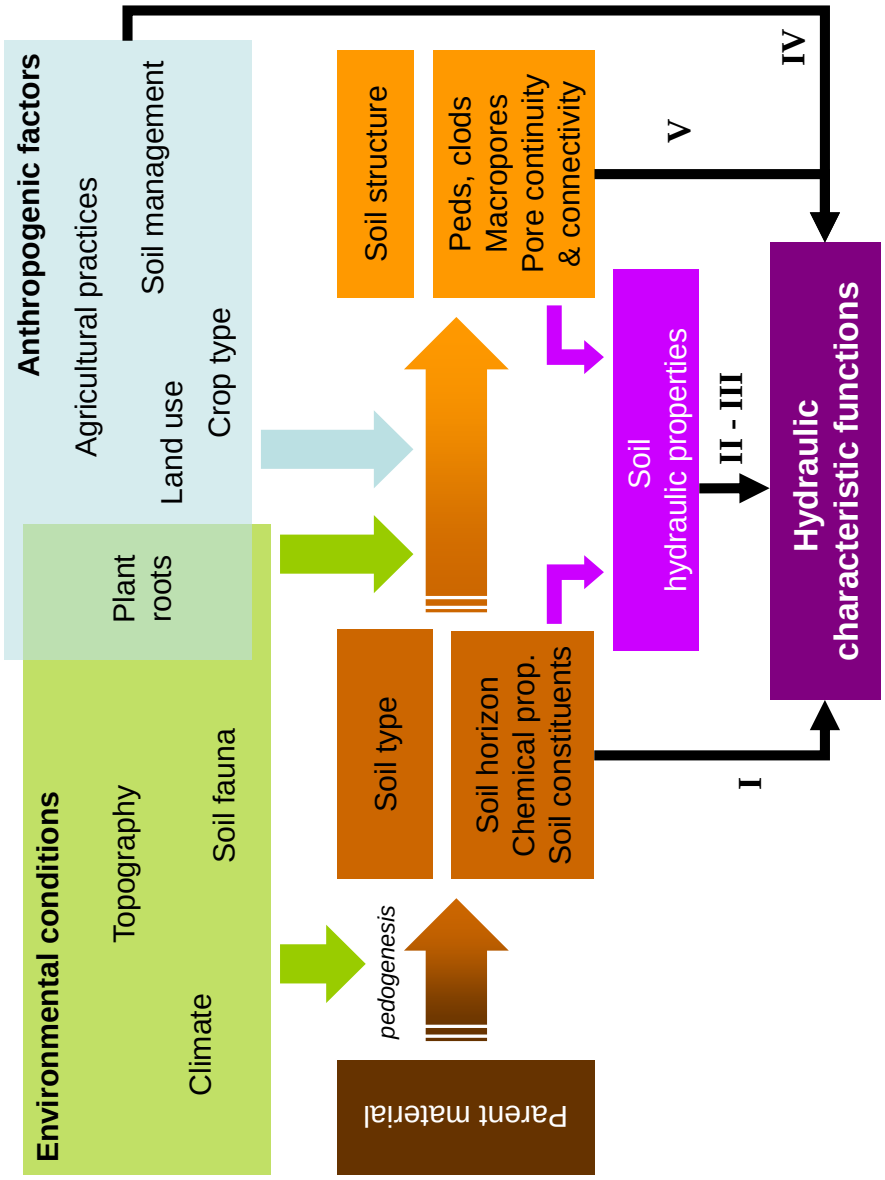

Figure 1: Hypotheses of this on relationships between soil formation factors and hydraulic properties. Chapters are shown with black arrows and roman numerals.

soil hydraulic properties requires that the measurement methods be sensitive enough close to saturation.

In this thesis, two methods for measuring soil hydraulic properties and their sensitivity to the soil structure effect are investigated: a laboratory method, a multistep outflow (MSO) system and, to a lesser extent, an in situ (suction infiltrometer) method.

What are the sources of uncertainty on directly and inversely obtained hydraulic properties? The assessment of hydraulic properties is plagued with uncertainties. The measurement technique itself induces an undetermined amount of error since it can directly alter the soil properties. Many techniques are based upon modelling approaches which require assumptions that generate further uncertainty. The large spatial variability of soil hydraulic properties, both over different soil horizons and between adjacent pedons, also raises the question of the representative volume necessary to properly characterise a given soil. The measured properties are valid at the scale of the volume sampled by the technique only and their upscaling remains a challenge. Extrapolation to other conditions than those in which they were measured is a persistent issue. In this thesis, the various sources of uncertainty are investigated with a specific emphasis on characterising the source of variability between soils having the same texture.

Which structure indicators are the most relevant for predicting soil hydraulic properties and how can they be included in models? As mentioned above, structure is influenced by pedological, anthropogenic and environmental factors. They can be characterised by indicators that relate to the soil structure. Some indicators are more difficult to quantify than others. Texture, organic matter content and bulk density are easily measured and included as continuous inputs in PTF. Dummy variables can be created for horizon position (topsoil=1, subsoil=0) (Wösten *et al.*, 2001). Different PTF can be developed for different land covers. The effect of the land management practices, such as no tillage is difficult to include directly. Roots size and abundance as well as voids created by the soil fauna can be categorised and included in models as dummies or directly quantified. Pedality features can be quantified (Lin *et al.*, 1999 a) or used in non parametric models (Pachepsky and Rawls, 2003).

In this thesis, the relevance of different structure indicators to explain soil hydraulic properties is investigated and the prediction of soil hydraulic properties on the basis of quantified structure indicators is studied.

Outline of this thesis

Figure 1 outlines the main hypotheses on which this thesis is based. It also shows the links between soil structure indicators and hydraulic properties explored in the chapters of this thesis.

Chapter 1 develops PTF for the coupled prediction of the MRC and HCC based

on the classically used and easily quantified information (texture, organic matter content and bulk density).

Chapter 2 presents the development of a laboratory multistep outflow device (MSO) to characterise soil hydraulic properties. A sensitivity analysis on synthetic data verifies its suitability for retrieving the parameters of the most classical expression of the hydraulic functions (MV).

Chapter 3, we study the sources of errors and variability in the hydraulic properties measured with the MSO. We focus on several aspects. First, we examine different protocols for handling the data. Then we investigate the effect of the choice of the model describing the hydraulic functions and the uncertainty on the parameters. Finally, we consider the spatial variability of the properties.

Chapter 4 investigates the hydraulic properties of silt loam soils and how they relate to secondary information sources other than the texture. More specifically, it analyses the effect of the land cover and the horizon position in the profile.

Chapter 5, explores the link between soil hydraulic properties, soil type and structure features of tropical soils derived from volcanic ashes.

The main findings and future perspectives are summarised and discussed in the conclusion of this document.

Chapter 1

Revisiting Vereecken PTF: introducing a closed-form hydraulic model*

1.1 Introduction

Whatever the scale, soils are intrinsically heterogeneous and this heterogeneity controls their hydraulic behaviour (Vogel and Roth, 2003). At the landscape scale, improving and developing methods to assess the hydraulic properties of the representative soil types in a quick and exhaustive manner is a crucial topic in soil science research. Besides the development of new experimental techniques to determine soil hydraulic properties, much effort has been devoted to build pedotransfer functions (PTF). This term, first introduced by Bouma (1989), covers mathematical functions predicting soil properties from more readily available data (e.g. texture, soil organic carbon and bulk density). The main assumption underlying most PTF is that textural properties dominate the hydraulic behaviour of soils (Lilly and Lin, 2004). There are some limitations to the PTF presently available in the literature. First, most PTF do not incorporate any structural information of the soil. It is well known that structural properties such as aggregation and macro-porosity influence the soil hydraulic behaviour. Structural information is especially crucial in the wet range of the moisture retention characteristic and hydraulic conductivity function. This is well illustrated by the low accuracy and the uncertainty of the predictions of the saturated hydraulic conductivity, K_{sat}, from PTF based on textural properties, bulk density and soil organic matter. Nowadays, information about the soil structure is becoming increasingly available and is incorporated in predictive models (Pachepsky *et al.*, 2006b). Second, the reliability of PTF used in a geographical region different from the one for which

*Adapted from Weynants, M., Vereecken, H. and Javaux, M. Revisiting Vereecken Pedotransfer Functions: Introducing a Closed-Form Hydraulic Model. Vadose Zone Journal, 2009, 8, 86-95

they were originally developed is often limited due to geological, geohydrological, climatic and land use factors. Third, in the last two decades, simple nonlinear least squares optimisation techniques were the main tools to estimate hydraulic parameters and to derive PTF. Current computer capabilities allow the use of global search algorithms which can improve the estimation of hydraulic parameters and the development of PTF.

Based on the above considerations, we revisited the database of Vereecken, which contains data on Belgian soils. It was first used to derive PTF for predicting soil hydraulic parameters of the van Genuchten model for the moisture retention characteristic and of the Gardner model for the hydraulic conductivity from texture, bulk density and organic carbon content (Vereecken *et al.*, 1989a, 1990). These PTF have been reported by several authors to be among the most accurate they evaluated (e.g., Tietje and Tapkenhinrichs, 1993; Romano and Santini, 1997; Cornelis *et al.*, 2001; Mermoud and Xu, 2006). They are not based on a closed-form model of the soil hydraulic properties, however, and this formulation is preferred when simulating transfer in the vadose zone.

The main objectives of this chapter are: (i) to explore the efficiency of different optimisation methods, such as global search algorithms and a one-step method to derive PTF compared to the sequential estimation approach, performed with a local optimisation algorithm, used by Vereecken *et al.* (1989a, 1990), (ii) to investigate the existence and value of a threshold pressure head that distinguishes macroporous from matrix flow in the hydraulic conductivity and (iii) to provide PTF for the Vereecken *et al.* (1989a, 1990) database based on a closed-form expression of the soil hydraulic functions.

1.2 Material and methods

1.2.1 Datasets

The Vereecken (1988) dataset is used to develop the new PTF. The soil profiles were chosen to be representative of the main soils types of Northern Belgium. Figure 1.1 shows the major textural classes of the sampled soil profiles. A total of 39 soil profiles were sampled and described according to the Belgian soil taxonomy. Soil cores for determining the moisture retention curves (MRC) and hydraulic conductivity curves (HCC) were taken in the middle of each of the 182 horizons. Once the hydraulic measurements were done, the soil cores were used to determine the textural composition, the organic carbon content and the bulk density. The granulometric composition was measured using dry-sieving to separate the sand fractions and the pipette method to discern the finer particles. Nine fractions were thus determined that correspond to the Belgian classification scheme. The organic carbon content was determined by means of Walkley and Black (1934) method. The bulk density was measured on the 100 cm^3 soil cores used for the MRC, which were dried for 24 hours at 105 °C. The ranges in which the available properties vary are presented in Table 1.1. Soil water content was determined at five matrix suctions below pF 2 using a sandbox apparatus and at higher suctions with low- and high-pressure chambers. For HCC, two different methods were used: the crust method (Bouma *et al.*,

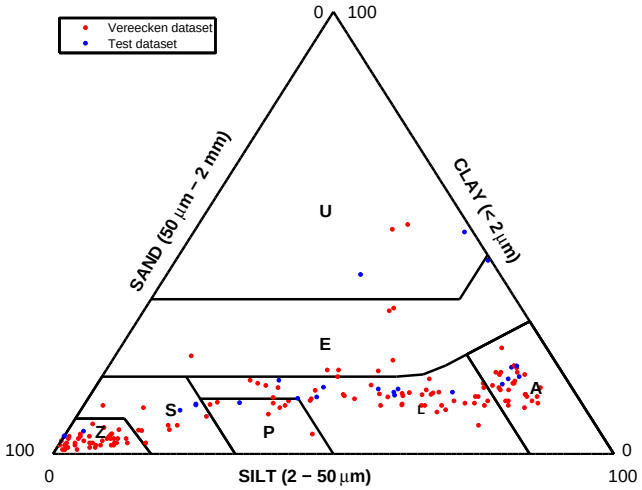

Figure 1.1: Belgian textural classes of the sampled soil horizons. Z = sand; S = loamy sand; P = light sandy loam; L = sandy loam; A = loam; E = clay; U = heavy clay. Training set in red, test set in blue.

1983) for the wet range and the hot air method (Arya *et al.*, 1975) for the dry range. Part of the raw data could not be retrieved so that the final data set only contains 136 HCC and 166 MRC.

To evaluate the reliability of the new pedotransfer functions, we also took advantage of an independent dataset containing moisture retention data collected in 48 horizons taken in 24 soil profiles sampled in forests of Flanders (North Belgium). It was developed in the framework of assessing the predictive quality and usefulness of the Belgian soil map and historical forest soil profile data for soil mapping purposes (Cornelis *et al.*, 2005). Each horizon was sampled twice using Kopecky rings of 100 cm^3. Cylinders with stones, charcoal, or roots larger than 2 mm in diameter were rejected and resampled in the same horizon. The particle-size distributions were determined on disturbed samples using a Coulter LS200 laser diffractometer (Beckman Coulter, Fullerton, CA). Organic matter content was determined using the Walkley and Black (1934) method. It ranges from 2.3 to 130.0 g kg^{-1}. Bulk densities were measured by weighing the 100 cm^3 sized undisturbed soil samples at 10 kPa and subtracting the corresponding mass of water measured on a 25cm^3 sized subsample. They vary from 0.76 to 1.78 Mg m^{-3}. For each soil ring, water content was measured at nine soil-matrix potentials to obtain the MRC. For the pressure potentials ranging from 1 to 10 kPa, the sand box apparatus (Eijkelkamp Agri-Equipment, Giesbeek, the Netherlands) was used. For higher potentials, subsamples were used in pressure chambers (Soilmoisture Equipment, Santa Barbara, CA). Undisturbed 20 cm^3 soil cores were used for measuring water content at 20 and 33 kPa, whereas two disturbed subsamples were used for water content determination at 1500 kPa. Unfortunately, this database contains no hydraulic conductivity measures and is therefore not suitable to evaluate the

PTF predicting the parameters of the conductivity model. As the extrapolation capacity of PTF is generally very bad, the test set was reduced to contain only the measurements for which the basic properties fall within the range of the training set. Therefore only 39 soil horizons were available to assess the reliability of the MRC PTF. The ranges of their properties are also presented in Table 1.1.

Texture fractions (sand: 50-2000 μm; silt: 2-50 μm; clay: < 2 μm), bulk density and organic carbon content are used as predictors for developing the new PTF.

Table 1.1: Ranges of soil basic properties for the training and test sets

	% sand	**%clay**	**BD**	**%OC**
min(training)	5.60	0	0.89	0.01
max(training)	97.80	54.50	1.77	6.60
min(test)	7.37	3.90	1.28	0.14
max(test)	96.10	42.70	1.59	6.08

%sand and %clay are the gravimetric percentages of sand (0.05-2 mm) and clay (<2 μm) particles; BD is the soil bulk density [g cm^3]; %OC is the gravimetric percentage of organic carbon.

1.2.2 Models

The major objective is to explore Vereecken's dataset using new optimisation methods and to assess the possibility of better estimating K_{sat} in order to improve the PTF of Vereecken using less parameters. Several models were fitted on the dataset. Table 1.2 displays their equations. For the retention curve only, several forms of the van Genuchten model [1980] were tested (m fitted (VG0), $m = 1$ (VG1), $m = 1 - 1/n$ (VG2)), but also the models proposed by Kosugi (1996); Brooks and Corey (1964); Ippisch *et al.* (2006), further referred to as KS, BC, IP respectively. The model referred here to as IP is actually the modified VG proposed by Vogel *et al.* (2001), rewritten by Ippisch *et al.* (2006). Concerning the hydraulic conductivity, the model of Mualem (1976), referred to as Mu, was coupled with several of the models used for the MRC. In its general form, it can be written (van Genuchten, 1980) as:

$$K(S) = K_o S^{\lambda} \left(\frac{\int_0^S 1/h(x)dx}{\int_0^1 1/h(x)dx} \right)^2 \tag{1.1}$$

where $K(S)$ is the unsaturated hydraulic conductivity [LT^{-1}] as a function of the relative saturation S; K_o is a hydraulic conductivity acting as matching point [L T^{-1}] at $h = 0$ (h is the suction head [L]); λ accounts for the tortuosity and the connectivity of the porous network. The model of Gardner (1958), as used in Vereecken *et al.* (1990), was also tested. The equations are also displayed at Table 1.2.

Table 1.2: Models of water retention and hydraulic conductivity tested on the training set

	Retention $S = \frac{\theta - \theta_r}{\theta_s - \theta_r}$		Conductivity
VG	$S = (1 + (\alpha\lvert h\rvert)^n)^{-m}$	MuVG	$K = K_o \left[S^\lambda \left(1 - \left(1 - S^{n/(n-1)} \right)^{1-1/n} \right)^2 \right]$, if $m = 1 - 1/n$
IP	$S = 1$ for $\lvert h\rvert \leq \lvert h_e\rvert$ $S = \frac{1}{S_c}(1 + (\alpha\lvert h\rvert)^n)^{-m}$ for $\lvert h\rvert > \lvert h_e\rvert$ with $S_c = [1 + (\alpha\lvert h_e\rvert)^n]^{-m}$	MuIp	$K = K_o$ for $S \leq 1$ $K = K_o S^\lambda \cdot \left[\frac{1-(1-(S \cdot S_c)^{1/m})^m}{1-(1-S_c^{1/m})^m} \right]^2$ for $S < 1$
KS	$S = \frac{1}{2}(\theta_s - \theta_r)\, erfc \left[\frac{\ln\left(\frac{h}{h_{0.5}}\right)}{\sigma\sqrt{2}} \right]$	MuKS	$K = K_{sat} \cdot S^{1/2} \left\{ \frac{1}{2} erfc \left[\left(\ln \frac{h}{h_m} \right) \frac{1}{\sigma\sqrt{2}} + \frac{\sigma}{\sqrt{2}} \right] \right\}^\gamma$
BC	$S = 1$ for $\lvert h\rvert \leq \lvert h_b\rvert$ $S = \left(\frac{h_b}{h}\right)^\lambda$ for $\lvert h\rvert > \lvert h_b\rvert$	Gard.	$K = K_{sat}\,(1 + (b\lvert h\rvert)^n)^{-1}$

S relative saturation [-], θ water content [$cm^3\ cm^{-3}$], h matric potential [cm], K soil hydraulic conductivity [cm d^{-1}], K_{sat} conductivity at saturation [cm d^{-1}], K_o conductivity acting as a matching point at 0 potential [cm d^{-1}]

We slightly modified the retention models by considering the moisture variation along the sample height, as suggested by Peters and Durner (2006). Rather than estimating the pressure head corresponding to the measured water content at half the sample height, its whole length is used. The measured water content is assumed to be the sample average water content, which varies in the sample. This can lead to more accurate results, especially near saturation where water content may greatly vary along short pressure intervals for coarse or macroporous soils. The water content is now expressed as :

$$\bar{\theta} = \frac{1}{L} \int_{h_l}^{h_u} \hat{\theta}(\boldsymbol{\beta}, h) dh \tag{1.2}$$

with $\bar{\theta}$ the measured water content, corresponding to the mean of the actual water content in the sample of total height L. h_l and h_u are the pressure heads at the bottom and at the top of the sample respectively. $\boldsymbol{\beta}$ is the vector of parameters of the chosen model.

As MuVG in Table 1.2 is intended to simulate the hydraulic conductivity in the soil matrix domain, a distinction is made between K_o and K_{sat}. The former acts as a matching point at $h = 0$, without considering the macropores. The latter is the effective saturated conductivity. To take macroporosity into account, multimodal models (e.g. Priesack and Durner, 2006) could have been fitted on the measurements, but the number of parameters would have been too large with regard to the number of data. Hence, we opted for the introduction of a threshold value h_t, from which macropores do not influence the HCC. Since too few measures are available in the wet range, h_t could not be estimated by optimisation, but we fixed it at -6 cm where our first unsaturated conductivity measurements occur. This value is also in concordance with the review of Jarvis (2007). He writes that macropores can be defined as pores having an equivalent cylindrical diameter larger than 0.3-0.5 mm, which is equivalent to a water entry pressure head of -6 to -10 cm, according to the Young-Laplace equation[†].

1.2.3 Pedotransfer functions

Method of building PTFs

The classical sequential method to build PTF consists in (1) fitting the hydraulic models on the measurements in order to derive the model's parameters; (2) building regression equations from the fitted parameters, using for example a stepwise method to choose the relevant variables entering the PTF. Although widely used, this method has several drawbacks: (i) PTF coefficients are obtained from uncertain hydraulic parameters but uncertainty on these hydraulic parameters is usually not taken into account; (ii) the final uncertainty of the PTF coefficients is therefore hard to assess and ; (iii) the forward model is largely overparameterised. We therefore opted for another method, proposed by Scheinost *et al.* (1997), which optimises the PTF' coefficients in one step.

[†] $h = \frac{2\gamma \cos\theta}{\rho g R}$, with h the pressure head, γ the surface tension, θ the contact angle between the two fluids, ρ the fluid density, g the gravitational acceleration, R, the radius of the capillary

Table 1.3: Empirical relationships between the hydraulic parameters and their predictors.

$\theta_r = a_1 + b_1\,\text{clay} + c_1\,\text{OC}$
$\theta_s = a_2 + b_2\,\text{clay} + c_2\,\text{BD}$
$\alpha^\star = a_3 + b_3\,\text{clay} + c_3\,\text{sand} + d_3\,\text{BD} + e_3\,\text{OC}$
$n^\star = a_4 + b_4\,\text{clay} + c_4\,\text{sand} + d_4\,\text{sand}^2$
$K^\star = a_5 + b_5\,\text{clay} + c_5\,\text{sand} + d_5\,\text{BD} + e_5\,\text{OC}$
$\lambda = a_6 + b_6\,\text{clay} + c_6\,\text{sand} + d_6\,\text{BD} + e_6\,\text{OC}$
$\alpha^\star = \ln(\alpha)$, $n^\star = \ln(n-1)$, $K^\star = \ln(K_o)$
BD is bulk density, OC is organic carbon content

Empirical relations between each of the parameters of the hydraulic model and the potential predictors (i.e., variables entering the PTF) must be set a priori. The coefficients of the PTF are then directly fitted to the retention and conductivity observations through the hydraulic model (Eqs. in Table 1.2) using non-linear regression. We further improved this method by allowing a stepwise optimisation process to only keep significant regression coefficients. With this stepwise extended method, uncertainty in the final PTF coefficients can be fully characterised. The main drawback of the method is that the equations of the relationships between the parameters and their predictors have to be set a priori. They must also be kept relatively simple to maintain the number of coefficients low enough for the optimisation. Table 1.3 presents the equations chosen in this study for the MuVG model (Eqs. VG and MuVG in Table 1.2). For the retention parameters, we based our a priori relations on the equations retained by Vereecken for his published PTF [1989]. Regarding the Mualem-van Genuchten model, we entered in the the equations all our available predictors without any transformation. The coefficients of these equations are optimised through a stepwise procedure that minimises the objective function presented hereafter. The stepwise procedure drops the less relevant predictors. In case some coefficients are not significantly different from zero (p-value > 0.05), the optimisation is performed again without the coefficient with the highest p-value, and so on until all the coefficients included in the model have a p-value < 0.05. The results from a stepwise procedure depend on the chosen path to remove the non significant coefficients. Even if it does not necessarily lead to the best performance, removing the coefficient with the larger p-value is a common practice and seems the most objective choice.

As parameter K_{sat} is not included in this set of PTF, another regression equation is developed to predict it, using a stepwise regression procedure.

Objective functions

The objective functions for the MRC and HCC are classical sum of squares, based on the direct models presented in Table 1.2. Note that for HCC, observations for $|h| < |h_t|$ were not included in the optimisation process, since $K_o \neq K_{sat}$ for soils with macropores. The value of h_t was chosen equal to 6 cm

of suction, which falls in the range of 6-10 cm proposed by Jarvis (2007) and beneath which we did not have other measurement data than the saturated conductivity itself.

For the coupled optimisation, objective functions of both MRC and HCC were combined to end up with Eq. 1.3.

$$\Phi(\boldsymbol{\beta}) = \sum_{i=1}^{n_1} v_i \left[\bar{\theta}_i - \frac{1}{L} \int_{h_{lb_i}}^{h_{ub_i}} \hat{\theta}(\boldsymbol{\beta}_{\mathbf{MRC}}, h_i) dh \right]^2 + \sum_{j=1}^{n_2} w_j \left[\ln(K_j) - \ln\left(\hat{K}(\boldsymbol{\beta}_{\mathbf{HCC}}, h_j) \right) \right]^2 \quad (1.3)$$

where v_i and w_j are used to balance the two parts of the function. A different method was applied to compute the weights for the choice of the model to be applied on the dataset and for building the PTF. In the first case, when the MRC or HCC models were directly fitted on the data, the weights that were used are the inverse of the variance of the model errors, according to the maximum likelihood.
In the second case, the PTF were first fitted once separately for the MRC and for the HCC parameters, and the variances of the errors for the whole dataset for the MRC, σ_θ^2, and the HCC, σ_K^2, were computed. The weights were also computed as the inverses of these variances. The same weights were hence applied for all the MRC data on the one hand and for all the HCC data on the other hand. The weights have here no statistical meaning but are just a way to balance the two parts of the objective function. Applying the same weight to all the data of one kind prevents some data that would have been badly fitted in the first optimisation to be condemned to never improve.

Optimisation algorithm

The optimisations are performed using a Global Multilevel Coordinate Search (GMCS) combined with a local Nelder-Mead Simplex algorithm (NMS), as proposed by Lambot *et al.* (2002). GMCS is an algorithm written in Matlab®(The MathWorks™) for bound constrained global optimisation using function values only, based on a multilevel coordinate search that balances global and local search. The local search is done via sequential quadratic programming (Huyer and Neumaier, 1999). In the approach used in this study, a global search is first performed by omitting the local search algorithm in order to avoid unnecessary function evaluations. Then a local search with NMS is realised on the parameters set provided as output of GMCS calculations.

Accuracy and reliability

The accuracy and the reliability of the newly developed PTF are evaluated using the criteria presented in Table 1.4.

Table 1.4: Statistics for evaluating the PTF accuracy

Statistic	Formula	Optimal value
Root Mean Square Error	$\mathrm{RMSE} = \sqrt{\frac{1}{N-p}\sum_{i=1}^{N}\left(\hat{y}_i - y_i\right)^2}$	0
Mean Absolute Error	$\mathrm{MAE} = \frac{1}{N-p}\sum_{i=1}^{N}\lvert\hat{y}_i - y_i\rvert$	0
Mean Relative Error	$\mathrm{MRE} = \frac{1}{N-p}\sum_{i=1}^{N}\frac{\hat{y}_i - y_i}{y_i}$	0
Coefficient of determination	$\mathrm{R}^2 = 1 - \frac{N-1}{N-p}$ $\left\{1 - \left[\frac{N\sum_{i=1}^{N} y_i\hat{y}_i - \sum_{i=1}^{N} y_i \sum_{i=1}^{N}\hat{y}_i}{\sqrt{N\sum_{i=1}^{N} y_i^2 - \left(\sum_{i=1}^{N} y_i\right)^2}\sqrt{N\sum_{i=1}^{N}\hat{y}_i^2 - \left(\sum_{i=1}^{N}\hat{y}_i\right)^2}}\right]^2\right\}$	1
Model Efficiency	$\mathrm{EF} = 1 - \frac{(N-1)\sum_{i=1}^{N}(\hat{y}_i - y_i)^2}{(N-p)\sum_{i=1}^{N}(y_i - \bar{y})^2}$	1

N: number of observations; p: number of parameters y: observations; $\hat{y}$: simulations

Uncertainty

The uncertainties are evaluated during the PTF calibration process. Assuming that measurements errors are normally distributed and that the sum of squares is locally linear in the parameters, we approximated the variance-covariance matrix of the coefficients $\mathbf{C}$ as suggested by Kool and Parker (1988).

$$\mathbf{C} \cong \frac{\boldsymbol{e}'_w \boldsymbol{e}_w [\mathbf{J}'_w \mathbf{J}_w]^{-1}}{N-p} \tag{1.4}$$

where $\mathbf{J}$ is the Jacobian matrix, i.e. the jth column of $\mathbf{J}$ is the partial derivative of the simulated data with respect to the jth coefficient. $\boldsymbol{e}$ is the vector of differences between the measurements and the simulated data. Index w means that the matrix has been multiplied by the Cholesky decomposition of the weight matrix. This is the diagonal matrix formed by the elements of the vector of the weights. The covariance matrix obtained by this way allows us to evaluate confidence intervals for the regression coefficients as well as their correlation matrix. The statistic $t = \frac{\hat{\beta}_i}{\sqrt{C_{ii}}} \sim St(N-p)$ and its associated p-value give an indication of the statistical significance of the $\hat{\beta}_i$ coefficients.

1.3 Results and discussion

1.3.1 Water retention and hydraulic conductivity models

In order to develop the new PTF on the basis of a relevant model for the description of the soil hydraulic functions, we fitted several models on the training dataset, presented in Table 1.2. The parameters of the models were optimised using the global algorithm GMCS. The average RMSE obtained with the different models are presented in Table 1.5. Comparing the performances of the van Genuchten model with parameter m equal to 1 (VG1) and to $1-1/n$ (MuVG) shows that VG1 is better. Comparing the RMSE distributions of the two models showed that their mean RMSE are significantly different (p-value = 0.0171). This corroborates the findings of Vereecken *et al.* (1989a). Figure 1.2 presents an example of the difference in the shapes of the retention curve. VG1 fits slightly better the decrease of water content. The predictions of both models mainly differ in the wet and dry ranges. Besides, near saturation, the curves do not behave the same way. With $m = 1$, n can be < 1, which leads to a decreasing slope rather than to the sill observed with $m = 1 - 1/n$

Table 1.5: Average (mean) and standard deviation (std) of the RMSE of coupled models and of association of VG1 and Gardner (1958).

	RMSE	MuVG	MuKS	MuIP	VG1+Gardner
MRC	mean	0.0175	0.0297	0.0200	0.0132
	std	0.0077	0.0148	0.0079	0.0059
HCC	mean	0.7324	6.6019	0.7050	0.9587
	std	0.3533	4.9710	0.2557	0.4773

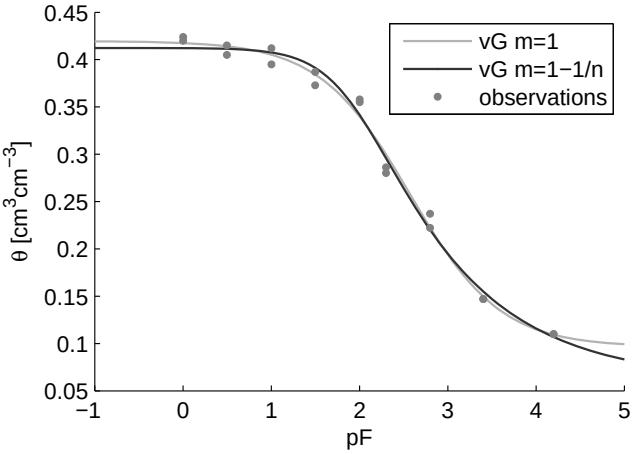

Figure 1.2: Example illustrating the difference of shape between the van Genuchten model with $m = 1$ and with $m = 1 - 1/n$

and $n > 1$. The retention model of Ippisch *et al.* (2006), here referred to as IP, is a rewriting of the modified VG introduced by Vogel *et al.* (2001). It introduces an air-entry point in the VG model, that does not lead to great changes in retention, but can improve the behaviour of the simulated HCC near saturation, mostly when $n < 2$. When the air-entry point, h_e, is 0, the model reduces to MuVG. However, it has an extra parameter that must be optimised. Concerning the combination of MRC and HCC, Table 1.5 shows that, if VG1 proved to better simulate MRC than VG2, Gardner performs worse than MuVG. Model MuKS performs the worst. Model MuIP performs the best, but it has an extra parameter compared to MuVG and its RMSE for the MRC is larger than the one of MuVG. Besides, MuVG is already implemented in many models. Hence, we chose the classic MuVG for the development of the new PTF.

1.3.2 Coefficients of PTF

Table 1.6 presents the predictors and their coefficients retained for each MuVG parameter in the new PTF.

Parameter θ_r does not appear in the table. The coefficients relating to this parameter were not retained by the stepwise procedure, finally setting it to be equal to 0. It is therefore excluded from the new PTF. This has already been observed in various PTF (e.g. Wösten *et al.*, 1999; Zacharias and Wessolek, 2007). Saturated water content, θ_s, is predicted with clay and bulk density (BD). As BD is directly related to the soil porosity F by the relation $F = 1 - \mathrm{BD}/\rho_s$ (ρ_s being the density of the solid particles of the soil), it is expected that the coefficient multiplying bulk density is negative (Scheinost *et al.*, 1997): soils with large porosity tend to retain more water near saturation. The predictors for parameter $\alpha^\star$ are sand, clay and organic carbon content.

Table 1.6: PTFs coefficients presented along with their confidence interval at 0.05 level (value +/- CI), the t statistic and its p-value. The names refer to those used in table 1.3.

parameter	var.	coef.	value	CI	t stat.	p-value
θ_s	intercept	a_2	0.6355	0.0219	56.9679	<0.0001
	clay	b_2	0.0013	0.0002	11.5132	<0.0001
	BD	c_2	-0.1631	0.0140	-22.8826	<0.0001
$\alpha\star = \ln(\alpha)$	intercept	a_3	-4.3003	0.1596	-52.8332	<0.0001
	clay	b_3	-0.0097	0.0063	-3.0132	0.0026
	sand	c_3	0.0138	0.0018	14.8296	<0.0001
	OC	e_3	-0.0992	0.0257	-7.5635	¡0.0001
$n^\star = \ln(n-1)$	intercept	a_4	-1.0846	0.0625	-33.9996	<0.0001
	clay	b_4	-0.0236	0.0022	-21.2222	<0.0001
	sand	c_4	-0.0085	0.0016	-10.3062	<0.0001
	sand^2	d_4	0.0001	0.0000	17.4583	<0.0001
$K^\star = \ln(K_o)$	intercept	a_5	1.9582	0.7543	5.0891	<0.0001
	sand	c_5	0.0308	0.0039	15.5281	<0.0001
	BD	d_5	-0.6142	0.4769	-2.5247	0.0116
	OC	e_5	-0.1566	0.0718	-4.2766	<0.0001
λ	intercept	a_6	-1.8642	0.4536	-8.0567	<0.0001
	clay	b_6	-0.1317	0.0231	-11.1891	<0.0001
	sand	c_6	0.0067	0.0044	2.9822	0.0029

The coefficients are effectual for length units expressed in centimetres, time units in days and mass units in grams.

The presence of clay and sand variables as predictors reflects the dependency of α to the geometrical mean particle diameter (Scheinost *et al.*, 1997) as both predictors fully characterise the soil texture. Parameter $n^\star$, which is linked to the shape of the particle-size distribution, is predicted using clay and sand contents as well as the square of the latter. $K^\star$ depends on sand content, bulk density and organic carbon. Parameter λ, which reflects tortuosity and connectivity of pores, depends on the clay and sand contents.

1.3.3 Performances of PTF

From the 25 coefficients proposed in Table 1.3, the stepwise procedure only retains 18 (see Table 1.6). In this section, the new PTF (referred to as WEY) are compared to the old ones (VER) and to two other published PTF: Hypres (Wösten *et al.*, 1999) and Rosetta (Schaap *et al.*, 2001). Hypres (HYP) was developed using multiple regressions on a European database, whereas Rosetta (ROS) is based on artificial neural networks built from soils in temperate to subtropical climates in North America and Europe.

Water retention curve

To evaluate the accuracy and the reliability of the PTF (see Table 1.7) for the moisture retention curve, we used a training and a test set. Using the training set, the performance of the new PTF (WEY) is almost as good as the old one

Table 1.7: Adjusted performance indicators of PTF for predicting the MRC. VER stands for Vereecken PTF, WEY stands for the new PTF, HYP stands for Hypres PTF, ROS stands for PTF implemented in Rosetta software. Bold characters present the best performing PTF, while italics present the worst.

	Training set			
Stat.	VER	WEY	HYP	ROS
RMSE	**0.0356**	0.0359	0.0464	*0.0593*
MAE	**0.0243**	0.0266	0.0327	*0.0447*
MRE	**0.0391**	0.0550	-0.0824	*-0.0970*
R^2	**0.9270**	0.9254	0.9002	*0.8784*
EF	**0.9265**	0.9253	0.8751	*0.7963*
	Test set			
Stat.	VER	WEY	HYP	ROS
RMSE	**0.094**	0.1013	0.1317	*0.1402*
MAE	**0.0790**	0.0866	0.1170	*0.1190*
MRE	*0.1418*	-0.0912	**-0.0520**	-0.3268
R^2	0.7628	**0.8359**	*0.5800*	0.8161
EF	**0.7360**	0.6945	0.4828	*0.4152*

(VER). Figure 1.3a shows that the spread of the water content values estimated with the PTF plotted against the observations is quite narrow, except for a few points that are overestimated. The mean relative error (MRE) is 40% larger than the value observed for the old PTF (VER). This means that the errors made on small water content values are larger with the new PTF (WEY). Nevertheless, the means of the relative errors averaged on each soil horizon are not significantly different ($p - value = 0.0522$). The results produced by HYP and ROS are comparable to those obtained with VER and WEY. Their performances are still a little worse, with ROS being worse than HYP. This illustrates the very specific character of hydraulic properties as related to soil-climate conditions. HYP developed from European soils performs better than ROS, which encompasses European and US soils. But HYP, as a pan-European set of functions, is less accurate than VER or WEY, developed for Belgian soils. It is however not a national measurement bias since the method used for determining the texture of the test set was different from the training set.

Testing the performances of the PTF with an independent dataset, we observed larger deviations compared to the training set. Fig. 1.3b illustrates for WEY and VER that the scattering around the straight line 1:1 is much broader than for the training set. Moreover, the high water content values are systematically underestimated. There are three main explanations to this. First, forest soils are typically highly structured and this is not directly included in the PTF. Information about the soil structure (such as the size and shape of the soil aggregates or pedological development of the profile) could be integrated in PTF, but it is mostly stored as qualitative and subjective data. A second reason may be the difference in the textural characterisations used for both data sets. Textural properties in the training set were determined using

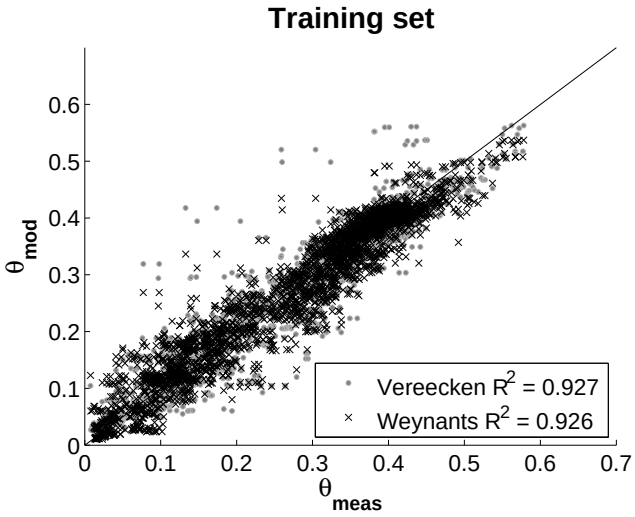

(a)

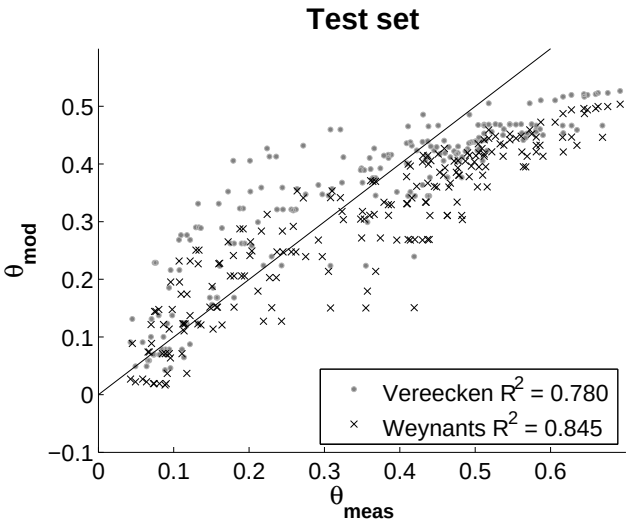

(b)

Figure 1.3: Predictions of water content plotted against observations according to Vereecken and Weynants PTFs, for training and test sets.

the classical combination of sieving and decantation whereas a laser method was used for the test set. A third reason may be the over parametrisation of the model. The comparison between the distribution of the relative errors of VER and WEY PTF show that their means are highly significantly different ($p-value \leq 0.001$). It is also worth to note that the performances of HYP and ROS on the test set are also far worse than on the training set. This pleads for the first reason proposed above since none of these PTF really consider the soil structure.

Hydraulic conductivity curve

The performances of the PTF to predict the hydraulic conductivity are presented in Table 1.8. Most of the indicators show a better performance of the new PTF (WEY). Only the mean of the relative errors (MRE) is large compared to the one observed with the old PTF (VER). Figure 1.4 displays the scattering of the data predicted with WEY and VER.

Results obtained with Hypres (HYP) and Rosetta (ROS) are also presented in Table 1.8. Relatively to the results of the MRC alone, their performances are worse. Depending on the indicator, ROS performs better than HYP or vice-versa. The results obtained for the MRC by the large-scale PTF were comparable to the local PTF. This is not true for the HCC where the need to take local specifications into account is more crucial.

Unfortunately, no test dataset containing independent hydraulic conductivity measurements is available in this study to evaluate the reliability of these

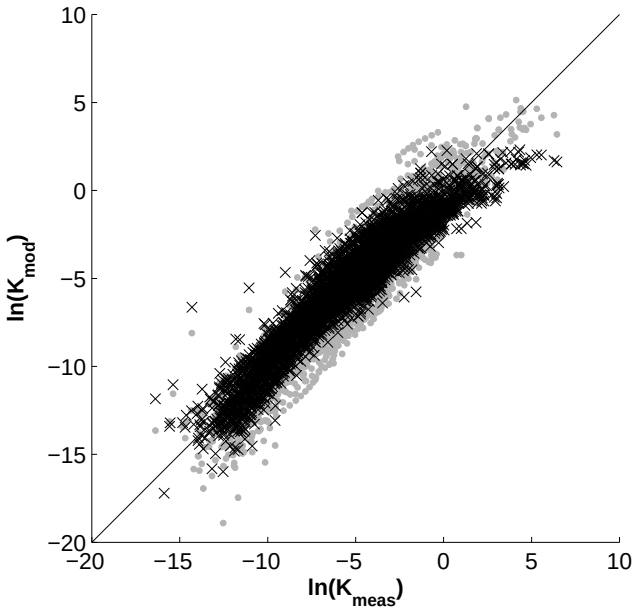

Figure 1.4: Predictions of unsaturated hydraulic conductivity according to Vereecken (grey circles) and Weynants (black crosses) PTF, for the training set.

Table 1.8: Adjusted performance indicators of pedotransfer functions predicting the hydraulic conductivity. VER stands for Vereecken PTF, WEY stands for the new PTF, HYP stands for Hypres PTF, ROS stands for PTF implemented in Rosetta software. Bold characters present the best performing PTF, while italics present the worst.

Stat.	VER	WEY	HYP	ROS
RMSE	1.3161	**1.0657**	2.5378	*3.0114*
MAE	1.0130	**0.8192**	1.6458	*2.1819*
MRE	**0.0337**	-0.0699	*0.2961*	0.0994
R^2	0.8777	**0.9064**	*0.7142*	0.8559
EF	0.8572	**0.9063**	0.4688	*0.2521*

PTF. Note that the measured saturated conductivity was not accounted for in these PTF.

Table 1.9 presents the coupled performance indicators obtained with the different PTF on the training set. The MRC and the HCC indicators are balanced using the inverse of the variances of the measurements. WEY performs the best except for the MAE, but only slightly better than VER. ROS and HYP are both worse.

K_o versus K_{sat}

The Mualem-van Genuchten model (MuVG) only describes hydraulic conductivity in the matrix flow domain. Therefore we did not include hydraulic conductivity measurements at and near saturation ($|h| \leq |h_t|$) in the optimisation process. Predictions of the estimated K_{sat} using the same variables as in the PTF did not produce satisfactory results, even when using various transformations of the variables (maximum obtained $R^2 = 0.25$). Figure 1.5 shows the three first components of the principal component analysis realised on $\ln(K_{sat})$ and the predictors used for the PTF (% sand, % clay, % OC, BD). These three components explain 83.58 % of the total variance. $\ln(K_{sat})$ mainly contributes to the third component whereas the different predictors are more represented by the first and the second component. This means that these predictors are not suitable to predict the saturated conductivity. Two reasons could explain why K_{sat} cannot be predicted by basic soil properties. First, it is well known that it is mainly affected by macropores that are not directly linked to the tex-

Table 1.9: Global adjusted performances, balanced by $1/\sigma^2_{meas}$. Bold characters present the best performing PTF, while italics present the worst.

Stat.	VER	WEY	HYP	ROS
RMSE	0.1905	**0.1878**	0.2654	*0.4441*
MAE	**0.1189**	0.1190	0.1703	*0.2309*
MRE	-0.0361	**0.0157**	*-0.1327*	-0.0142
R^2	0.9818	**0.9822**	0.9689	*0.9580*
EF	0.9220	**0.9241**	0.8492	*0.7600*

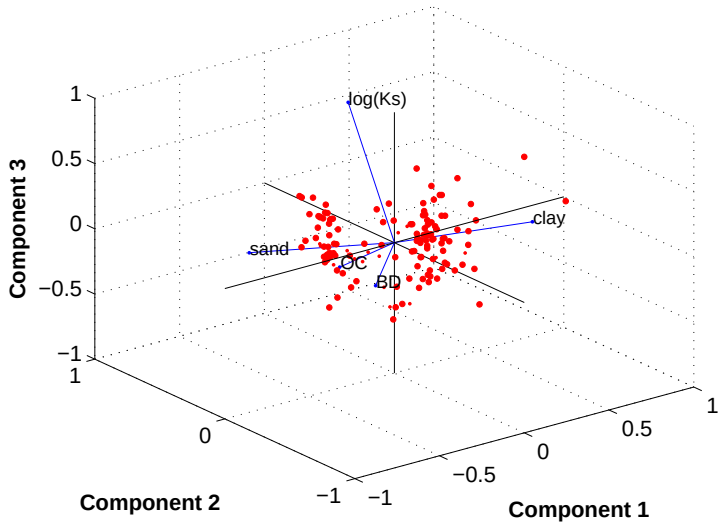

Figure 1.5: Principal component analysis of the saturated hydraulic conductivity and its potential predictors: sand and clay contents, bulk density and organic carbon content. The dots show the scattering of the dataset in the space of the three first components, explaining 83.58% of the total variance.

tural properties of soils. Therefore other variables that are more related to soil structure (e.g. the profile development, the horizon, the land use, the presence of roots,...) could be added for developing new PTF for K_{sat}. Second, the measurement support or the amount of samples are not adequate to characterise K_{sat}. Conductivity measurements are indeed highly scale-dependant and sensitive to the measurement method, especially close to saturation (Javaux and Vanclooster, 2006; Mallants *et al.*, 1998). As pedotransfer functions are usually used for large-scale studies, excluding any non significant very localised effect (namely the location of one or several macropores) is justified. However, there is a need to develop new methods to characterise effective large scale K_{sat} based on other indicators like soil surface structural properties, agricultural practices or crops.

The distribution of the ratio $\ln(K_{sat})/\ln(K_o)$ by soil type can be used to assess the presence of soil macroporosity. Figure 1.6 presents a boxplot of the ratio for each textural class. The dispersion of the ratio tends to increase for soils having a decreasing content of sand (sand (Z) $<$ silt loam (L) $<$ silt (A)). The number of observations available for the other classes is too low to draw conclusions with this respect. However, plotting sand content against the ratio as shown in Fig. 1.7 supports the finding that the ratio $\ln(K_{sat})/\ln(K_o)$ shows a larger spread for soils with a low content of sand. Nothing can be concluded about the clay content, for which the sampling does not encompass the whole textural range. This suggests that fine textured soils are more prone to macroporous flow. However, measurements in fine-textured soils are more prone to errors from side-effects.

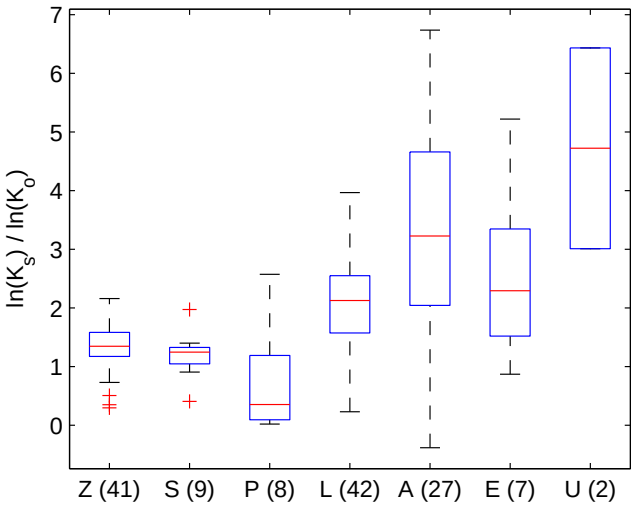

Figure 1.6: Boxplot of the ratio $\ln(K_{sat})/\ln(K_o)$ for each textural class available in the Vereecken dataset. Letters refer to the Belgian classification, see Fig. 1.1. The number in parentheses gives the amount of observations in each class. The box has lines at the lower quartile, median, and upper quartile values. Whiskers extend to the most extreme values within 1.5 times the interquartile range from the ends of the box. Outliers are displayed with a + sign.

Uncertainties and correlations

The one-step inversion method allows a direct quantification of the PTF uncertainty and the correlation matrix of their coefficients. Contrary to the sequential method, the final uncertainty encompasses at the same time dataset experimental errors, model errors and uncertainty due to fitting PTF to the dataset. The values of the PTF coefficients, their confidence intervals and their significance are presented in Table 1.6. These uncertainties along with the correlation matrix shown in Table 1.11 can be used to perform uncertainty analysis for specific flow problems.

The correlation matrix of the hydraulic parameters predicted with the PTF (see Table 1.10) reveals that $\alpha^\star$ and $K^\star$ on the one hand and $n^\star$ and λ on the other hand are very strongly correlated. The regression between parameters

Table 1.10: Correlation matrix of the hydraulic parameters predicted with the new PTF for the training set

	θ_s	$\ln(\alpha)$	$\ln(n-1)$	$\ln(K_o)$	λ
θ_s	1.0000	-0.5949	-0.6164	-0.4796	-0.6859
$\ln(\alpha)$	-0.5949	1.0000	0.9153	0.9882	0.8421
$\ln(n-1)$	-0.6164	0.9153	1.0000	0.8778	0.9409
$\ln(K_o)$	-0.4796	0.9882	0.8778	1.0000	0.7754
λ	-0.6859	0.8421	0.9409	0.7754	1.0000

Table 1.11: Correlations between the regression coefficients predicting the hydraulic parameters

	a_2	b_2	c_2	a_3	b_3	c_3	e_3	a_4	b_4
a_2	1	-0.4446	-0.9884	-0.0675	-0.0169	0.0469	0.4366	0.0295	-0.0091
b_2	-0.4446	1	0.3369	-0.0954	0.3737	-0.0984	-0.0996	-0.1768	0.2298
c_2	-0.9884	0.3369	1	0.1067	-0.0233	-0.0403	-0.45	-0.0193	-0.0167
a_3	-0.0675	-0.0954	0.1067	1	-0.6753	-0.8281	-0.2096	-0.5632	0.2584
b_3	-0.0169	0.3737	-0.0233	-0.6753	1	0.4513	0.1134	0.1935	-0.221
c_3	0.0469	-0.0984	-0.0403	-0.8281	0.4513	1	-0.0427	0.5579	-0.2634
e_3	0.4366	-0.0996	-0.45	-0.2096	0.1134	-0.0427	1	0.0232	0.0213
a_4	0.0295	-0.1768	-0.0193	-0.5632	0.1935	0.5579	0.0232	1	-0.7127
b_4	-0.0091	0.2298	-0.0167	0.2584	-0.221	-0.2634	0.0213	-0.7127	1
c_4	-0.0523	0.018	0.0581	0.2973	-0.2027	-0.2765	-0.0684	-0.6258	0.2082
d_4	0.0247	0.1029	-0.0464	-0.0697	0.1659	-0.0828	0.0745	0.2574	0.0664
a_5	-0.0292	0.0779	0.0294	0.0494	0.2069	-0.0934	-0.0282	-0.0577	-0.1603
c_5	0.0563	-0.2308	-0.0278	-0.3989	-0.031	0.6983	-0.0781	0.4413	-0.1235
d_5	-0.0002	-0.0238	0.0024	0.1476	-0.2114	-0.1048	-0.0203	-0.1262	0.2106
e_5	0.2678	-0.0682	-0.2752	-0.1336	0.0827	-0.0262	0.6137	0.0581	-0.0392
a_6	-0.0039	0.0785	-0.011	-0.6118	0.6412	0.4931	0.049	0.5504	-0.5793
b_6	0.0068	-0.1226	0.0063	0.4855	-0.7063	-0.3646	-0.051	-0.4204	0.5854
c_6	-0.0046	-0.0365	0.0138	0.5784	-0.5486	-0.4995	-0.0392	-0.5294	0.529

	c_4	d_4	a_5	c_5	d_5	e_5	a_6	b_6	c_6
a_2	-0.0523	0.0247	-0.0292	0.0563	-0.0002	0.2678	-0.0039	0.0068	-0.0046
b_2	0.018	0.1029	0.0779	-0.2308	-0.0238	-0.0682	0.0785	-0.1226	-0.0365
c_2	0.0581	-0.0464	0.0294	-0.0278	0.0024	-0.2752	-0.011	0.0063	0.0138
a_3	0.2973	-0.0697	0.0494	-0.3989	0.1476	-0.1336	-0.6118	0.4855	0.5784
b_3	-0.2027	0.1659	0.2069	-0.031	-0.2114	0.0827	0.6412	-0.7063	-0.5486
c_3	-0.2765	-0.0828	-0.0934	0.6983	-0.1048	-0.0262	0.4931	-0.3646	-0.4995
e_3	-0.0684	0.0745	-0.0282	-0.0781	-0.0203	0.6137	0.049	-0.051	-0.0392
a_4	-0.6258	0.2574	-0.0577	0.4413	-0.1262	0.0581	0.5504	-0.4204	-0.5294
b_4	0.2082	0.0664	-0.1603	-0.1235	0.2106	-0.0392	-0.5793	0.5854	0.529
c_4	1	-0.8735	0.0476	-0.2388	0.0311	-0.0821	-0.3019	0.2812	0.2625
d_4	-0.8735	1	0.0005	-0.1093	0.0098	0.0767	0.1065	-0.1463	-0.0577
a_5	0.0476	0.0005	1	-0.1142	-0.9516	-0.4311	0.071	-0.1243	-0.0618
c_5	-0.2388	-0.1093	-0.1142	1	-0.1172	-0.1272	0.0268	0.0011	0.0553
d_5	0.0311	0.0098	-0.9516	-0.1172	1	0.3878	-0.1045	0.1334	0.0876
e_5	-0.0821	0.0767	-0.4311	-0.1272	0.3878	1	0.134	-0.1442	-0.1057
a_6	-0.3019	0.1065	0.071	0.0268	-0.1045	0.134	1	-0.9093	-0.9443
b_6	0.2812	-0.1463	-0.1243	0.0011	0.1334	-0.1442	-0.9093	1	0.7943
c_6	0.2625	-0.0577	-0.0618	0.0553	0.0876	-0.1057	-0.9443	0.7943	1

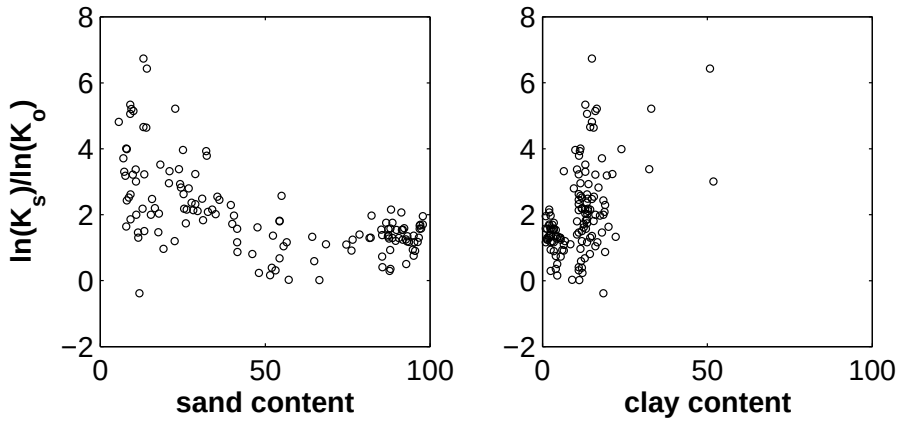

Figure 1.7: Ratio $\ln(K_{sat})/\ln(K_o)$ versus sand and clay content

$\ln(K_o)$ and $\ln(\alpha)$, obtained from fitted HCC and MRC functions (as in section 1.3.1, see above) produced the relation $\ln(K_o) = 8.94 + 1.78\ln(\alpha)$ with a coefficient of determination (R^2) of 0.59. $1/\alpha$ corresponds to the inflection point of the MRC described by VG. We can relate it to K_o using a set of physics laws. First Poiseuille's law[‡] explicitly relates the volumetric laminar stationary flow of an incompressible uniform viscous liquid through a cylindrical tube with constant circular cross-section to the internal radius of the tube at power 4. By Jurin rule, $1/\alpha$ is inversely proportional to the average pore radius. Combining these two laws with Darcy's law[§], we can conclude that $\ln(K_o)$ is linearly linked with $\ln(\alpha)$, with a slope of 2, which is close to the value of 1.78 obtained in the regression above. The intercept should be equal to $\ln\left[\left(\frac{\rho g}{2\gamma\cos\theta}\right)^2 \frac{|\Delta P|}{8\eta L}\right]$, which is 12.35 in the units used here. Again this value is not far from 8.94. Note that this strong correlation does not exist between α and K_{sat}, as experimental K_{sat} is mainly influenced by the macropore network ($R^2 = 0.0101$).

Both λ and n influence the general slope of the HCC and MRC. It is therefore expected that the same type of information will affect these parameters and that they therefore will be correlated. These strong correlations suggest that the parameters specific to the HCC in MuVG model could be predicted using the optimised parameters of the MRC modelled with VG2. This interesting suggestion deserves further investigation. Rosetta (Schaap *et al.*, 2001) already proposes to predict K_o and λ from the VG parameters optimised on measurement data on the basis of the work of Schaap and Leij (2000a).

[‡] $\phi = \frac{dV}{dt} = v\pi R^2 = \frac{\pi R^4}{8\eta}\left(\frac{-\Delta P}{\Delta x}\right) = \frac{\pi R^4}{8\eta}\frac{|\Delta P|}{L}$

[§] $q = \frac{\phi}{A} = K\frac{\Delta H}{L}$, with q the flux density, ϕ the discharge, A the unit cross-sectional area, K the proportionality factor called hydraulic conductivity, $\frac{\Delta H}{L}$ the hydraulic gradient

1.4 Conclusion

New PTF are developed for Belgium based on Vereecken dataset. The new PTF, developed using MuVG, perform as good as the ones published by Vereecken *et al.* (1989a, 1990), based on Gardner and VG1 models, and they use less coefficients (18 vs 26), less parameters (6 vs 7) and have better accuracy for $K(h)$. The one-step inversion method coupled with a stepwise optimisation procedure led to a consistent parameters set for PTF. In addition, it allows the direct quantification of the correlation matrix and the uncertainties on the parameters predicted by the PTF. The strong correlations observed between some parameters can be explained thanks to physical reasoning. The possibility of predicting the HCC parameters from the MRC parameters is suggested but needs to be further investigated. Besides, we showed that close to saturation conductivity measurements cannot be predicted based on any of the available variables. Instead, the new PTF predicts the saturated hydraulic conductivity for the matrix K_o, with high accuracy. The resulting PTF hence predict the hydraulic conductivity in the soil matrix and not in the macropores. There is therefore a need for developing alternative methods to asses relevant K_{sat} values based on other predictors, experiments or support scales. Improved K_{sat} could then be linked to the hydraulic conductivity at the h_t value. The function between $h = 0$ and $h = h_t$ could be chosen based on experimental datasets. We advise that more systematic measurements should be performed in the range 0-15 cm to further investigate the optimal threshold value h_t.

Further research could focus on the improvement of the prediction if any information about the soil structure is introduced in the model. As shown here, predictions using texture, bulk density and organic carbon content fail to predict the hydraulic characteristics of highly structured soils or the hydraulic conductivity near saturation. Structure related information could consist in pedological data, as gathered during soil survey (Lin *et al.*, 2006a,b; Pachepsky *et al.*, 2006b). Information about land use and crop management, which strongly affect the soil surface, can also be taken into account (Jarvis, 2007).

Acknowledgements

The test set used in this study was set up in the framework of project 00/05 of the VLINA research program (1995-2001), which was funded by the Ministry of the Flemish Community and conducted by Ghent University and the Institute for Forestry and Game Management.

Chapter 2

Development of a Multistep Outflow device

Multistep outflow (MSO) method (VanDam *et al.*, 1994) is used to obtain parameters of the hydraulic characteristic curves via inverse modelling of Richards equation. It is based on the measurement of the outflow from an initially saturated soil sample submitted to increasing steps of suction/pressure. Samples are placed on porous plates and a suction is applied at their basis or a pneumatic pressure is exerted at their top. MSO principal advantages are its ability to provide information on both the hydraulic conductivity curves (HCC) and moisture retention curves (MRC) of the soil sample and its relative easy implementation. Eching and Hopmans (1993) showed how multistep outflow, combined with an automated monitoring of the suction, led to a unique solution comparable to independent measurements for samples of four contrasted soil textures. In their review, Durner *et al.* (1999) compare the MSO and the one-step methods and conclude to the excellent performances of the former for a large range of textures. Bagarello *et al.* (2000) showed that MSO produced HCC comparable to thos obtained from field suction infiltrometer measurements. However, MSO experiments are also prone to errors. Experimental errors can affect the quality of the results. Wildenschild *et al.* (2001) highlighted different processes that could contribute to the rate-dependancy observed in their experiments. Unrealistic applied boundary conditions could also affect the results. VanDam *et al.* (1994) mentioned that sudden pressure changes are not encountered in nature and are susceptible to cause unrealistic fluxes. Errors can also come form the inversion procedure. In presence of macropores, the model might not be adapted to the considered soil (Laloy *et al.*, 2010). In this chapter we first describe the criteria we chose for developing the device, its implementation and its evolution. This first section is very descriptive, but its purpose is to serve as a reference for future users of the MSO. In a second section, we enumerate the sources of error that were detected along the use of the device and the solutions we found to take them into account. And finally, we present a sensitivity analysis of the parameters of Mualem-van Genuchten (van Genuchten, 1980) model (Eq. 3.1, 3.2) (MV).

2.1 Development

The requests for the device were: (i) a high accuracy close to saturation, (ii) a large sampling volume, (iii) an automated monitoring of outflow and tension. Soil structure effects can be very local and working with small volumes of soil makes generalisations of the measured properties hazardous. However, working with very large volumes of soil *ex situ* demands material resources that are not easily put into action. A compromise had to be found. We chose to work with undisturbed soil samples of 1 L, contained in PVC cylinders with a section of around 100 cm^2.

Initially the device was designed to work with a pneumatic pressure at the sample upper boundary. An overall view of its functioning is illustrated at Figure 2.1. Ten samples can be subjected to MSO experiment in parallel. Samples contained in PVC cylinders are placed in hermetic cells. The bottom of each sample lies on a highly conductive nylon porous plate (EcoTech, Germany). An opening allows the outflow to drip out of the lower part of the cell. A valve allows to bleed the air out of the cell for the saturation process or to drain out the excess of water prior to the experiment. The pneumatic pressure is applied on the upper part of the cell thanks to a pressure regulator (EcoTech, Germany) controlled by the computer program. This regulator can control the incoming pressure with a precision of 1 hPa in the range between 6 and 1000 hPa. The outflow is collected in 0.5 L buckets placed on scales. Hollenbeck and Jensen (1998a) recommand weight measurement of the outflow over a burette connected to the cell outlet. The scales have a 0.02 grams precision and a maximum capacity of 600 grams. They are connected to the computer via ZigBee® protocol using Xbee® wireless RF modules (Digi International Inc., Minnesota, USA). Tensiometers can be inserted in the samples to monitor the soil suction head along the experiment. We chose miniature tensiometers (EcoTech, Germany), connected to a AM16/32 multiplexer (Campbell Scientific Ltd., UK). The data are collected by a CR800 datalogger (Campbell Scientific Ltd., UK), connected to the computer via RS232. The program controlling the MSO experiment is written in Java (Melebeck, 2009). Close to saturation, the pressure regulator could not provide us with the accuracy we wanted. Therefore, we developed a suction functioning mode for measurements between saturation and *circum* 80 cm of suction head (Figure 2.2). In this configuration, columns are supported by a board and connected from the outlet with a flexible tube to overflow setups placed on top of the scales. This tube is filled with water so that a continuum of water is maintained between the sample and the overflow bucket. By lifting the board, higher suctions can be applied. The board is secured with cables to a frame consisting in two metallic poles fixed to a stabilising base. The level is handled thanks to a system of pulley and gears. The handle of the pulley allows the level of the board to be controlled with a 2 mm precision.

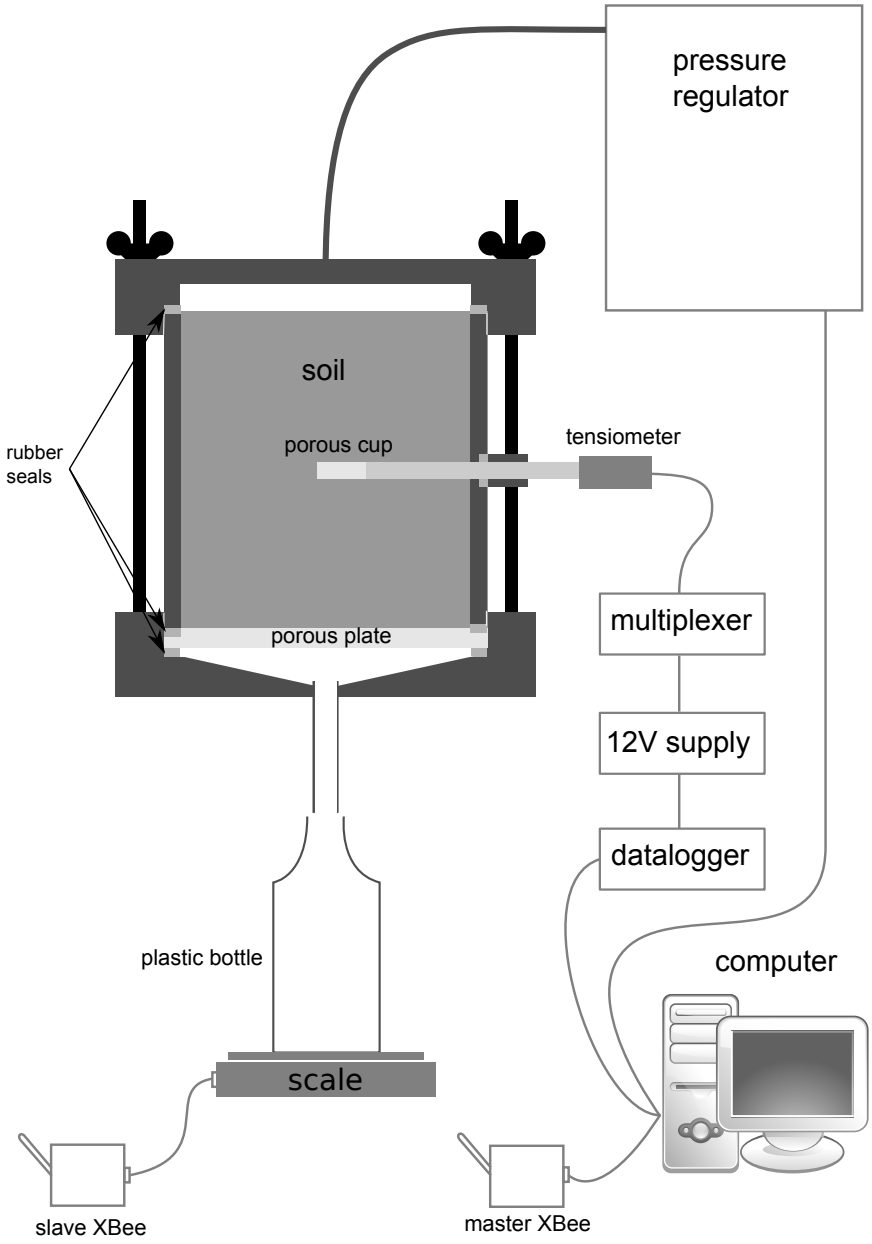

Figure 2.1: Schematic view of the multistep outflow device functioning in pressure mode

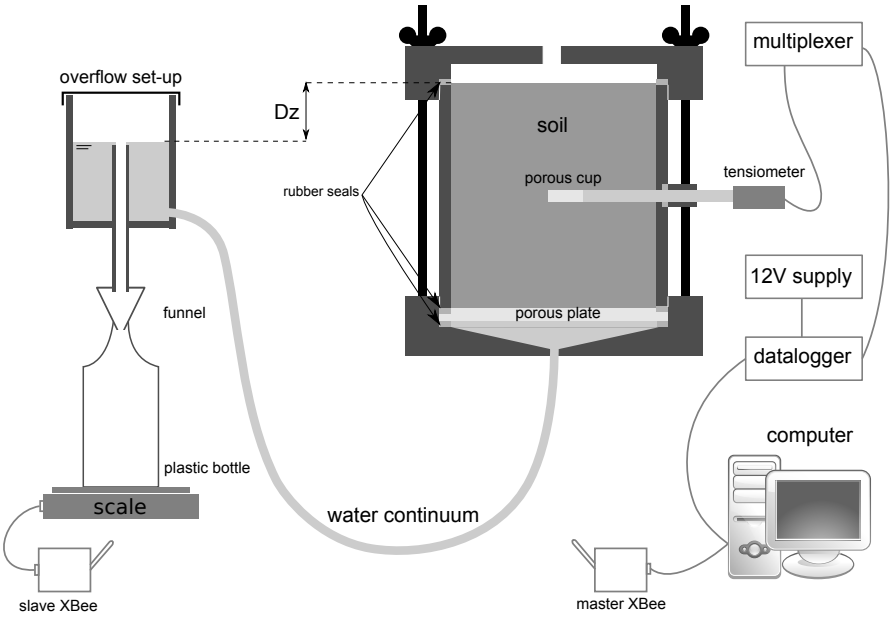

Figure 2.2: Schematic view of the multistep outflow device functioning in suction mode

2.2 Sources of errors

Errors on the hydraulic properties estimated from MSO experiments can have various origins. We can distinguish errors due to the modelling (forward and inverse) and experimental errors (Laloy *et al.*, 2010). Even if we assume that the former is negligible, the latter may lead to erroneous parameters estimation. Estimating hydrodynamic parameters by inverse modelling on the basis of data of poor quality does not make any sense. In this section, we inventory the potential sources of experimental errors and how to minimize them.

2.2.1 Errors affecting the outflow

Errors on the volume of the sample have considerable consequences. First, it affects the estimation of the soil bulk density. This property is used for calculating the volumetric water content at the end of the experiment. It is also used to compute the outflow itself. Indeed Hydrus1D, as a one dimension model, works with flow rates expressed in length by time units [L T^{-1}]. The raw data from the scales must hence be divided by the section of the sample. Errors on the volume of the sample hence lead to errors in the water balance. If the volume is underestimated, the bulk density is overestimated, and the volumetric contents are also overestimated. The outflow will in that case also be overestimated.

Ignoring the evaporation from the collecting bottles may lead to an underestimation of the outflow. It can easily be corrected using a simple model of the evaporation process, considering the room and the water temperatures and the surface of the bottle.

When working in pressure mode, water can be stored beneath or inside the porous plate and released with the exertion of pressure, producing an excess of outflow.

When saturating the samples bottom-up, water can accumulate in the plate and be released during the experiment. When working with 1 L samples, the effect is limited. However when working with smaller samples, the volume of water accumulated in the plate is large relatively to the sample volume. In that case, the suction mode must be avoided.

Starting from a saturated sample can cause artificial rapid flows along the sides of the PVC cylinder. It is best to start the experiment with the water table at the bottom of the sample and to be sure to have let drain it long enough for the equilibrium to be restored.

2.2.2 Errors affecting the boundary conditions

The porous plates are covered with a synthetic membrane which is very fragile. Small scratches on that membrane decrease its air-entry point. If there is a small hole, the boundary condition can be maintained, but if it is too big, the pressure regulator may not be able to reach the desired pressure, the actual boundary condition is then not known anymore and the results cannot be interpreted. The plates must hence be handled with great care and their quality checked prior to each experiment.

When working in suction mode, the board supporting the samples must be levelled with the board supporting the overflow set-up. As the device is meant for high-precision close to saturation, a small error can lead to a bias in the applied suction head which would lead to erroneous results.

When working in pressure mode, the stability of the applied pneumatic pressure must be ensured. The pressure regulator would not be accurate enough for applying pressures less than 10 hPa.

2.2.3 Errors affecting the measured suction head

The suction head inside the samples is monitored by mini tensiometers inserted through a hole in the cylinder. The quality of the measurement will be affected if the contact between the porous cup and the soil is not properly maintained. Also, the tensiometers have to be properly calibrated so that the voltage they measure can be transformed into suction head. The calibration is to be checked regularly.

2.3 Sensitivity analysis

When equilibrium is not reached at the end of a suction/pressure step,MSO results are difficult to use directly. As for other transient experiments, inverse

modelling is required to obtain the HCC of a soil sample undergoing a MSO experiment. This means that a model has to be applied and that the shape of the hydraulic functions are not completely free. The water flow inside the soil has been modelled by the one-dimensional Richards equation, with Hydrus1D (Simunek *et al.*, 2005).

In this section, a sensitivity analysis of the parameters of the MV model (the most widely used) is realised from synthetic data. A virtual MSO experiment was simulated using Hydrus1D with the MV model of the MRC and HCC. The real samples are contained in 1 L PVC cylinders of 10 cm high. We hence set the height of the soil profile in Hydrus1D to 10 cm. The parameters of a loam are chosen in the Rosetta database (see Table 2.2). The length units are in centimetres and the time units are in minutes. The initial conditions are a hydraulic equilibrium with an aquifer level at the top of the profile.

$$t = 0, \quad 0 < z < L, \quad h(z) = -z + L$$

The boundary conditions are a no-flux at the top and a variable pressure head at the bottom.

$$t > 0, \quad z = L, \quad q(z,t) = 0$$

$$t > 0, \quad z = 0, h(z,t) = \mathsf{BC}$$

Boundary conditions for the virtual experiment are similar to real ones (see Table 2.1).

Table 2.1: Bottom boundary conditions (BC) of the virtual MSO experiment

Time	Step Duration	Pressure head
0h 00	30min	0 cm
0h 30	30min	-2 cm
1h 00	30min	-4 cm
1h 30	30min	-6 cm
2h 00	30min	-8 cm
2h 30	30min	-10 cm
3h 00	30min	-20 cm
3h 30	30min	-30 cm
4h 00	10h	-40 cm
14h 00	10h	-80 cm
1d 0h 00	10h	-160 cm
1d 10h 00	10h	-320 cm
1d 20h 00	20h	-640 cm
2d 16h 00	20h	-960 cm
3d 12h 00	-	END

The synthetic datasets generated from the virtual experiment consist in time series of outflow and pressure head in the middle of the sample. Points of the MRC are also added.

A global objective function is defined to assess the identifiabilitly of the parameters of the MV formulation of the hydraulic properties. It consists in the sum of three sub-objectives:

$$\mathbf{\Phi}(\boldsymbol{\beta}) = \phi_q(\boldsymbol{\beta}) + \phi_h(\boldsymbol{\beta}) + \phi_\theta(\boldsymbol{\beta}) \tag{2.1}$$

where the subobjectives are written:

$$\phi_q(\boldsymbol{\beta}) = \frac{1}{N_q S_q^2} \sum_{i=1}^{N_q} [q(t_i) - q(t_i, \boldsymbol{\beta})]^2 \tag{2.2}$$

$$\phi_h(\boldsymbol{\beta}) = \frac{1}{N_h S_h^2} \sum_{i=1}^{N_h} [h(t_i) - h(t_i, \boldsymbol{\beta})]^2 \tag{2.3}$$

$$\phi_\theta(\boldsymbol{\beta}) = \frac{1}{N_\theta S_\theta^2} \sum_{i=1}^{N_\theta} \left[\bar{\theta}(h_i) - \int_{h_i - L/2}^{h_i + L/2} \theta(h_i, \boldsymbol{\beta}) \right]^2 \tag{2.4}$$

where
$\boldsymbol{\beta}$ is the vector of parameters for which the objective function is calculated
q is the cumulative outflow [cm min^{-1}]
h is the pressure head [cm] halfway down the profile
θ is the volumetric water content [-]. $\bar{\theta}(h)$ is the water content of a profile of height L, when a suction h is applied halfway down the profile height.
N is the number of data, specific to each type of measurement.
S_q^2, S_h^2, S_θ^2 are the measurement error variances for the cumulative flux, the pressure head and the water content, respectively. These were estimated from the measurement errors of the different devices used to obtain the measurements.

For this sensitivity analysis, we calculated cross-sections of the different sub-objective functions around the minimum. Only two parameters vary at a time in a range of plausible values (Table 2.2), the others remain fixed to their true value. The ranges of variation are discretised into 51 steps. Each sub-objective was evaluated separately in order to assess its performance for retrieving the different parameters of MV.

Table 2.2: Variation ranges of the parameters

Parameter	True value	Lower	Increment	Upper	Units
θ_r	0.067	0	4×10^{-3}	0.2	cm^{3}cm^{-3}
θ_s	0.45	0.3	6×10^{-3}	0.6	cm^{3}cm^{-3}
α	0.02	0.001	1.8×10^{-2}	0.9	cm^{-1}
n	1.41	1.01	0.14	8	-
$\log_{10} K_s$	$\log_{10}(0.0075)$	-3	0.062	0.1	$\log_{10}$(cm min^{-1})
λ	0.5	-5	0.2	5	-

The response surfaces allow us to analyse the sensitivity of the objective function (OF) in planes of the parametric space. The gradient of the OF around

its minimum gives an idea of its sensitivity on small changes of the parameters. Its observation can show the existence of local minima or of a very insensitive minimum, which would cast doubt on the uniqueness of the solution. With response surfaces, we look at two parameters at a time, all the others remain fixed to their true values. There could hence be some local minima that are not grasped by this approach. Nevertheless, it already gives us a first tool to evaluate the well-posedness of the problem, *i.e.* (i) a solution exists, (ii) the solution is unique, (iii) the solution depends continuously on the data, in some reasonable topology.

Some of these response surfaces are represented at Figures A.1, A.2 and A.3. The base 10 logarithm of the OF is represented for couples of parameters, for each subobjective ($\phi_q, \phi_h, \phi_\theta$) and for their sum ($\mathbf{\Phi}$). The contribution of each subobjective to the global OF can hence be assessed.

Table 2.3 summarises the general quality of the OF for the identification of the parameters. In the next paragraphs, the identification of all parameters is

Table 2.3: Quality of the identification of the parameters by the objective function (Eq. 4.3) and its components (Eqs. 2.2, 2.3, 2.4).

	θ_r	θ_s	α	n	$log_{10}(K_s)$	λ
ϕ_q	–	–	-	+	+/-	+
ϕ_h	–	–	+	-	+/-	+
ϕ_θ	–	+	-	+	+/-	-
$\mathbf{\Phi}$	–	-	+	+	+/-	-
Corr.	θ_s	θ_r	K_s, λ	-	λ, α	K_s, α

discussed.

2.3.1 Saturation and retention water content - θ_s and θ_r

There is a strong correlation between these two parameters, at least concerning the outflow (ϕ_q) and the suction head (ϕ_h) objectives. This is expected as none of these objectives brings information on the absolute value of the water content during the experiment. The information is relative to the initial conditions of wetness. This has already been observed by Hopmans *et al.* (2002). This means information on the absolute value of the water content is essential. It can be brought by a sub-objective in the OF or by fixing the value of parameter θ_s to an independently measured value.

In the present case, ϕ_θ can help bringing this lacking information. It also shows correlation between the two parameters, but in the opposite direction as the two other sub-objectives. The sum of all three sub-objectives allows the identification of these parameters, but the contribution of ϕ_θ to $\mathbf{\Phi}$ is smaller than the one of ϕ_q and ϕ_h. Besides a large uncertainty remains on the identification of θ_r, mostly because of the boundary conditions of the MSO.

2.3.2 Parameter α

Parameter α is linked to the inflection point of the MRC and thus to the soil pore size distribution. It is non linearly correlated to several other parameters. ϕ_θ is not very sensitive to α, at least towards θ_r (non linear correlation) and n. Its identification towards parameter n is difficult with outflow (ϕ_q), but tensiometers bring valuable information. α is correlated to parameters K_s and λ. Its identification towards these parameters is less easy. In general, identification of parameter α is possible based on the combination of the sub-objectives.

2.3.3 Parameter n

Parameter n is a shape parameter, controlling the slope of the MRC. Parameter n is correlated to other parameters to different extents. Outflow (ϕ_q) shows slight correlations towards θ_r and θ_s, whereas water (ϕ_θ) content show strong non linear correlations. For the same parameters, the tensiometers show the best sensitivity. Identification of n towards α is difficult using the outflow (ϕ_q) due to non linear correlation. In the same cross-section, tensiometers are insensitive to n and water content shows a local minimum not far from the minimum. Adding the sub-objectives ends up in a relatively good definition of both parameters. In the planes (n, K_s) and (n, λ), a non-linear correlation is visible for ϕ_q and ϕ_h. However the steep gradients around the minimum make its identification possible and show that the OF is very sensitive to this parameter.

Hydrus1D does not converge for values of n very close to 1. Besides, when $n > 2$, problems of convergence occur if λ becomes negative. This is caused by decreasing $K(h)$ curves for certain couples of parameters. These combinations of parameters are rejected before running the model.

2.3.4 Saturated hydraulic conductvity - K_s

Saturated hydraulic conductivity is a physical parameter, measurable in the field or in the lab. However, it is better to consider K_s parameter in MV as a fitting parameter (Schaap and Leij, 2000a). The estimated parameter is an extrapolation on the basis of the available information and, as such, cannot be interpreted as the true saturated conductivity. An MSO experiment does not hold enough information to properly identify the true saturated hydraulic conductivity. A logarithmic scale is often adopted for representing this parameter because of its large variation with no zero values.

A relatively good identification of $\log_{10}(K_s)$ is possible thanks to the combination of ϕ_q and ϕ_h (ϕ_θ is unsensitive to K_s since it does not depend on that parameter). However a large uncertainty remains in the plane (K_s, λ), as a the correlation between these two parameters is large.

2.3.5 Parameter λ

λ is a shape parameter of the HCC. It is linked to the tortuosity of the porous system. In the original model of Mualem 1976, it is set to 0.5. However several authors changed this initial value to increase the flexibility of the model (Schaap and Leij, 2000a, e.g.). When it takes negative values, it does not have any physical meaning (Durner *et al.*, 1999).

Its identification is difficult with the MSO experiment. The minimum of the OF is not well identified in all planes of the parametric space. Particularly, the gradients around the minimum in the planes (λ, θ_r), (λ, θ_s), (K_s, λ) are not very steep. In the plane (n, λ), ϕ_q is insensitive to λ, but ϕ_h allows $\mathbf{\Phi}$ to be sensitive enough. In the plane (α, λ), ϕ_q allows a good identification of λ.

2.4 Conclusion

In this chapter, we described a multistep outflow (MSO) device. This device provided measurements used in the next chapters. We presented the sources of experimental errors and ways to limit them. Based on a virtual experiment and on cross-sections of terms of the objective function, we evaluated the identifiability of Mualem-van Genuchten (van Genuchten, 1980) model (Eq. 3.1, 3.2) (MV) parameters. Not all parameters are as easily identified. θ_r and θ_s are strongly correlated and are not well identified. α and n are well identified. K_s and λ are less easily identified, but the minimum of the objective function (OF) is still relatively well defined. MV parameters can hence be retrieved using MSO experiments, but the outflow only is not enough. Tensiometers are necessary to constrain the solution but they lack information on the absolute water content. Moisture retention at several suctions can help fill in this gap.

Chapter 3

Tackling the sources of uncertainty in multistep outflow experiments*

3.1 Introduction

Modelling hydrological processes at all scales requires information on soil hydraulic properties. These properties, namely the relationship between the soil hydraulic conductivity, its moisture content and its hydraulic potential, are highly variable in space and time and their measurement is tedious and time-consuming. Particularly, the characterisation of the unsaturated hydraulic conductivity remains a challenge in soil hydrology. Today, the multistep outflow (MSO) technique, originally developed by VanDam *et al.* (1994), has become a standard method to assess hydraulic soil properties in the laboratory (see e.g. VanDam *et al.*, 1994; Hollenbeck and Jensen, 1998b; Zurmuhl and Durner, 1998; Javaux and Vanclooster, 2006; Vogel *et al.*, 2008). This approach is based on transient experiments where a soil sample saturated with water is progressively drained by applying successive pressure steps. Authors generally use either positive air pressure at the top or negative pressure steps at the bottom of the sample (e.g. Puhlmann *et al.*, 2009). Typically, the parameters of the Mualem-van Genuchten (van Genuchten, 1980) model (Eq. 3.1, 3.2) (MV) are obtained from the inverse solution of the 1-D Richards equation, based on measured cumulative outflow data and water potential or moisture content time series at given locations. Recently, other formulations of soil hydraulic properties have also been used to inverse MSO data (Zurmuhl and Durner, 1998; Ippisch *et al.*, 2006; Iden and Durner, 2007).
Four main advantages of MSO can be cited. First it is faster then other laboratory techniques, such as evaporation or crust methods. Second, both the

*Adapted from Weynants, M., Laloy, E. and Javaux, M. Soil hydraulic properties obtained from multistep outflow: impact of model choice, protocol and spatial variability on the uncertainty at the horizon scale, *submitted to Journal of Hydrology*

retention and the conductivity curves can be obtained at the same time. Third, it is an inverse method where several input data can be used: combined use of cumulative outflow and pressure head in the objective function greatly improves the optimisation (Eching and Hopmans, 1993). Fourth, uncertainty can be associated with optimised hydraulic functions. However, MSO technique has also several drawbacks. First, the inversion problem may be ill-posed. Users have also reported problems of model adequacy (e.g. Iden and Durner, 2007), like the impossibility of fitting both the pressure head and outflow time series. Hollenbeck and Jensen (1998a) report poor reproducibility of transient flow experiments with small step changes and non-unique system response for large step changes. Besides, MSO users mention unexpected high outflow at low suction levels. Most of them therefore omit the first step to limit errors caused by experimental artefacts that may appear in a saturated medium (either unsaturated pores or saturated artificial macropores at the boundaries of the sample). Wildenschild *et al.* (2001) underline the flow rate dependency of multistep outflow experiments. They suggest five physical processes to explain their observations: (i) entrapment of water occurring at high flow rates; (ii) pore water blockage; (iii) air entrapment that might compromise the continuity of the air phase in the soil; (iv) air-entry value effect; (v) dynamic contact angle effect. They conclude that these phenomena are mostly prevalent in the coarse textured soils and at high flow rates.
The final optimised parameters sets may hence suffer from uncertainties due to several sources that are developed hereafter.

(i) Even if the inversion problem is well posed, it may need complex algorithms to get the true solution. When the number of parameters to be optimised is large or when the parameters are correlated, the solution can suffer from non-uniqueness or the objective function can include local minima. In the latter case, the inversion requires a global algorithm to find the global minimum.

(ii) The question of the model adequacy is not only typical to MSO but is present as for all inverse modelling techniques. In MSO, one important assumption is that samples are "homogeneous", which is seldom the case for real soils (Durner *et al.*, 2008). Laloy *et al.* (2010) numerically investigated the impact of soil heterogeneity on the effective parameters obtained with MSO and found that a one-dimensional model could reproduce water flow in a macroporous medium only if the model would take this structure into account.

(iii) The spatial variability of hydraulic properties of sediments has been analysed by Botros *et al.* (2009) using MSO experiments. They suggest that the horizontal continuity of the hydraulic properties is about one order of magnitude larger than in the vertical dimension. This means that hydraulic properties are more variable in the vertical dimension than in the horizontal one. Sampling the different horizons of a soil profile is hence more informative than replicating samples within a single horizon. The question of the ideal sample volume has been tackled by numerous authors (e.g. Mallants *et al.*, 1997a) and is not related with the MSO technique itself. However this is an important question in order to be sure that the hydraulic properties are indeed represen-

tative of the support volume. The optimal support volume is closely linked with the definition of the elementary representative volume.

(iv) Experimental artefacts and unconsidered physical processes can lead to inaccurate results, as already suggested by some authors (e.g. Hollenbeck and Jensen, 1998a; Wildenschild *et al.*, 2001).

Uncertainty in the final estimate of soil hydraulic properties originates from different sources: the model adequacy, the soil representative volume (if one exists) versus support volume, and from the protocol itself (uncertainty in the initial and boundary conditions, measurements errors and artefacts). These sources of uncertainty can also be correlated. For instance, too large pressure steps close to saturation may render a double porosity soil invisible to the MSO operator and therefore give a good unimodal model adequacy. Puhlmann *et al.* (2009) optimised MSO pressure regimes for different texture groups from synthetic experiments and information content. Nowadays a lot of efforts is devoted to characterise the fitting uncertainty by use of complex algorithms, but it is worth wondering whether the prediction uncertainty is not more affected by the spatial variability, the experimental errors or by the choice of the hydraulic model.

In this study, we propose to compare several sources of uncertainty for silt loam hydraulic parameterisations. These soils, prone to structural heterogeneity, have large agronomic interest and have been broadly investigated. We focused our investigation on three soil horizons with contrasted structural features and estimated the sources of uncertainty due to the protocol, the model, the parameters uncertainty and the spatial variability. With these tools, we want to answer more specific questions:

- In what combination of model and protocol can we be the most confident to obtain soil parameters?
- What is the main source of uncertainty of the hydraulic properties inverted from MSO experiments: the choice of protocol, the model, the parameters uncertainty, or the spatial variability?
- How does uncertainty related to MSO experiments, spatial variability and model choice affect predictions?

3.2 Material and methods

3.2.1 Field sampling and laboratory measurements

Nine undisturbed soil samples of 1 L (10 cm high, 11.25 cm diameter) were extracted from the silt-loam region of Belgium. The soil cores were taken in triplicate from three soil profiles, as shown at Figure 3.1, under different land covers, i.e. forest, grassland and crop (F, G and C). At the same sites, triplicates of 100 cm^3 undisturbed soil cores were also taken. Table 3.1 presents the clay, silt and sand contents of the analysed horizons, along with their organic carbon content and bulk density. The sampled soil horizon morphology and structure was described using the FAO guidelines (FAO, 2006). In the forest

Table 3.1: Mass percentages of clay, silt, sand and organic carbon in the analysed horizons and bulk density (g cm^{-3}) values.

	Clay	Silt	Sand	OC	BD
F	10.70	74.55	14.76	1.32	1.19
G	17.64	70.30	12.05	3.14	1.27
C	19.14	70.52	10.35	1.52	1.51

horizon (F), the structure is defined as weak with fine subangular blocks with more or less plane fractures. The macroporosity is visible and it has a high root density. The cropland horizon (C) presents a strong and medium blocky angular structure with few to common fine (0.5-2 mm) to medium (2-5 mm) pores and few medium sized (2-5 mm) roots. In the grassland horizon (G), the structure consists in moderate and fine blocks, with few fine (0.5-2 mm) pores and many fine (0.5-2 mm) roots.

Moisture retention measurements were performed with a sand-box system on the 100 cm^3 samples at the following pressure heads applied at the bottom of the soil cores: 0, −0.5, −1, −2, −3, −4, −5, −6.5, −8, −10, −15, −20, −30, −40, −80 cm. A pressure plates apparatus was used for lower pressure heads (−1000, −3000, −12600 cm).

MSO experiments were performed on the undisturbed 1L soil cores. They were placed in hermetic cells on top of synthetic high conductivity porous plates (EcoTech, Germany). Automated mini-tensiometers (EcoTech, Germany) were inserted horizontally in the samples, 5 cm from the bottom. Experiments began with the water table at the top of the soil samples (pressure head at the lower boundary $h = +10$ cm, after 60 hours of equilibrium). Desaturation was then conducted applying suction steps with a hanging water column connected from the cell outlet to a reservoir monitored by a scale (Fig. 2.2). The following steps were approximately applied: +10; +8; +6; +4; +2; 0; −2; −4;

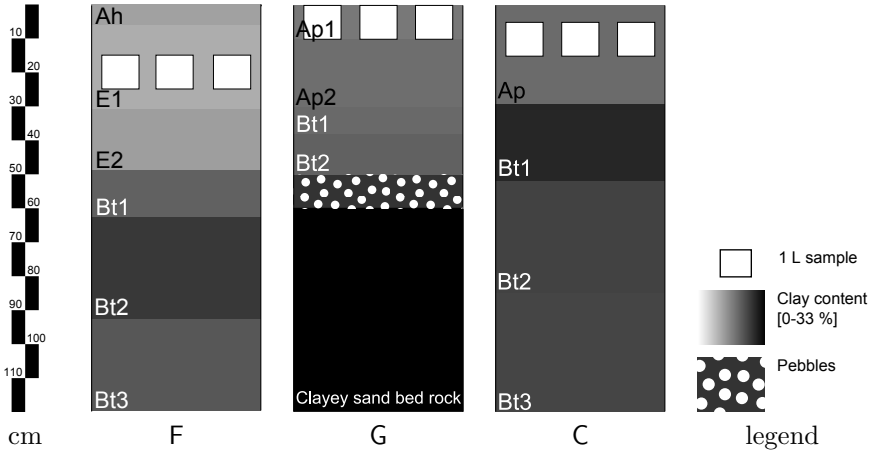

Figure 3.1: Illustration of the sampled soil profiles and position of the 1 L samples

−6; −8; −10; −15; −20; −30; −40; −80 cm. The first 14 steps were applied during approximately 30 minutes each whereas the last two were maintained during at least 6 hours. The next steps (−160; −320; −640; −960 cm) were performed by applying air pressure at the top of the cells using a pressure regulator (EcoTech, Germany) as depicted in Fig. 2.1. The outflow was recorded in real time using scales (accuracy: 2×10^{-4} cm water height) connected to a computer. It is important to note that, as the handling of the suction device was not automated, we could not conduct all the experiments in the exact same conditions of suction steps durations and levels.

3.2.2 Methodology

In order to test the effect of the experimental protocol and the inverted model on the optimised hydraulic properties, the following methodology was used. For each experimental dataset, we inverted the parameters of three models describing the hydraulic functions, according to three different inversion protocols. Then, statistical analysis was performed for each combination of protocol/soil horizon/model to test (a) the intra-horizon variation in the MSO measurements, (b) the goodness of fit, and (c) the variation and uncertainty of the optimised characteristic curves and of the results of numerical extrapolation experiments.

Forward modelling

We used Hydrus1D (Simunek *et al.*, 2005) to model soil pressure head and outflow time series with Richards equation. The soil domain is configured with a logarithmic density of nodes to ensure a high resolution at the bottom of the profile, where the hydraulic gradient is expected to be larger. The porous plate is explicitely modelled. Its properties are set so that its air-entry point does not occur in the range of pressure head explored during the MSO experiment. Its saturated hydraulic conductivity is calculated from the constructor indications ($K_{s,plate}$ = 0.00056 cm min^{-1}, on a 0.025 cm height). The top boundary condition is set to a zero flux, whereas the bottom boundary condition is set to a variable pressure head, corresponding to the suction/pressure steps applied on the MSO device during the experiment. The initial boundary condition is considered to be a hydrostatic equilibrium.

The moisture retention and hydraulic conductivity curves are described using three different sets of functions. The first model is the classical Mualem-van Genuchten (van Genuchten, 1980), further referred to as MV. The relative saturation is expressed as:

$$S = (1 + (\alpha|h|)^n)^{-1+1/n} \tag{3.1}$$

where S is the relative saturation [-]: $S = \frac{\theta-\theta_r}{\theta_s-\theta_r}$, θ the water content [L^3 L^{-3}], h the pressure head [L], α [L^{-1}] and n [-] are shape parameters.
It is coupled in a closed-form expression with the Mualem (1976) hydraulic

conductivity model.

$$K = K_o \left[S^{\lambda} \left(1 - \left(1 - S^{n/(n-1)} \right)^{1-1/n} \right)^2 \right] \tag{3.2}$$

where K is the soil hydraulic conductivity [L T^{-1}] and K_o is the conductivity at 0 cm [L T^{-1}] and λ [-] is a shape parameter related to the pores connectivity.

The second model, proposed by Durner (1994), is based on the MV model but introduces a bimodal pore system, with the linear superposition of two (or more) functions of the soil hydraulic properties. We further refer to this model as DR.

$$S = w_1 \left(1 + (\alpha_1 |h|)^{n_1}\right)^{-1+1/n_1} + w_2 \left(1 + (\alpha_2 |h|)^{n_2}\right)^{-1+1/n_2} \tag{3.3}$$

$$\begin{aligned} K = K_o \frac{(w_1 S_1 + w_2 S_2)^{\lambda}}{w_1 \alpha_1 + w_2 \alpha_2} \\ \left[w_1 \alpha_1 \left(1 - \left(1 - S_1^{n_1/(n_1-1)} \right)^{1-1/n_1} \right) \right. \\ \left. + w_2 \alpha_2 \left(1 - \left(1 - S_2^{n_2/(n_2-1)} \right)^{1-1/n_2} \right) \right]^2 \end{aligned} \tag{3.4}$$

where w_i are weighting factors of the different pore regions ($\sum(w_i) = 1$), and α_i, n_i and λ_i are shape parameters for each hydraulic function (i=1,2).
Third, Gerke and van Genuchten (1993a) dual porosity model (Eq. 3.5, 3.6) (DUAL) considers the porous system as two separate porous media, with transfer between them. The hydraulic properties functions write:

$$\begin{aligned} \theta = (1 - w_f) \left[\theta_{r,m} + \frac{\theta_{s,m} - \theta_{r,m}}{\left(1 + (\alpha_m |h|)^{n_m}\right)^{1-1/n_m}} \right] \\ + w_f \left[\theta_{r,f} + \frac{\theta_{s,f} - \theta_{r,f}}{\left(1 + (\alpha_f |h|)^{n_f}\right)^{1-1/n_f}} \right] \end{aligned} \tag{3.5}$$

$$K_m = K_{o,m} \left[S_m^{\lambda_m} \left(1 - \left(1 - S_m^{n_m/(n_m-1)} \right)^{1-1/n_m} \right)^2 \right] + \Gamma_w \tag{3.6}$$

$$K_f = K_{o,f} \left[S_f^{\lambda_f} \left(1 - \left(1 - S_f^{n_f/(n_f-1)} \right)^{1-1/n_f} \right)^2 \right] - \Gamma_w \tag{3.7}$$

Parameters for the fracture and the matrix are indexed with f and m respectively (θ_r, θ_s, α, n, K_o and λ). The parameters indexed with w are relative to the transfer between the two pore systems. Γ_w is the water transfer between the two pore systems. It is defined as:

$$\Gamma_w = \frac{\beta}{a^2} K_w(h) \gamma (h_f - h_m) \tag{3.8}$$

where β is a geometry factor [-], a is the characteristic length of the matrix structure [L], K_w is the effective hydraulic conductivity at the interface between the pore systems [LT^{-1}], and γ is a scaling coefficient. Gerke and van Genuchten (1996) evaluated K_w as

$$K_w(h) = 0.5\,[K_w(h_f) + K_w(h_m)] \tag{3.9}$$

In Hydrus 1D (Simunek, 2009, personal communication), K_w is computed as:

$$K_w(h) = \frac{K_{o,w}}{K_{o,m}} 0.5\,[K_m(h_f) + K_m(h_m)] \tag{3.10}$$

so that the shape of the curve is given by the matrix conductivity curve but its value is given by $K_{o,w}$.

The number of parameters depends on the model. Not all parameters were optimised. Saturated water content was either optimised or fixed to $\theta_{sat,MSO}$, the water content at the beginning of the experiment, calculated by a mass balance. Table 3.2 details the optimised and fixed parameters for the three models.

For DUAL, the observed pressure head was compared with the simulated pressure head of the matrix (h_m), as suggested by Simunek (2009, personal communication) for redistribution experiments.

The concepts underlying the three models are summarized at Figure 3.2. Their parametrisation is chosen so that the three cases are very different. The continuum is represented according to Köhne *et al.* (2009): MV and Durner (1994) bimodal model (Eq. 3.3, 3.4) (DR) have a uniform flow domain, whereas DUAL has two. For the latter, we limited the transfer to a very small value, given the restricted water exchange between the matrix and biopores, due to water repellent coatings (Jarvis, 2007). Distinction between MV and DR comes from the unimodal or bimodal pore size density. It must be noted that the apparent soil retention curve obtained by traditional experimental methods would be similar between DR and DUAL, as both lead to a bimodal moisture retention curves (MRC).

Protocols

When using MSO, very large flow rates can be observed close to saturation. These are difficult to simulate with classical models. Hence, many users omit

Table 3.2: Optimised and fixed parameters for the three tested models

Model	Optimised	Fixed
MV	θ_r; α; n; K_o; λ	$\theta_s = \theta_{s,MSO}$
DR	θ_r; α_1; n_1; K_o; λ; w_2; α_2; n_2	$\theta_s = \theta_{s,MSO}$
DUAL	$\theta_{r,m}$; α_m; n_m; $K_{o,m}$; λ_m; w_f; $\theta_{r,f}$; α_f; n_f; $K_{o,f}$; λ_f	$\theta_{s,m} = \frac{\theta_{s,MSO} - w_f}{1 - w_f}$; $\theta_{r,f} = 0$; $\beta = 10^{-20}$; $\gamma = 0.4$; $a = 1$; $K_{o,w} = K_{o,m}$

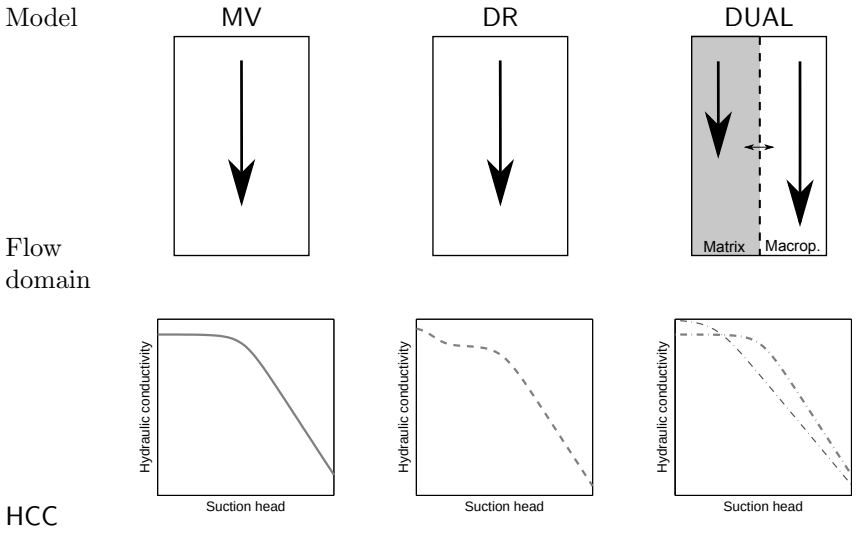

Figure 3.2: Illustration of the concepts underlying the models used for describing the soil hydraulic functions: flow domain and shape of the hydraulic conductivity curve (HCC).

data coming from the first step for the inverse procedure (Laloy *et al.*, 2010). To study the relevancy of such an approach, we developed an experimental protocol starting from complete saturation of the sample and we progressively lowered the water table. For each MSO experiment, simulations were designed with three different initial conditions. Protocols p_{10}, p_0 and p_{-5} correspond to different initial levels of the water table: $h = 10$; $h = 0$; $h = -5$ cm. As a hydraulic equilibrium is assumed at the beginning of the experiment, the initial conditions for p_{10} are at $z = 0$, $h = 0$ and at $z = -10$, $h = 10$ cm, with z the vertical dimension [L], positive upwards, and h the pressure head [L]. Since under these conditions the whole sample is saturated, results are very sensitive to any artefact in the experimental setup. Therefore, we also simulated MSO experiments with p_0 for which at $z = 0$, $h = -10$ and at $z = -10$, $h = 0$ and with p_{-5} for which at $z = 0$, $h = -15$ cm and at $z = -10$, $h = -5$ cm. These initial conditions are represented in Figure 3.3.

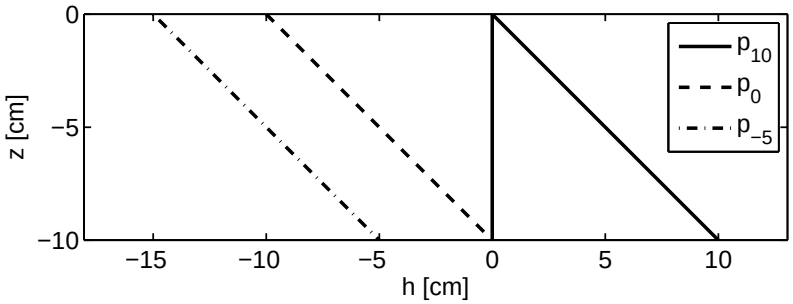

Figure 3.3: Initial conditions of the three simulation protocols. h is the pressure head, z is the vertical length, wit $z = 0$ at the top of the sample. The plain line is for p_{10}, the dashed line for p_0 and the dot/dash line for p_{-5}.

Objective function

During MSO experiments, we monitored the cumulative flux at the outlet and the pressure head in the middle of the 1 L. sample. We also measured water retention pairs on other smaller samples. These three types of data (i, j and k) were included in the objective function, Φ (Equation 3.11). It is a sum of squares balanced by the measurement errors variances and the number of data.

$$\begin{aligned}\Phi(\boldsymbol{\beta}) = &\frac{1}{2}\left(\Delta q_{cum}\right)^{-2}\frac{1}{N_1}\sum_{i=1}^{N_1}\left(q^{\star}_{cum,i} - q_{cum,i}\left(\boldsymbol{\beta}\right)\right)^2 \\ &+ \frac{1}{2}\left(\Delta h\right)^{-2}\frac{1}{N_2}\sum_{j=1}^{N_2}\left(h^{\star}_{j} - h_{j}\left(\boldsymbol{\beta}\right)\right)^2 \\ &+ \frac{1}{2}\left(\Delta \theta\right)^{-2}\frac{1}{N_3}\sum_{k=1}^{N_3}\left(\bar{\theta}^{\star}_{k} - \frac{1}{L}\int_{h_{l,k}}^{h_{u,k}}\theta_k\left(\boldsymbol{\beta}\right)dh\right)^2 \end{aligned} \quad (3.11)$$

where $\boldsymbol{\beta}$ is the vector of parameters, q_{cum} is the cumulative outflow [cm], and Δq_{cum} its experimental error [cm], h is the pressure head in the soil [cm] and Δh is its experimental error [cm], $\bar{\theta}$ is the volumetric water content [$\mathrm{cm^3 cm^{-3}}$] measured on a sample of height L [cm] and $\Delta\theta$ its experimental error [$\mathrm{cm^3 cm^{-3}}$]. h_l and h_u are the lower and upper values of h for measurement k (Peters and Durner, 2006). N_1, N_2 and N_3 are the numbers of observations for the three types of data. The starred symbols are the observed values.

The measurement errors were calculated using the precision of the different measurement devices. Δq_{cum} was estimated to 0.015 cm, Δh to 1.4 cm and $\Delta\theta$ to 0.01 $\mathrm{cm^3 cm^{-3}}$.

Inversion algorithm

Parameters of the three models (MV, DR and DUAL) were calibrated for each MSO experiment and for each protocol (Fig. 3.3) by minimising the objective

function Φ (Eq.3.11). AMALGAM-SO (Vrugt *et al.*, 2009) is used for optimising the parameters sets. To assess the uncertainty on the optimised parameters, we also performed inversions with the DiffeRential Evolution Adaptive Metropolis (DREAM) Markov Chain Monte Carlo (MCMC) algorithm (Vrugt *et al.*, 2008b), using a logarithmic version of the objective function, in accordance to the maximum likelihood and bayesian theories. A complete description of the model and application to MSO experiments is given by Laloy *et al.* (2010).

3.2.3 Statistical analyses

The results of the experiments and the inversions are compared according to two criteria: the goodness of fit and the intra-horizon variability. In addition, numerical extrapolation experiments are conducted to analyse the behaviour of the hydraulic functions with parameters optimised from MSO experiments under different boundary conditions.

Goodness of fit

Goodness of fit for each of the three objectives in Φ (Eq. 3.11) is estimated with the adjusted root mean squared error, defined as:

$$\mathrm{RMSE} = \sqrt{\frac{\sum_{i=1}^{N} \left(y_i^\star - y_i\right)^2}{N - p}} \tag{3.12}$$

where $y^\star$ and y are the observed and the fitted data respectively. N is the number of data available for the type of data considered and p the number of optimised parameters to simulate y.

This RMSE is calculated for the different scenarios (combinations of horizon, model and protocol) with the optimum parameters sets. This performance indicator gathers at the same time the experimental errors, the model errors and the error due to the use of a certain inversion protocol. It is used in an analysis of variance with three factors (horizon, model, protocol). Multiple comparisons of the means are performed using Scheffé's method, allowing estimates of all possible contrasts among the factors levels means (Scheffe, 1952). Thanks to this analysis, the best combination of model and protocol can be assessed for each horizon.

Intra-horizon variability

The intra-horizon variability is assessed using a statistical indice R that summarizes the variation between the characteristic curves of a single horizon (Govaerts, 2009, personal communication). The R value can be calculated for each scenario (combination of horizon, model and protocol) at every value of pressure head h. For the hydraulic conductivity curve, we can write:

$$R_K(h) = \max_m \log K_m(h) - \min_m \log K_m(h) \tag{3.13}$$

where $\log K_m(h)$ is the the logarithm of the hydraulic conductivity at pressure head h, $m = 1, 2, 3$ is the replicate identifier in the horizon of interest.

R can also be integrated on a range of pressure heads, with N the number of pressure head values considered:

$$\bar{R_K} = \frac{\sum_{p=1}^{N} R_K(h_p)}{N} \tag{3.14}$$

$\bar{R_K}$ can be calculated on different ranges of pressure heads according to what part of the porosity is of interest. For example, to test the variability on macropores, one can compute $\bar{R_K}$ only for pressure head corresponding to pores of diameter larger than 0.15 mm ($h > -10$ cm). Using the same equations, we can compute the variation between cumulative outflow curves ($\bar{R_q}$) or monitored water potential curves ($\bar{R_h}$). An analysis of the variance can then be performed on the values of $\bar{R}$.

Extrapolation experiments

Extrapolation experiments are numerically simulated in order to assess the impact of hydraulic property variations at the horizon scale under different boundary conditions. An infiltration experiment is simulated with Hydrus1D on a 10 cm depth soil layer. The bottom boundary condition is free drainage. The initial conditions are set to $h = -500$ cm on the whole profile. Two scenarios of constant rainfall are applied. In scenario 1, a high flux of 0.0112 cm min^{-1} is simulated during 20 minutes. This boundary condition was chosen to activate the macroporal system included in certain models. In scenario 2, a low flux of 2×10^{-4} cm min^{-1} (2.9 mm d^{-1}) is applied during 500 minutes to observe the soil behaviour far from saturation.

The pressure head and water content profiles are observed after a cumulative infiltration of 0.5 cm and 0.05 cm for scenarios 1 and 2 respectively. We also compare the depths of the infiltration front among models and replicates. The cumulative infiltration can be expressed as: $I = \int i dt = \int \theta dz$, with i the instantaneous infiltration [LT^{-1}], t the time [T], θ the volumetric water content [-] and z the depth [L]. Provided that the front does not reach the bottom of the profile, it can also be expressed as $I = [\theta_{end} - \theta_{ini}]_{z=0} \Delta z$, as illustrated at Figure 3.4, with indexes *ini* and *end* standing for the beginning and the end of the infiltration experiment. Hence the front depth can be approximated with the following equation:

$$\Delta z = \frac{I}{[\theta_{end} - \theta_{ini}]_{z=0}} \tag{3.15}$$

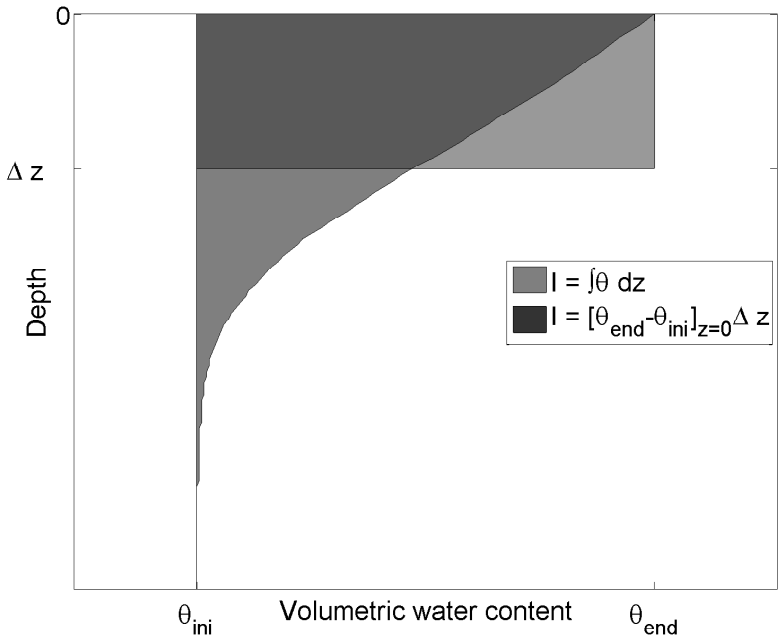

Figure 3.4: Concept of calculation of the infiltration front depth. I is the cumulative infiltration at the end of the experiment, θ is the volumetric water content, z is the depth, indexes ini and end stand for the beginning and the end of the experiment.

3.3 Results and discussion

3.3.1 Experimental results: inter-horizon differences

Figure 3.5 shows cumulative outflow and pressure head monitored during the MSO experiments. For each horizon (F, C and G), results are shown for the triplicates. Large differences in cumulative outflow occur at the beginning of the experiments, whereas pressure head time series look more similar. In order to compare intra-horizon variability of the outflow, the pressure head and the water content, we computed the variation between replicates (Eq. 3.13). For the outflow, we computed R on the water volume drained during a given step to eliminate the serial correlation of the measurements. For the pressure head, we computed R at the end of the same steps. The variation in the water content measurements is computed at each available pressure head value.

Outflow and pressure head variation between replicates (Figs. 3.6a and 3.6b) follow the same trend for the threes soils. Large outflow variation during the first step ($h = +10$ cm to $h = 0$ cm) is clearly visible here, as commonly observed in MSO experiments. As the equivalent pressure head applied at the bottom of the sample decreases (becomes more negative), the variation tends to decrease.

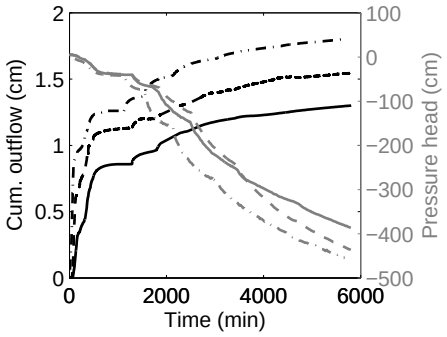

(a) Crop (C)

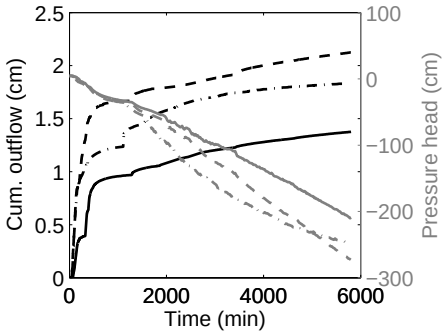

(b) Grass (G)

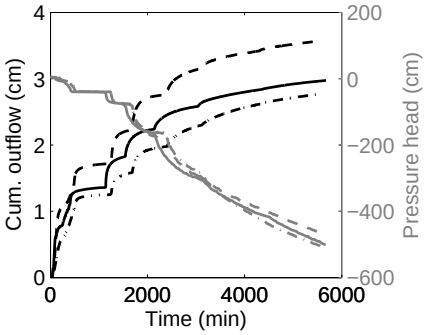

(c) Forest (F)

Figure 3.5: MSO measurements for the triplicates of each horizon. The dark grey curves (ascending) show the cumulative outflow as a function of time (left axis). The light grey curves (descending) represent the pressure head measured by tensiometers inserted in the middle of the samples as a function of time (right axis). Each triplicate is shown with a different line style.

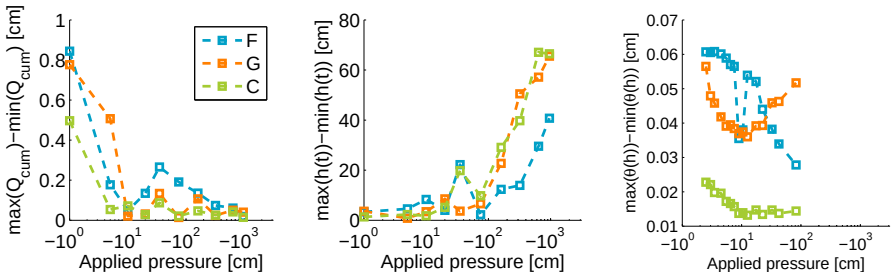

(a) Outflow accumulated between pressure steps

(b) Pressure head

(c) Water content

Figure 3.6: Observed variation in cumulative outflow, pressure head and water retention measurements at the horizon scale, for the three horizons (F: blue, G: orange, C: green), at the end of several pressure steps.

Contrary to the outflow, variations in pressure head between replicates increase with applied pressure steps. the smallest variation is here observed in the F horizon. The small differences close to saturation reflect the small time needed to reach a homogeneous static equilibrium with the applied boundary condition. As boundary pressure increases, soil matric conductivity decreases and equilibrium takes more time to be reached, outlining conductivity differences between replicates.

Regarding retention data (Fig. 3.6c), the three horizons present different behaviours. Horizon C shows a small variation on the whole explored pressure head range. For horizon F, variation decreases when the applied pressure head decreases. Horizon G presents an increasing variation at pressure heads smaller than -100 cm.

In general, variation of outflow and water content tends to decrease when the pressure head becomes more negative. This is consistent with the hypothesis that the hydraulic behaviour is the most variable close to saturation.

To compare the horizons on the whole pressure head range, we averaged the variations for all steps. We then ranked the horizons according to their variation in cumulative outflow monitored during MSO experiments and in water retention measurements. Horizons F and G show almost as much variation, with variation in F (0.19 cm / 0.04 cm^3cm^{-3}) slightly greater than in G (0.16 cm / 0.05 cm^3cm^{-3}), whereas horizon C (0.09 cm/ 0.01 cm^3cm^{-3}) shows much less.

We can conclude that horizon C is a relatively homogeneous horizon with small variation in retention curves and observed MSO dynamics. It is expected that agricultural soils will generally be more homogeneous. For horizons F and G, variation in outflow is larger close to saturation and remains slightly larger at smaller pressure heads. Retention curves are also more variable. This suggests that, in upper horizons of soils under grassland and forest, the soil may be more prone to preferential flow and is more heterogeneous than in agricultural soils.

3.3.2 Goodness of fit: protocol and model effects

An example of observed and simulated cumulative outflow and pressure head time series are presented in Figure 3.7. It shows observations of an MSO experiment realised on a sample from the forest horizon and simulations obtained with model DR with the three inversion protocols in different colours. RMSE values for the three terms of the objective function, obtained with the different models and protocols, are presented averaged by horizon in Table 3.3. Overall, fitting performance are good for cumulative outflow and pressure head. Close to saturation, simulations fit less well to the data than at smaller pressure heads (see example in Figure 3.7). Fits are less good for retention curves. Especially, the dry ends are often overestimated (for example, see Figure 3.8). This probably because the large amount of information given by the MSO in the wet range controls the fitting. Differences between RMSE are tested with ANOVA3 and multiple comparison of means ($\alpha = 0.05$). For protocol p_{10}, the best model for the three horizons is DR. For protocol p_0, DR and DUAL are almost as good and $\text{RMSE}_{q_{cum}}$ are smaller than for p_{10}. For protocol p_{-5}, the three models are equivalent. In general DR results in better fits (smaller RMSE), while DUAL and MV give less good results. A better performance of DUAL with protocol p_{10} would suggest that the soil is highly structured and that a model consider-

Table 3.3: Adjusted root mean squared errors (RMSE) averaged by horizon of the fit of Hydrus-1D simulated MSO experiments to observed data. For each horizon (C, F and G), the different terms of the objective function (cumulative outflow: q_{cum}; suction head: $h(t)$; volumetric water content: $\theta(h)$) according to different models (DR, DUAL, MV) are shown, for all protocols (p_{10}, p_0, p_{-5}).

p_{10}		DR	DUAL	MV
$q_{cum}(t)$	C	0.09	0.15	0.18
	F	0.12	0.21	0.21
	G	0.08	0.16	0.20
$h(t)$	C	12.80	22.80	24.63
	F	12.42	18.71	19.04
	G	11.55	16.36	16.16
$\theta(h)$	C	0.04	0.06	0.05
	F	0.04	0.05	0.07
	G	0.09	0.12	0.08

p_0		DR	DUAL	MV
$q_{cum}(t)$	C	0.04	0.04	0.07
	F	0.06	0.08	0.09
	G	0.06	0.05	0.11
$h(t)$	C	12.54	18.17	18.08
	F	12.38	14.51	14.50
	G	12.18	12.87	13.15
$\theta(h)$	C	0.04	0.05	0.06
	F	0.04	0.04	0.04
	G	0.09	0.09	0.09

p_{-5}		DR	DUAL	MV
$q_{cum}(t)$	C	0.03	0.02	0.03
	F	0.04	0.05	0.05
	G	0.03	0.04	0.08
$h(t)$	C	12.87	17.19	17.49
	F	12.58	13.70	13.71
	G	12.33	13.05	14.90
$\theta(h)$	C	0.04	0.04	0.06
	F	0.04	0.03	0.04
	G	0.08	0.13	0.08

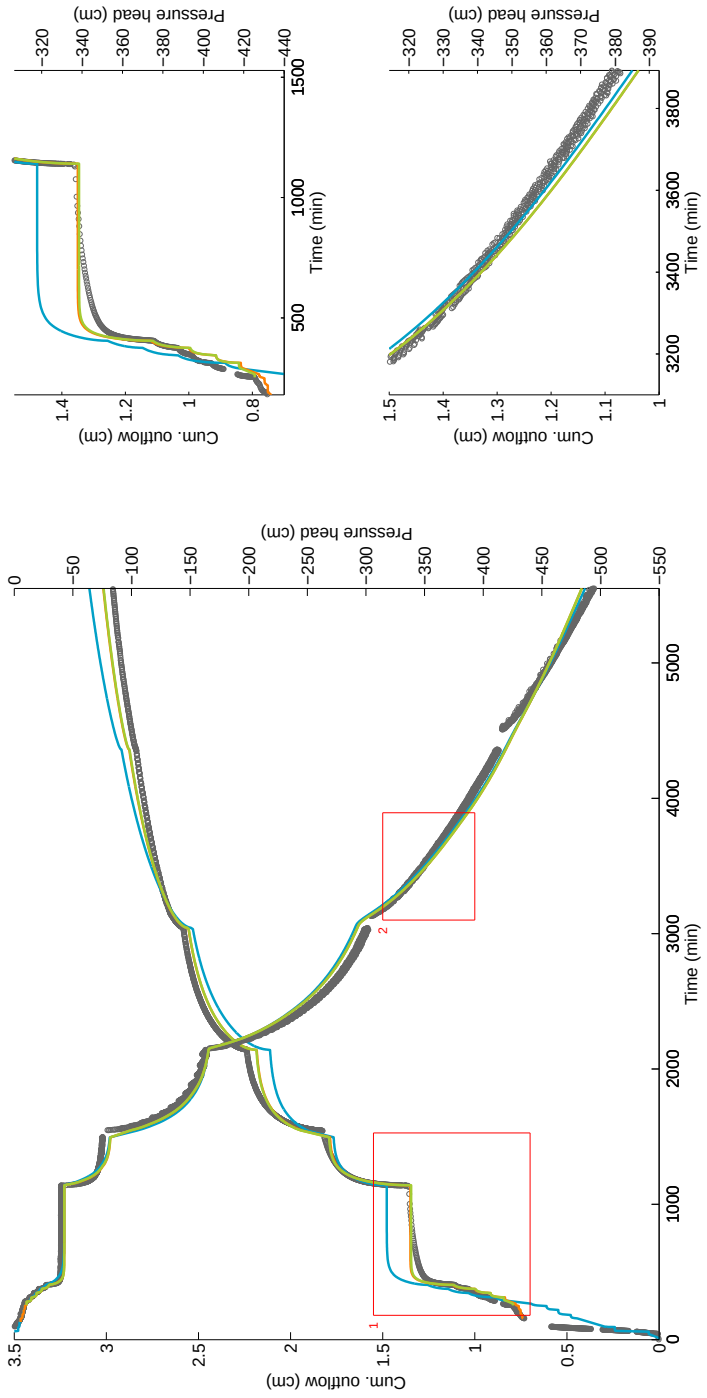

Figure 3.7: Observed (grey circles) and simulated cumulative outflow (ascending curves, left axes) and pressure head (descending curves, right axes) with the three protocols (p_{10} in blue, p_0 in orange and p_{-5} in green), for one exemplary sample of horizon F, with model DR.

ing macropores better simulates its hydraulic behaviour. This is however not the case here. On the other hand, the worse performance of model MV on the whole dataset (p_{10}) than when simulating with p_0 or p_{-5} could be an argument in favour of structured soils. If structural macropores were present, a single porosity model could not grasp the soil hydraulic behaviour provided that the MSO is sensitive to the effects of macropores (Laloy *et al.*, 2010). Improvement of RMSE through protocols is not observed with DR.

$\text{RMSE}_{q_{cum}}$ for protocol p_{10} averaged for all horizons and models (0.16) is significantly larger than for protocols p_0 (0.07) and p_{-5} (0.04). Users generally report discarding data between $h = 0$ and $h = -3$ cm. But in this case, the difference in RMSE between protocols p_0 and p_{-5} was not significant (p-value < 0.05). None of the tested models is able to reproduce the processes occurring when the water table is above the bottom of the sample (larger RMSE with p_{10}). The large flow rates observed in these conditions can be explained either by a dead volume or by the soil structure. When the soil core does not perfectly fit to the PVC tube, water can accumulate along the column wall. At the beginning of the experiment, water could also accumulate at the top of the sample if it is not properly levelled or if there is an error in the estimation of the water table level. Both extra water storage should mainly affect the first steps of the experiment when the water level is above the bottom of the soil column. However, Laloy *et al.* (2010) highlighted the risk of using a single permeability model when discarding data from the first steps. Indeed, not considering the macropores and their interaction with the soil matrix may lead to an underestimation of the matrix pressure head. Another potential source of large flow rates under protocol p_{10} would be continuous structural macropores. These could cause rapid flow that may not be modelled by a single-porosity model. From Table 3.3, we see that for a given horizon, the decrease in RMSE for model DR from protocols p_{10} through p_{-5} is less than for the two other models, suggesting that this model is not as strongly affected by the protocol. Surprisingly, DUAL did not show significantly smaller RMSE even if it should be able to reproduce rapid flow in part of the domain (in macorpores or artefacts from the experimental set-up).

Protocol p_0 and model DR produce the best fits for the three horizons. As experimental artefacts canot be discrimintaed from real macropores, results obtained with protocol p_0 will be more thoroughly studied in the rest of the text.

3.3.3 Comparison of optimised hydraulic curves

Moisture retention curves obtained with protocol p_0 for each horizon and each model are shown in Figure 3.8. Visually confirming results from Table 3.3, we observe that fits are the worse for horizon G. For horizon C, they are bad mostly in the dry end. Fits for horizon F are relatively good. The poor quality of the fit highlights the difficulty of optimising both the HCC and the MRC. However, it is important to note that moisture retention measurements were not performed on the samples used for the MSO measurements, but on small (100 cm^3) soil cores taken in the same horizons.

Hydraulic conductivity curves (HCC) of each horizon and each model obtained with protocol p_0 are presented in Figure 3.9. For each combination, the triplicates are shown. For a given model, the curves shapes are generally comparable. They are the most similar for MV and the most different for DUAL. The effect of horizon, model and protocol can be assessed using MANOVA1, with conductivity at several pressure head values (-1; -3; -10; -30; -100; -300 cm) as input variables. Horizons cropland (C) and grassland (G) have $K(h)$ curves different from horizon forest (F), considering all models and protocols. Comparing the $K(h)$ curves for the different models, it appears that the ones modelled with DR are significantly different from those modelled with MV

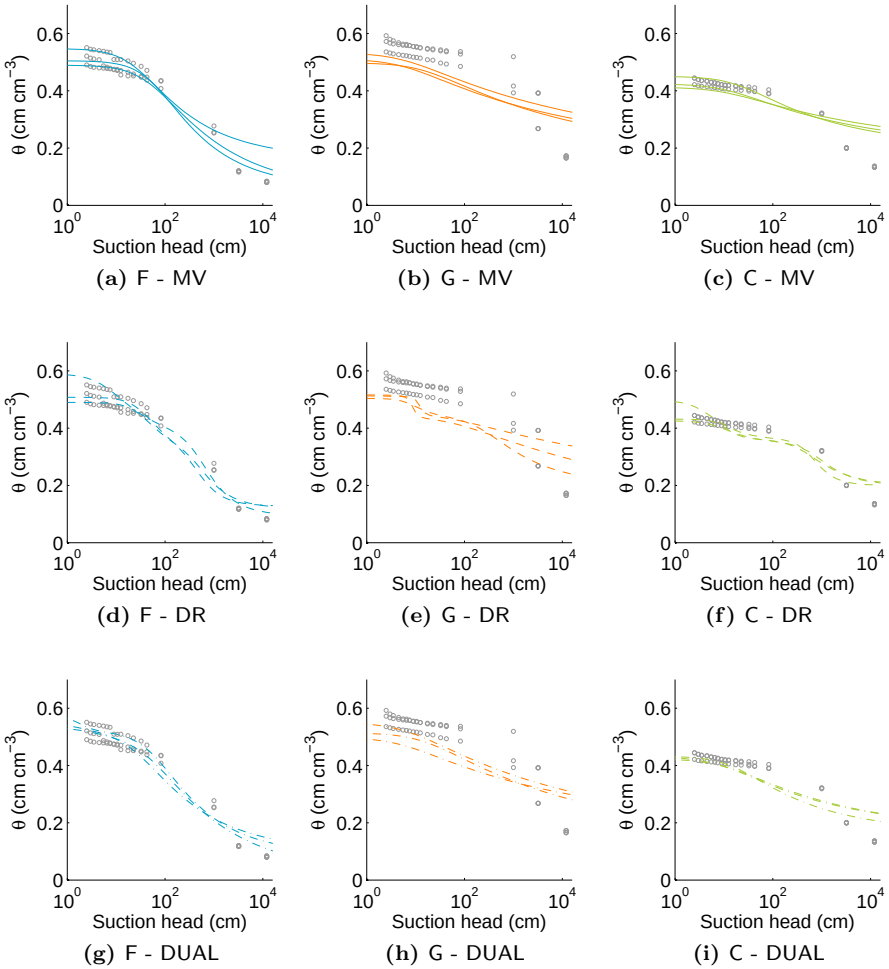

Figure 3.8: Moisture retention curves obtained from inversion of MSO experiments for the triplicates of each horizon (F, G, C) with three models (MV, DR, DUAL), using unsaturated experimental data (protocol p_0)

and DUAL (p-values are <0.01 and 0.03, considering all horizons and all protocols). When looking at the effect of the protocol, we observe that the curves obtained with p_{10} are different from those obtained with p_0 and p_{-5} (p-values are 0.02 and 0.34). It is expected that the replicates will show a comparable $K(h)$ curve far from saturation but could diverge close to saturation due to structural features, if any.

We tested this hypothesis by comparing the similarity between HCC of a single horizon along the explored pressure head range, using $\bar{R}$ index (Eq. 3.14). We hence divided the pressure head range into three pressure head classes corresponding to the macro-, the meso-, and the micro-porosity. The macropores

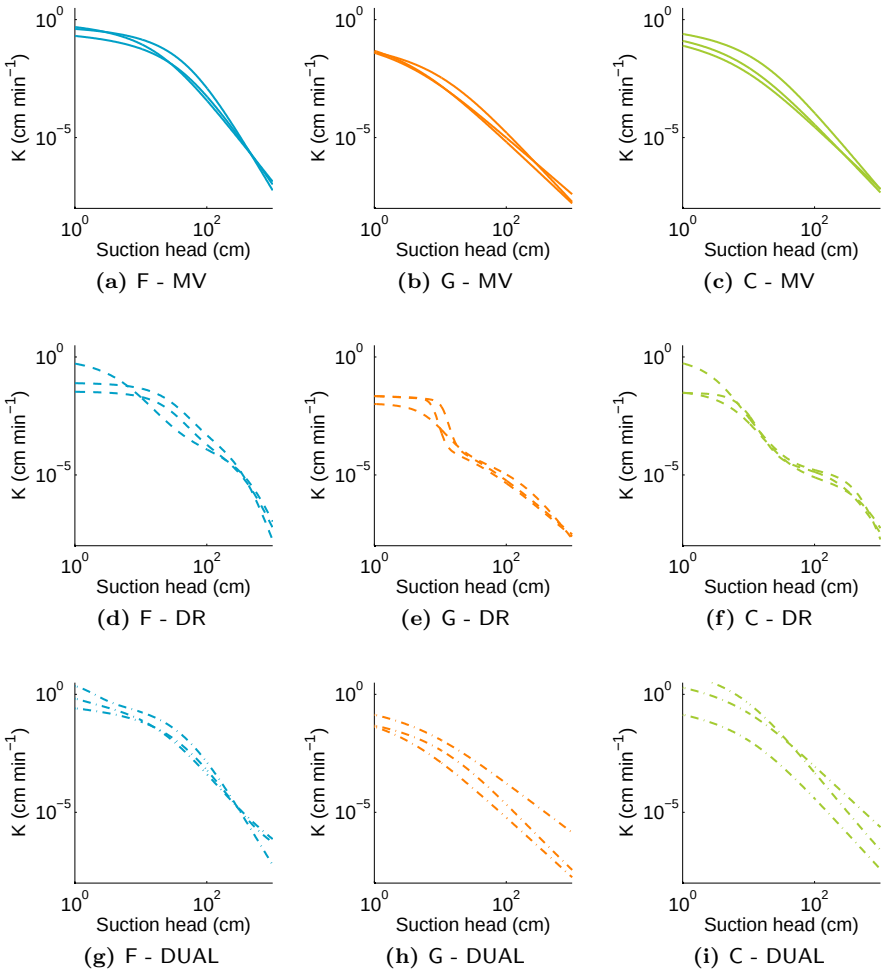

Figure 3.9: Hydraulic conductivity curves obtained from inversion of MSO experiments for the triplicates of each horizon (F, G, C) with three models (MV, DR, DUAL), using unsaturated experimental data (protocol p_0)

Table 3.4: $\bar{R}$ values of the conductivity curves for three categories of pores (Macropores: diameter $\geq$ 0.3 mm; Mesopores: 0.3 mm $>$ diameter $\geq$ 30μm; Micropores: diameter $<$ 30μm), for three models (DR, DUAL, MV) and three horizons, using protocol p_0

		Macro	Meso	Micro
C	DR	1.1669	0.4584	0.7480
	DUAL	3.5260	3.1809	3.6127
	MV	1.5800	1.7164	0.7860
F	DR	1.8161	1.8824	0.8642
	DUAL	1.2747	1.1991	0.9591
	MV	0.9753	1.1119	0.6114
G	DR	1.1127	0.9792	0.6924
	DUAL	2.2012	2.7837	3.8633
	MV	0.7246	0.9858	0.7639

are pores greater than 0.3 mm, corresponding to pressure heads greater than -10 cm (Jarvis, 2007). The micropores have diameters smaller than 30μm, corresponding to pressure heads smaller than -100 cm. The mesopores are the pores between those first two categories. Values of $\bar{R_K}$ calculated for protocol p_0, for the three pore categories are presented in Table 3.4. For DR, variation tends to be the largest in the macroporosity and the smallest in the microporosity. The use of DR gives the possibility of a large variability between replicates close to saturation, where the largest pores influence the hydraulic behaviour, but it tends to bring the hydraulic curves closer to each other when only the micropores are at work. For model MV, $\bar{R_K}$ values tend to be the greatest in the mesoporosity. This is due to differences in the values of parameter α. For DUAL, $\bar{R_K}$ values are large relatively to the other models in the three pore categories. The large $\bar{R_K}$ values observed for DUAL in the pressure head range corresponding to micropores is probably an evidence that this model is not capable of apprehending the hydraulic behaviour of the three studied horizons in a robust way. It can also be the consequence of using an over-parametrised model that is too sensitive to the discrepancies between replicates. However, since the fitting performances of DUAL were not better than for the other models, this result could be explained by the relatively poor convergence rate of Hydrus 1D with this formulation of the soil hydraulic characteristic curves. On the opposite, MV cancels the variability between replicates. It shows a bit larger variability in the middle range. The smaller number of degrees of freedom of this model as compared to DR and DUAL leads to a decrease of the intra-horizon variability. This could indicate that this simpler model is capable of characterising the common behaviour of each horizon in an "effective way". It is however likely that this model will fail to properly simulate the soil hydraulic behaviour close to saturation.

Figure 3.10 shows 95 % confidence intervals to MRC and HCC obtained from inversions of MSO experiments with DREAM algorithm. They illustrate the uncertainty of the parameters compared to the spatial variability (replicates) for each model (MV, DR, DUAL) and horizon (F, G, C). The uncertainty of

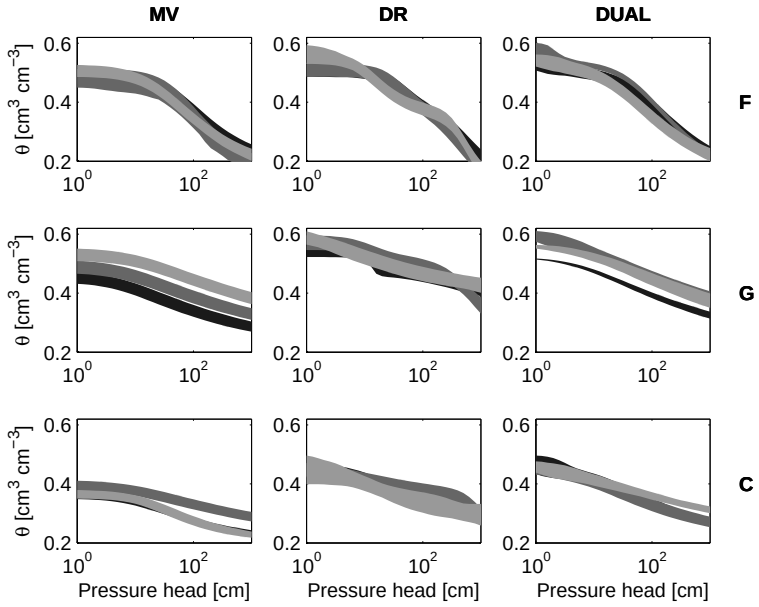

(a) Moisture retention curves

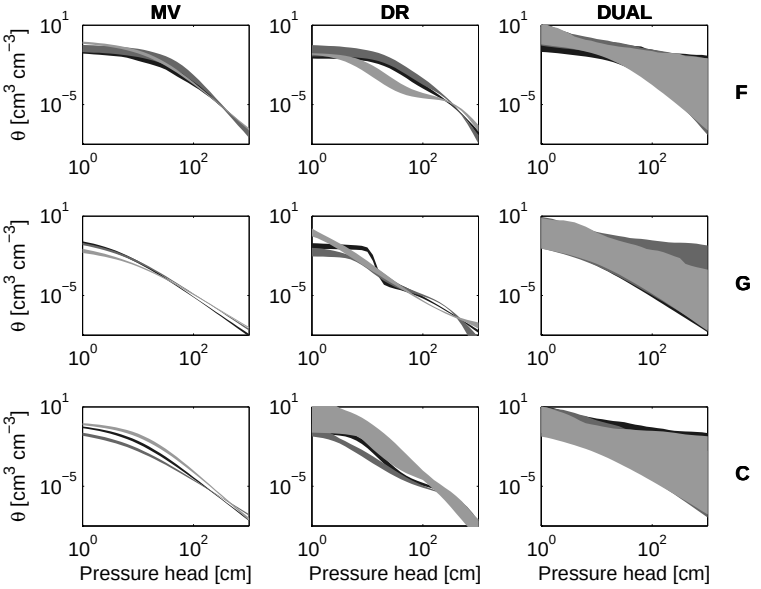

(b) Hydraulic conductivity curves

Figure 3.10: 95 % confidence intervals on hydraulic curves obtained from inversions of MSO experiments with DREAM algorithm and protocol p_0. Replicates are shown in different levels of grey.

the parameters, which depends on the experimental and model error, does generally not completely encompass the spatial variability. For MV and DR, the uncertainty of the parameters is larger for MRC than for HCC. For DUAL, it is the contrary. Interestingly, we observe an increasing uncertainty of HCC for increasingly complex models, i.e. when a larger number of parameters have to be optimised. Even if the fitting performances of DR are the best, they do not necessarily lead to the smallest parameters uncertainty.

3.3.4 Extrapolation experiments

Figure 3.11 shows boxplots of the infiltration front depth, Δz (Eq. 3.15), obtained by simulating a 0.0112 cm min^{-1} infiltration rate on an initially dry soil ($h = -500$ cm) and observed after 5 mm of cumulative infiltration. The three models are used, with 2500 parameters sets from the posterior parameters distribution obtained with DREAM for each replicate of each horizon with protocol p_0. With MV, the three replicates of each horizon show very few variation. The distributions of the front depth are very narrow (even if there are a lot of outliers, mostly in horizon F) and the medians are similar. Hence, using MV, the uncertainty and the spatial variability are small, even if the fitting of the model is not the best. With DR, there is a slightly larger uncertainty, but also a much larger spatial heterogeneity. Indeed, the median values of Δz are very different between the three replicates, especially in horizon G. With DUAL, the uncertainty is larger than with the other two models and the differences between the replicates are smaller than with DR, but still larger than with MV. This is partly due to the poor convergence rate of Hydrus 1D with this model. This is also due to the large number of parameters optimised for DUAL and to the existence of correlations between them.These observations are in accordance with what could have been expected from the confidence intervals of the hydraulic curves shown in Figure 3.10. From the point of view of the replicates, in horizons F and G, MV and DR agree on the predictions, while DR produces different results. In horizon C, the agreement between the models is less good, mostly for replicate A. The uncertainty brought by the models is hence large. To assess whether it is larger than the spatial variability, estimations of the standard deviation of the different distributions can be compared. Table 3.5 gives the estimated standard deviations of Δz calculated on the distributions merged either for the three replicates of each horizon (first three columns), or for the three models (last three columns). It shows that MV, which produced the poorer fits, is less affected by the spatial variability than DR and DUAL. On the contrary, DR, which showed the best fits, is the most affected by the spatial variability. Table 3.5 also shows that the variability observed when merging the three models tends to be larger than the spatial variability, except for samples from horizon G modelled with DR and from horizon C modelled with DUAL which have particularly large values of $\sigma_{(\text{merged replicates})}$. This suggests that the choice of the model is more important than the replication of samples.

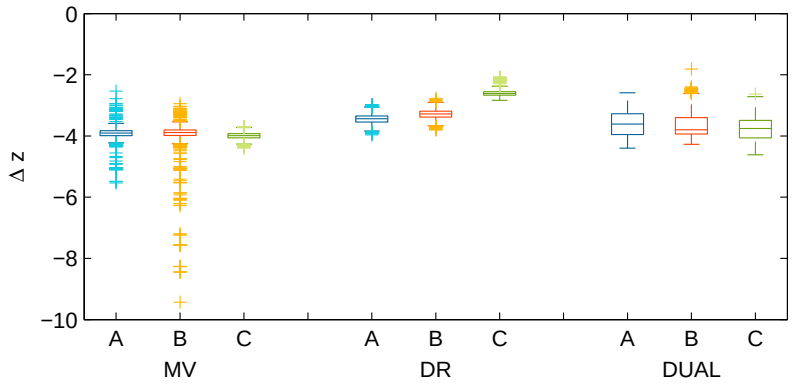

(a) F

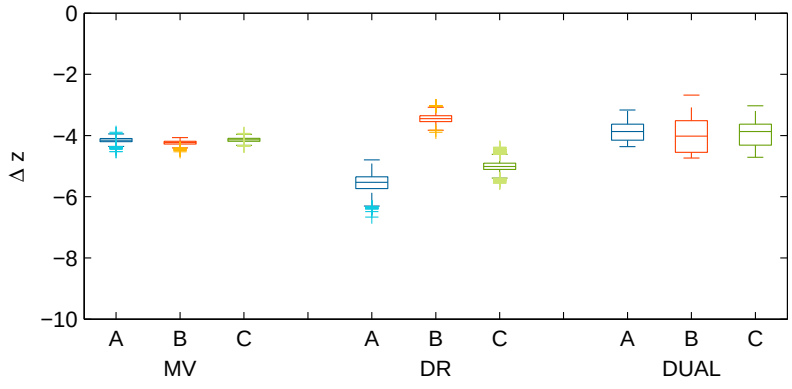

(b) G

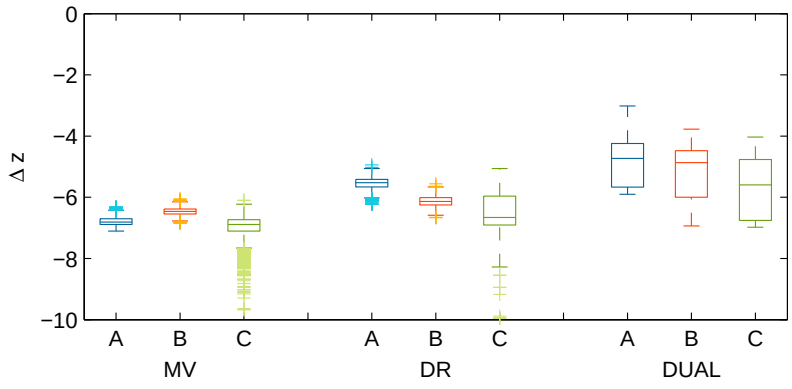

(c) C

Figure 3.11: Boxplots of the infiltration front depth (Δz) simulated with 2500 parameters sets from the posterior distribution obtained with DREAM algorithm for each horizon (subfigures a, b and c), each model (MV, DR, DUAL) and each replicate (A, B, C).

Table 3.5: Estimated standard deviations of distributions of infiltration front depths Δz, merged according to the replicates and to the models. Units are in cm and the maximum infiltration depth is 10 cm.

	$\sigma_{\text{(merged replicates)}}$			$\sigma_{\text{(merged models)}}$		
	MV	DR	DUAL	A	B	C
F	0.2722	0.3975	0.3798	0.3241	0.4318	0.6654
G	0.0831	0.9139	0.4156	0.7684	0.4601	0.5224
C	0.3320	0.5060	0.9270	0.8965	0.7411	0.9438

3.4 Conclusion

In this study we wanted to answer three questions relative to the use of multistep outflow (MSO) experiment to characterise the hydraulic behaviour of structured soils.

First, the best combination of model and inversion protocol was assessed. From the analysis of the RMSE values for all considered scenarios, it appears that Durner (1994) bimodal model (Eq. 3.3, 3.4) (DR) is the most appropriate in this case. Given the good results obtained with the DR for all three protocols, the setup seems suitable to determine the hydraulic properties of soil considering its structure, that implies fast flow close to saturation. We would have expected the Gerke and van Genuchten (1993a) dual porosity model (Eq. 3.5, 3.6) (DUAL) model to confirm these findings, but its performance with protocol p_{10} was not as good as with DR. However, we made strong restrictions on the DUAL parametrisation: we fixed the transfer between the two pore system Γ_w to a very small value by fixing K_w to K_m and β to 10^{-20}. This impeded the model flexibility. Also, the convergence rate of DUAL with Hydrus 1D was very small. This may have interfered with the minimum search. Even with flexible models, a consequence of a nice fit of the wet end of the retention curve is a poorer fit of the dry end, with water content at retention often hitting its upper boundary. This is either due to a wrong or too flexible model or to a lack of data in the dry range. Regarding the protocol, starting the experiment with a saturated sample, it is better to let it drain and begin modelling only after the water table reaches the bottom of the sample (protocol p_0).

The second objective was to identify the main source(s) of uncertainty in the hydraulic conductivity obtained with simulated MSO experiments. Using DiffeRential Evolution Adaptive Metropolis (DREAM) algorithm, the predictive uncertainty could be assessed. This analysis confirmed Laloy *et al.* (2010) observation that good fitting performances are not necessarily associated with small uncertainty on the parameters. To separate the effects of the model and the spatial variability, we compared the variation in the measurements. between the three sampled horizons. We assessed this variation with a summarising value $\bar{R}$, comparable between horizons and different simulation scenarios. We found that samples originating from the horizon under crop (C) had a more homogeneous hydraulic behaviour than the ones coming from a soil under for-

est (F) or grassland (G).
In addition, using the parameters optimised from MSO experiments in a numerical infiltration experiment, we showed that the choice of the model has more impact on the results than the spatial variability at the horizon scale. The choice of the model is hence not neutral. As a consequence, it would be interesting to have access to secondary information that could help the user to choose the most appropriate model given the characteristics of the soil at hand. This analysis also showed that samples originating from different land covers showed distinct behaviours. We could therefore enlarge this study to a larger database to explore the effect of land cover on the hydraulic properties. Finally, we would encourage researchers to focus on the choice of the models rather than on the replication of samples (and experiments).

Chapter 4

Impact of land cover and horizon depth on hydraulic properties of silt loam soils*

4.1 Introduction

Historically, pedotransfer functions (PTF) have been mainly developped for cropped soils in agricultural areas (Vereecken *et al.*, 2010). For managing forests or grasslands for instance, it is of interest to know whether PTF apply as well under other land covers. However, soil structure can be quite different under different land covers because of different amounts and pools of organic matter in the upper horizon, because of the tillage practices and also due to very different types of roots. In combination with the textural and chemical properties of the soil particles, land cover may therefore deeply affect close to saturation soil hydraulic properties. Land cover could be incorporated into current PTF to improve their predictions, particularly close to saturation.

Loess and loess-like deposits cover 10% of the Earth's surface and bear some of its most productive soils (Smalley *et al.*, 2001). In Europe, a belt of loess extends from Brittany (France) to Ukraine and Russia (Haase *et al.*, 2007). Typical loess is a clastic sediment of aeolian origin and consists mainly of silt (with a mode in the coarse silt). Loamy and silty soils are widely used for agricultural purposes, because of their high fertility due to their large available water and cation exchange capacity (CEC). Their texture makes them easy to till. Besides, their clay content allows for structuration of the particles, which potentially generates large pores. As their textural properties are quite homogeneous, the loess derived soils are good candidates to test the effect of structuring features on hydraulic properties.

*Adapted from Weynants, M. and Javaux, M. (in preparation). Impact of land cover and horizon depth on close to saturation hydraulic properties of silt loam soils, *To be submitted to European Journal of Soil Science*

When studying the unsaturated hydraulic conductivity of such soils, it may occur that their behaviour can not be entirely explained by classical predictors such as texture, bulk density or organic carbon content. Other factors structure the soil and affect its behaviour close to saturation. The question that arises is how to characterise and use them as model inputs. In this study, we rely on the hypothesis that land cover controls the root architecture, the soil microfauna and to some extent the land management. The presence of structure features also vary in depth. They are generally more present in the surface horizons than in the subsoil. Horizon position in the profile has already been used as PTF input (Wösten *et al.*, 1999). We therefore want to investigate the use of the land cover and horizon position as indicators of soil structure.

We focus our study on the wet part of moisture retention curves (MRC) and hydraulic conductivity curves (HCC) of Luvisols, particularly on horizons with texture classified as silt loam. This preoccupation comes from the conclusion of a previous study (Chapter 1, published byWeynants *et al.* (2009)) in which a difference is made between K_0 and K_{sat}, the former being the fitted hydraulic conductivity at zero potential, the latter being the actual saturated hydraulic conductivity. An arbitrary upper limit of potential $h = -6$ cm was used as the limit of unsaturated conductivity data used to fit the Mualem-van Genuchten model (Mualem, 1976; van Genuchten, 1980). This limit was chosen according to Jarvis (2007). But its physical meaning was not tested on the available data. It would hence be worth to confront the hypothesis of $h_0 = -6$ cm against real retention and conductivity data close to saturation.

The objective of this study is to investigate whether the macroporosity and the structure observed in silt loam horizons of Luvisols are only due to their texture or whether the land cover has an influence on their development. For this purpose, we create a database of Luvisols, with high resolution moisture retention and hydraulic conductivity measurements in the wet range. We then analyse the potential links between, on the one hand, the texture, the horizon position in the profile and the land cover and, on the other hand, hydraulic properties.

4.2 Materials and methods

4.2.1 Field sampling and pedological measurements

The sampling zone is located near Louvain-la-Neuve (Belgium), in the loess belt. The climate is maritime temperate, with precipitations uniformely distributed all year long (760 mm/yr). The effect of soil structure on hydraulic properties of silt loam soils is investigated on the basis of a new database. We selected eleven sampling locations under different land covers. The profiles were all chosen for their relatively homogeneous texture. They are all developed in an eolian loess deposited on a sand bedrock. The depth of the loess deposit is very variable and, for some profiles, the sand bedrock is quite shallow. The soil profiles were described and laboratory measurements were made on samples taken in each horizon.

At each location, we dug out 1.2 m deep pits for describing the soil profiles. One face was flattened for describing the soil profile horizons. We followed the guidelines suggested by the FAO (2006). The following general characteristic features were collected: date, author, location, weather conditions, land use, history, topography, drainage class, parent material, bedrock, rock fragments. For each horizon, we also characterised its delimitation, colour, distinctness, topography, texture, structure (grade, type, size), roots (abundance, size), pores (type, abundance, size).

We extracted several undisturbed soil samples in all horizons. We first collected two or three samples contained in PVC cylinders (height: 10 cm, diameter: 11.25 cm) for subsequent multistep outflow (MSO) experiments. The cylinders were pushed into the soil thanks to a steel cylinder with a cutting edge placed under the PVC tube, and another one placed above on which we hit with a heavy hammer. The cylinder was cautiously maintained vertical during the operation. In addition, smaller samples were taken using 100 cm^3 steel rings (Kopecki) for moisture retention curve and other laboratory measurements.

Soil texture analysis was performed on 10 grams subsamples. Organic matter and peds were destroyed before the soil was sieved and settled in a $(NaPO_3)_6$ solution, used as dispersing agent. Four textural classes were characterised: sand (50-2000 μm), coarse silt (20-50 μm), fine silt (2-20 μm) and clay ($< 2\mu$m). pH, carbon and nitrogen contents were also measured.
For the sake of clarity, each profile will be referred to by three or four uppercase letters and one number. The letters represent the broad location of the profile (LAU = Bois de Lauzelle; MAR = Centre Alphonse de Marbaix (P = prairie, C = culture); GEN = Gentinnes; LLN = Louvain-la-Neuve; MSG: Mont-Saint-Guibert; SMG = Sart-Messire-Guillaume). The number identifies the profile in the area. In addition, a letter in parentheses gives the land cover at the sampling location: forest (F), grassland (G) and cropland (C).

4.2.2 Soil hydraulic properties

Multistep outflow (MSO) experiments were carried out on undisturbed samples 10 cm high and 11.25 cm in diameter. Experiments combined the suction and the pressure modes of the MSO device described in detail in Chapter 2). We applied low suctions (+10 to −80 cm of water column) during short periods of time (from one to eight hours) and then longer higher pressure steps (equivalent to −160 to −960 cm). The protocol was slightly modified from one experiment to another resulting in small discrepancies in the number of suction steps and their duration. Mini tensiometers (EcoTech, Bonn, Germany) were horizontally inserted at 5 cm depth. The outflow, the applied pressure and the suction inside the samples were monitored during the experiments. The water content at the end of the experiments was measured by gravimetric method. Finally, 74 experiments produced usable results. For some experiments, the tensiometers failed to produce reliable data. In that case pressure head measurements have been partly or entirely removed from the final database.

Prior to MSO experiments, saturated hydraulic conductivity was measured with a constant head method. Saturated samples placed atop porous plates in hermetic cells were subjected to a constant head with a Mariotte's bottle. The

cumulative outflow was measured during two minutes. The test was repeated three times and the measurements were averaged. Saturated conductivity was calculated from Darcy's law.

MRC were measured on 100 cm^3 with sand-box apparatus and pressure chamber methods. From 0 to −70 cm of pressure head, we used the sand-box apparatus with undisturbed 100 cm^3 soil samples contained in steel rings (Kopecki). A fine suction-wise resolution was applied close to saturation (0, −0.5, −1, −2, −3, −4, −5, −6.5, −8, −10, −15, −20, −30, −40, −80 cm). The rings were then placed in a low pressure chamber for measurements at 0.3 and 1 bar (−300 and −1000 cm). Unfortunately, these measurements were not reliable for all samples due to failure of the pressure regulation system. The samples were then destroyed for measurements at 3 and 12 bar (−3000 and −12000 cm) in high pressure chambers. Bulk density was measured after drying the samples during at least 48 hours at 105 °C.

4.2.3 Macroporosity indicators

We selected three indicators of the presence of macropores. First w_{pF0}, the gravimetric water content at $h = -1$ cm (pF 0). Unlike the volumetric water content, θ, the gravimetric water content, w, of soils with macropores should be strictly smaller than for soils without macropores. Indeed in terms of θ, a large saturated w could be compensated by a smaller bulk density. The second indicator is $(\theta_{pF0} - \theta_{pF1})/\theta_{pF0}$, the loss of water content between pF 0 and pF 1, relative to the water content at pF 0. The third indicator is simply the soil bulk density, ρ_b [g cm^{-3}]. Since we work with soils having the same texture, ρ_b is expected to be directly related with soil structure.

4.2.4 Statistical analysis

All analyses presented here were performed on horizons for which a silt content greater than 50 % was observed, so that the effect of texture on the variability of hydraulic properties was limited. All analyses were performed with Matlab® - Statistical Toolbox. Boxplots are widely used in the results section. The box represents the interquartile, with the median shown inside the box, and the whiskers extent to a 95 % confidence interval of the distribution of the data. Outliers are represented with crosses.

Equality of variances between groups (for example, land covers or horizon position in the profile) is tested with the Levene's test, which is indicated when samples distributions are not normal and are prone to outliers (Levene, 1960).

$$W = \frac{(N-k)}{(k-1)} \frac{\sum_{i=1}^{k} N_i \left(Z_{i.} - Z_{..}\right)^2}{\sum_{i=1}^{k} \sum j = 1^{N_i} \left(Z_{ij} - Z_{i.}\right)^2} \tag{4.1}$$

where, W is the test statistics, k is the number of groups, N is the total number of samples, N_i is the number of samples in the ith group, $Z_{ij} = \left|Y_{ij} - \widetilde{Y}_i\right|$, Y_{ij} is the value of the jth sample from the ith group, $\widetilde{Y}_i$ is the mean of the ith group, $Z_{..} = \frac{1}{N} \sum_{i=1}^{k} \sum_{j=1}^{N_i} Z_{ij}$ is the mean of all Z_{ij} and $Z_{i.} = \frac{1}{N_i} \sum_{j=1}^{N_i} Z_{ij}$

is the mean of the Z_{ij} for group i. The significance of W is tested against $F(\alpha, k-1, N-k)$ where F is a quantile of the F test distribution, with $k-1$ and $N-k$ its degrees of freedom, and α is the chosen level of significance (0.05). The null hypothesis of equality of the variance is rejected when the p-value is smaller than α ($W > F(\alpha, k-1, N-k)$).

Analysis of the variance (ANOVA) tests the null hypothesis that all samples are taken from the same distribution (equality of the means between groups). It relies on the hypotheses of independence of cases, normality and homoscedasticity (homogeneity of the variances between the different groups). It is based on the partitioning of the total sum of squares into the sum of squares of the errors and the sum of squares of the factors. The F-test is used to compare the variance between groups to the variance within groups.

When the null hypothesis of equality of the means is rejected, one may want to perform comparisons of the means, to find which groups have different means from one another. In this study, we use Matlab function multcompare that compares population marginal means using Tukey-Kramer or Scheffé's methods (Tukey, 1953; Scheffe, 1952).

4.2.5 Soil hydraulic models

For the sake of brevity, we do not repeat the hydraulic functions equations already exposed in previous chapters. Moisture retention curves (MRC) have been modelled with the following parameterisations: different forms of the van Genuchten model (1980), Brooks and Corey (1964), Kosugi (1996), Ippisch *et al.* (2006), all of them unimodal models (Equations can be found in Table 1.2), and two bimodal models: Durner (1994) (Eq. 3.3) and Dexter *et al.* (2008a), which writes:

$$w = A_1 \exp(-h/h_1) + A_2 \exp(-h/h_2) + C \tag{4.2}$$

where w is the gravimetric water content [g g^{-1}], h the suction head [cm], A_1, h_1, A_2, h_2 and C are fitting parameters, with $h_1 > h_2$. When plotting MRC as a function of $\log(h)$, inflection points are observed. For the bimodal models, they occur at suction heads $h_{i,\mathsf{DR}} = \alpha_i^{-1} m^{-1/n_i}$ for Durner (1994) bimodal model (Eq. 3.3, 3.4) (DR) and $h_{i,\mathsf{DX}} = h_i$ for Dexter *et al.* (2008a) model (Eq. 4.2) (DX). HCC have been modelled with Mualem-van Genuchten (van Genuchten, 1980) model (Eq. 3.1, 3.2) (MV) and DR models. The MSO experiments have been simulated with HYDRUS 1D (Simunek *et al.*, 2005). The soil is modelled with 50 nodes, logarithmically distributed so that the resolution is finer at the bottom, where large gradients of pressure head are expected. To take into account the effect of the porous plate on the outflow, the former has to be explicitly modelled. Its hydraulic properties are to be set so that it never desaturates during the MSO experiment. A first attempt consisted in modelling the plate using only the last node, setting its saturated hydraulic conductivity to 0.00053 cm min^{-1}. However, as this is not physically sound, in a second attempt, it was modelled on the two last nodes, with its hydraulic conductivity set to the measured value of 2.46×10^{-5} cm min^{-1}, for a 0.025 cm height. For further details, see chapter 3.

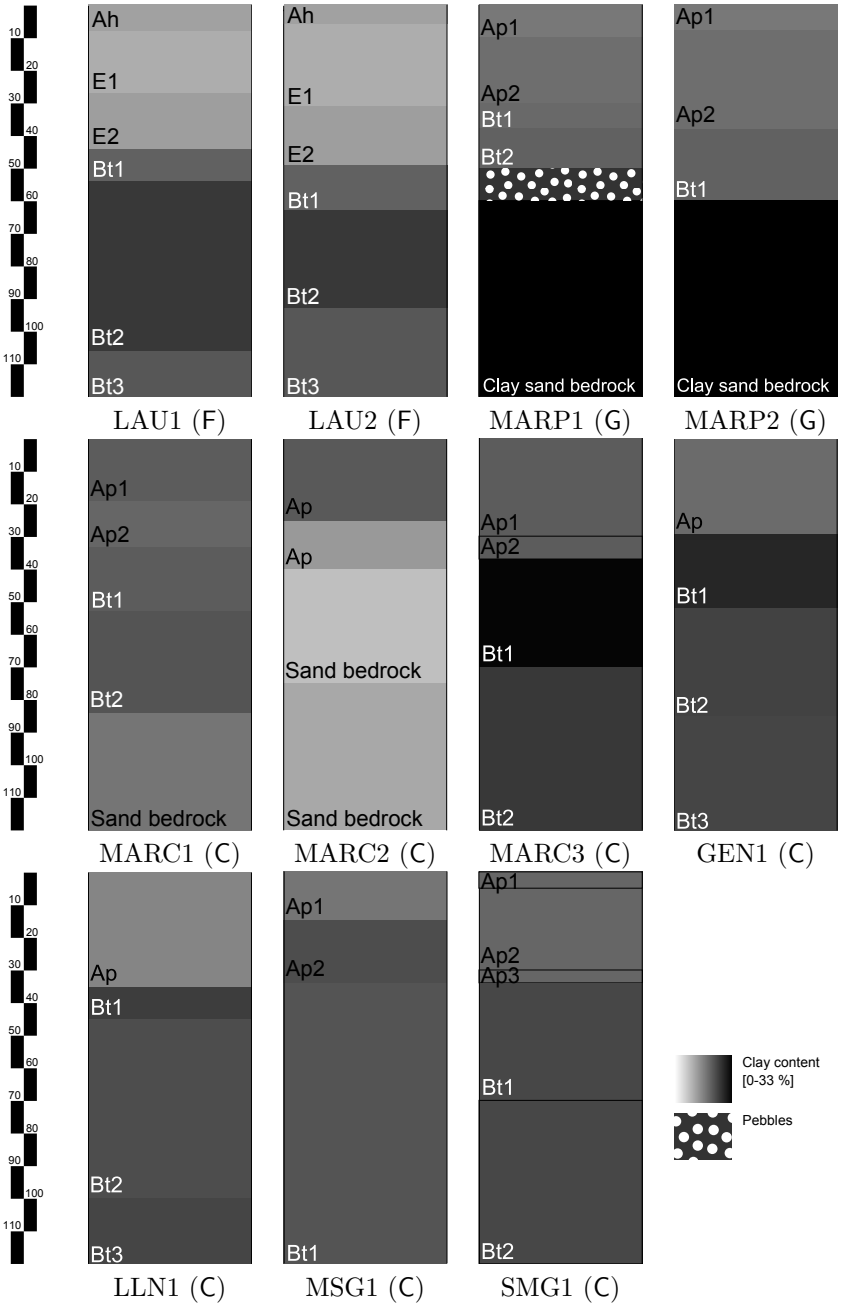

Figure 4.1: Illustration of the sampled soil profiles. All horizons thicker than 8 cm were sampled.

4.2.6 Inverse modelling

We fitted the different hydraulic models both on moisture retention measurements alone and, for MV and DR, on MSO and moisture measurements to obtain parameters representative for our samples. For the MRC, we fitted the models using Matlab lsqnonlin function, which is based on a Levenberg-Marquardt local minimum search. We used AMALGAM-SO global algorithm (Vrugt *et al.*, 2009) to inverse the MSO experiments and retrieve the parameters of the HCC and MRC. Protocol p_0 (Initial conditions: $z = 0$, $h = -10$ cm; $z = -10$ cm, $h = 0$ cm, see Chapter 3 for details) has been used for all inversions. The objective function is the sum of three sub-objectives. Each sub-objective is evaluated according to the log-likelihood theory. The global objective function is written as:

$$\Phi = \left(\sum_{j=1}^{3} \frac{1}{\sigma_j^2} \frac{\sum_{i=1}^{N_j} (y_i - \hat{y}_i)^2}{N_j} \right) \tag{4.3}$$

with y_i the observation and $\hat{y}_i$ its estimation. For each objective j there are N_j observations. Each objective is weighted by the inverse of the variance of its measurements errors σ_j^2.

4.3 Results

4.3.1 Database

The database contains three types of information: (i) *in situ* profile descriptions and horizon properties, (ii) MRC measurements and (iii) MSO measurements. Not all data are available for all entries. Typically, MSO measurements lack for the first sampled profiles, because of technical problems with the device. This section gives an overview of the database, according to each type of information.

Profile description and pedological data

Figure 4.1 illustrates the profile descriptions of the eleven soil profiles. Measurements were conducted in 2008 and 2009. Appendix B gives a description of each location, together with profile main features. Two profiles were excavated under beech forest and two under permanent grassland. Among the seven remaining profiles, located in croplands, there are various agricultural practices. Profile SMG1 was not tilled for the last 25 years. Profile GEN1 was recently worked with no tillage practices. The other profiles undergo traditional management. For sake of clarity land covers will be referred to in the text by upper letters : G for grassland, F for forest and C for cropland. Only samples with a silt content greater than 50% were kept for the subsequent analyses. Figure 4.2 shows the soil horizons on the USDA soil texture triangle. Colours refer to land cover (F, G, C). In the background, the silt loam samples (also extracted from the Belgian loess belt) from Harry Vereecken's database (1988) are given for comparison. Table 4.1 gives the minimum, median and maximum values of the soil particles classes, as well as of the organic carbon content and bulk density. We also included the median values of the previous attributes for each

Table 4.1: Minimum, median and maximum values of sand, silt, clay, organic carbon contents (%) and bulk density (g cm ^{3}) in the database.

	%Sa	%Si	%Cl	%OC	BD
min	0.51	50.24	10.70	0.00	0.79
median	11.06	68.03	21.53	0.29	1.48
max	28.63	76.41	32.53	6.28	1.64

Table 4.2: Median values of sand (%Sa), silt (%Si), clay(%Cl), organic carbon (%OC) contents and bulk density (BD) in the database, for the different land covers (F, G, C) and horizon positions (top, sub). n is the number of samples in each group.

	%Sa	%Si	%Cl	%OC	BD	n
F top	18.81	68.96	12.88	5.48	0.84	7
F sub	14.46	67.43	18.12	0.22	1.38	31
G top	12.05	68.41	18.97	1.16	1.52	11
G sub	8.53	68.03	23.95	0.42	1.51	12
C top	11.06	70.52	19.51	0.70	1.48	19
C sub	6.87	67.09	24.40	0.07	1.54	33

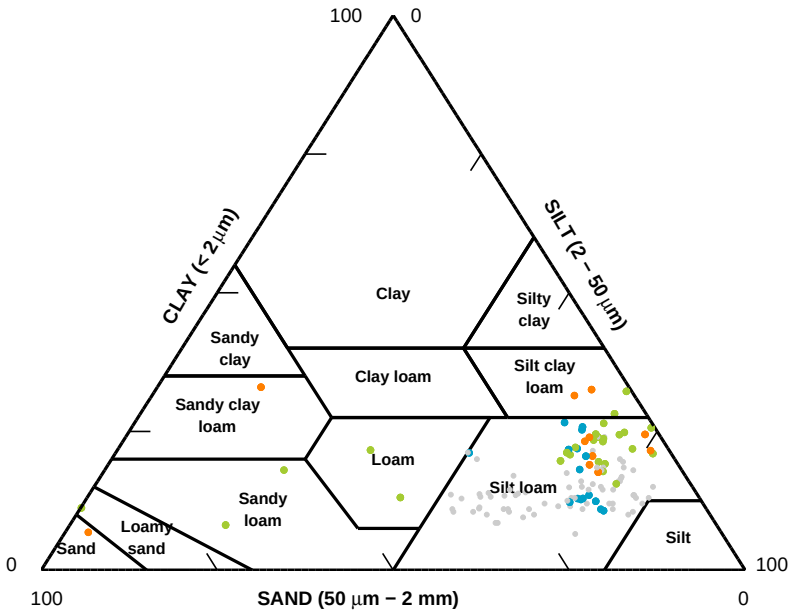

Figure 4.2: USDA soil texture triangle with sampled horizon textures. The coloured dots refer to sample land cover (Forest: blue, Grassland: orange, Cropland: green). The grey crosses represent the Silt Loam samples from the database of Harry Vereecken (1989a).

combination of land cover and horizon position in the profile. For the latter, we distinguish between surface horizons (Ap and Ah), further referred to as topsoil, and all subsurface horizons (E, Bt, Bh, C), referred to as subsoil. The number of samples available in each group is given in the last column.

Moisture retention curves

Moisture retention curves were measured on samples taken in 2 to 4 replicates in each horizon thicker than 8 cm. A total of 132 MRC were measured, representing 53 horizons. Discarding samples with silt content less than 50 %, the number of curves falls to 113 (42 horizons). Figure 4.3 shows the MRC data obtained in this study stratified by land use. In the background silt loam data from the database of Vereecken *et al.* (1989a) are also shown. MRC from this study coming from C (green) fall into the range of their data, that almost exclusively contain cropped soils. However, water content of some samples taken in F or G soils are significantly greater, before pF 2 (-100 cm of pressure head). Observing higher water contents in forest or grassland soils is expected, as those soils have generally larger organic carbon content and more roots, decreasing bulk density and increasing total porosity.

We can also compare our measurements with MRC obtained with the PTF developed in Chapter 1, as shown in Figure 4.4. Each subfigure presents the results for a different land use and a different horizon depth. The mean RMSE values are 0.11 for the forest, 0.08 for the grassland and 0.07 for the cropland. The better correspondence of PTF with samples from croplands is expected since PTF were trained on a database containing mostly samples from croplands (Vereecken *et al.*, 1989a). PTF largely underestimate measurements in the topsoil of forest soils. We observe the same for some samples in the topsoil

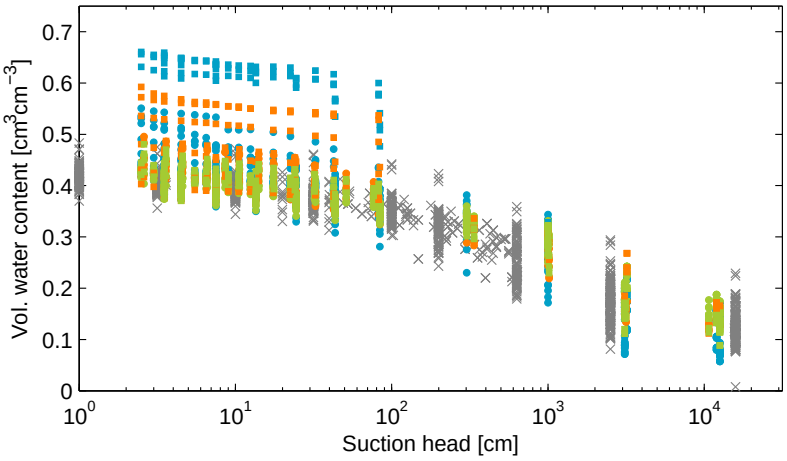

Figure 4.3: Moisture retention data obtained in this study (coloured ∘) compared to data measured by Vereecken *et al.* (1989a) on Belgian Silt Loam soils (grey ×). The colors refer to the land use (Forest: blue, Grassland: orange, Cropland: green)

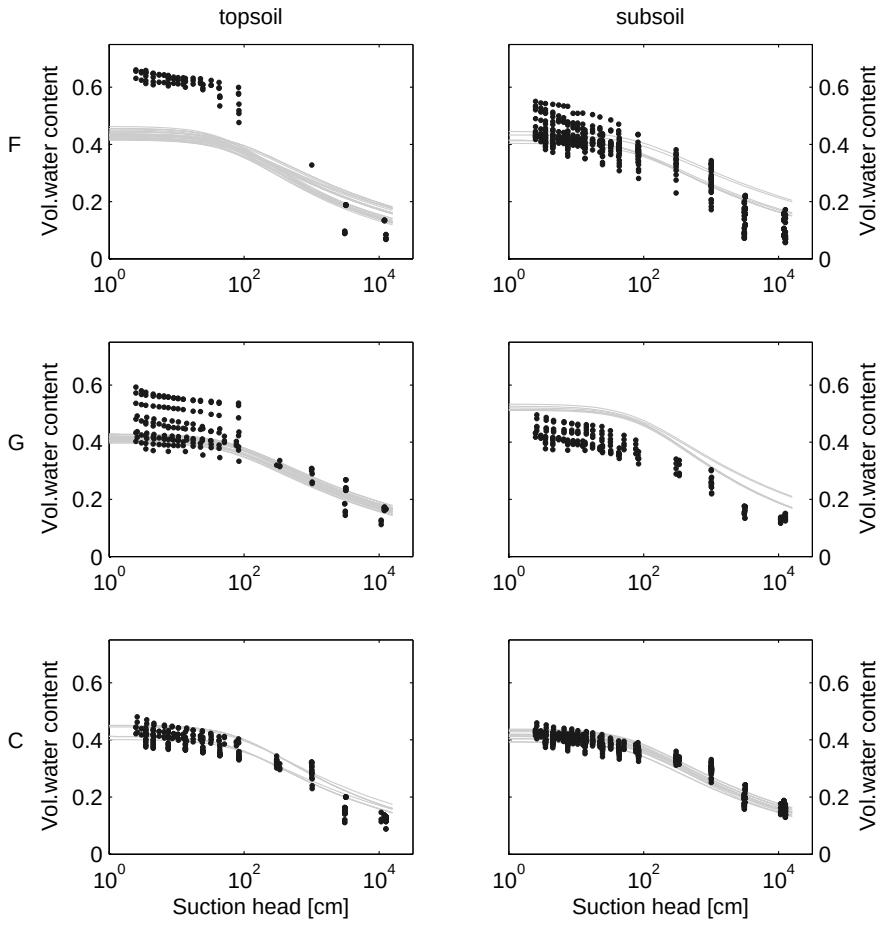

Figure 4.4: Moisture retention data obtained in this study (black dots) compared to curves obtained with PTF developed in chapter 1 (grey lines).

of grassland soils and in subsurface horizons of forest soils. In the subsurface horizons of grassland soils, PTF overestimate the measurements. In soils from cropland, PTF fit relatively well the data. This shows that PTF developed for soils from croplands are not suitable to predict MRC for soils from grassland or forest. It justifies the need to understand where the difference between these land covers lies. Figure 4.4 also shows that there are missing measurements at $h = -300$ and -1000 cm, mostly in the topsoil of forest and grassland soils.

Multistep outflow

The database contains the results of 74 MSO experiments. It is important to verify the water balance of the MSO experiments. It has been shown in

Chapter 2 that data with a wrong water balance should not be used. To assess the quality of our MSO data, we compared the total water content of the samples at the beginning of the experiment $\theta_{s,\mathsf{MSO}}$ to the maximum theoretical porosity, given by $1 - \rho_b/\rho_s$, with ρ_b the soil bulk density and ρ_s the density of the solid phase of the soil. The latter is generally approximated to 2.65 g cm^{-3}, but has to be adapted as a function of the gravimetric percentage of organic matter (OM). We hence calculated ρ_s as $2.65 - 0.01 \times \mathsf{OM}$ (Reid, 1973). Values of $\theta_{s,\mathsf{MSO}}$ larger than $1 - \rho_b/\rho_s$, cast doubt on the validity of the data. It is the case for 68 experiments out of 74. This could be explained by an excess of water, due to errors on the level of the water table or wall effects. It could also happen if the sample volume is underestimated. The volume impacts both $\theta_{s,\mathsf{MSO}}$ and ρ_b. This could be observed in case of swelling soils. With an increase in height of 1% (1 mm for a sample of 10 cm high), 12 samples rather 6 would satisfy our condition. With 5% swelling (5 mm), the number rises to 63. A swelling of 7.5% would explain the difference for all samples.

With our setup, we had no access to the samples when they were saturated. We could hence not assess the actual swelling and distinguish it from measurement errors on the water volume. However if we do not use the very first outflow data, when the water table is above the bottom of the sample, we eliminate the data that are the most prone to errors (see section 3.3.2, page 55). In that case, only 12 experiments should be ruled out if we do not consider swelling and only 7 if we allow an error of 1% on the volume (due to swelling for example). Combining this last restriction with the previous constraint of silt content greater than 50%, we obtain a set of 54 reliable and mass conservative MSO experiments.

4.3.2 Moisture retention curves

Moisture retention measurements

Figure 4.5 shows moisture retention curves (MRC) measured for three exemplary profiles under different land covers. In each subfigure, we show the measurements for all soil horizons of one profile. MARC3 is a soil planted with maize, LAU2 is under a beech forest, and MARP is a grassland soil. The different soil horizons are shown in different colours. MRC are relatively homogeneous along the cropland soil profile. Close to saturation, the water content tends to be larger in the Ap horizon, whereas at larger suctions, the illuvial horizons have larger water contents, due to an accumulation of clay. The curves cross around pF 2.3. In the forest profile, the surface horizon (Ah) is clearly distinct from the underneath horizons at least at pressure heads from 0 to -80 cm, which is expected given the large organic matter content of forest surface horizons. Unfortunately, data are missing between pF 2 and pF 3 because of instrument failure and we cannot assess the lower limit of this difference. The eluvial horizon (E) has a higher water content close to saturation than the underlying illuvial horizon (Bt), probably because the former contains more organic matter. At the dry end of the curve, the opposite situation is observed due to larger clay contents in the Bt horizons. In the grassland profile, a large variability is observed in the surface horizons (Ap), whereas the illuvial hori-

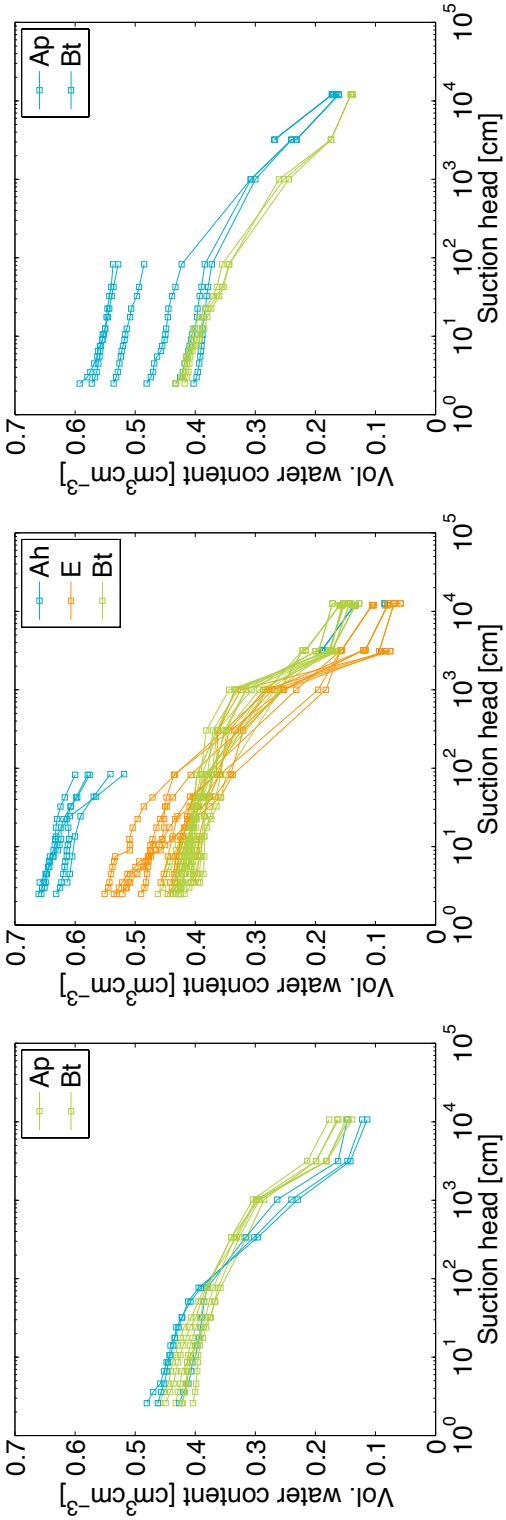

(a) MARC3 (C)

(b) LAU2 (F)

(c) MARP2 (G)

Figure 4.5: Moisture retention curves of three soil profiles (MARC3: tilled cropland (C), LAU2: beech forest (F), MARP2: grassland (G))

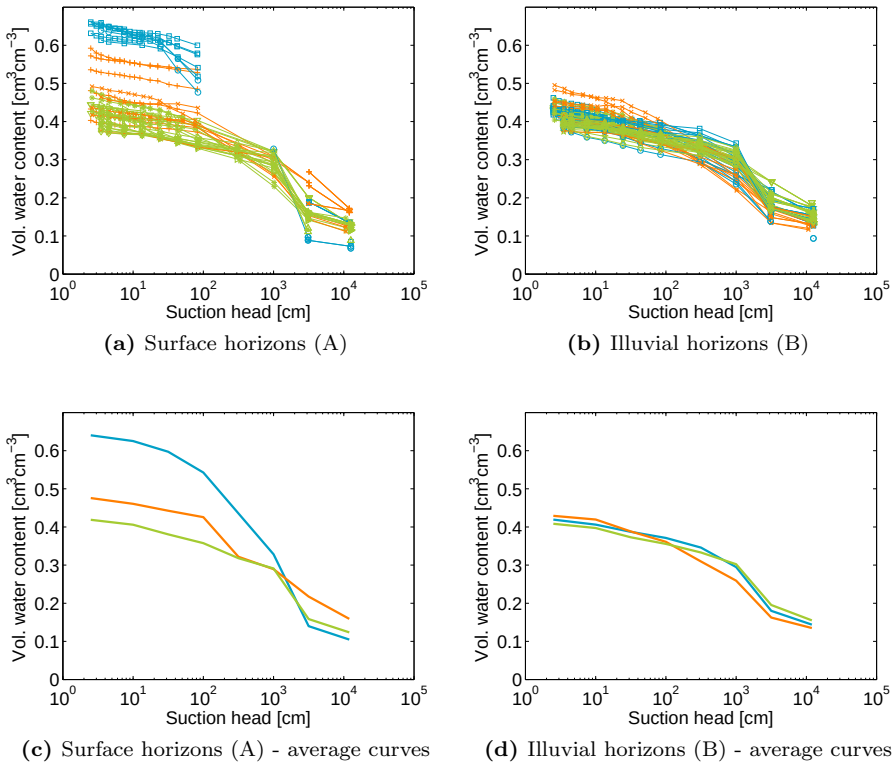

(a) Surface horizons (A)

(b) Illuvial horizons (B)

(c) Surface horizons (A) - average curves

(d) Illuvial horizons (B) - average curves

Figure 4.6: Moisture retention curves for surface (A) and illuvial (B) horizons, for all profiles (a and b) and averaged by land cover (c and d)

zon (Bt) shows very little. The water content at high suctions is lower in the Bt horizon than in the Ap horizons. This is unexpected given the larger clay content of the Bt horizon. However, this particular luvisol profile is not very advanced: the clay content is 18% in the Ap horizon and only 20% in the Bt horizon (see Appendix B).

Figure 4.6 shows the MRC for surface and illuvial horizons of all profiles and average curves by land cover. Variation between samples is larger in the surface horizons. Surface horizons from forest soils (blue) are distinct from cropland and grassland soils for pressure heads larger than -1000 cm (pF 3). Close to saturation and until pF 2, grassland soils tend to have larger water content than cropland soils. The largest variation is observed in the grassland surface horizons (orange). In the illuvial horizons (Bt), the average curves are not different from one land cover to another. The variation is constant along the investigated suctions (around 10% in volumetric water content). Observed differences could be attributed to the plant root-induced macro- and meso-structure.

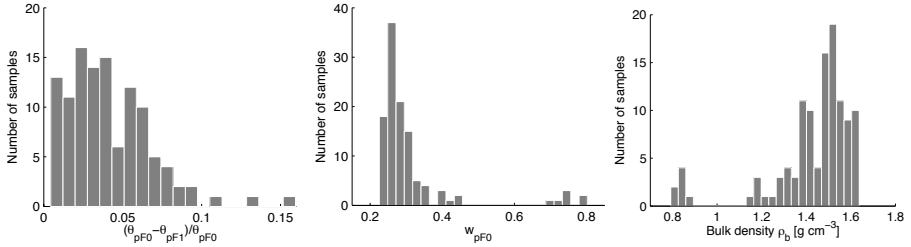

Figure 4.7: Histograms of the macroporosity indicators of Silt Loam samples.

Macroporosity indicators

Figure 4.6 shows that most differences between MRC occur close to saturation, we therefore focus our analysis on the impact of land cover and horizon position on macroporosity.

The histogram of the relative loss of water content between pF 0 and pF 1 for all Silt Loam samples is shown at Figure 4.7a. The loss varies between 2 and 16 % of the water content at pF 0. All samples loose water between pF 0 and pF 1. The distribution is asymmetric, with few samples losing more than 7% of their water. Figure 4.7b presents the histogram of w_{pF0}, the gravimetric water content at pF 0. The distribution is relatively narrow, between 0.25 and 0.35, except for seven samples having very large w_{pF0} values (more than 0.7). These are samples from Ah horizons of forest profiles with large carbon content (> 3.9 %) and bulk density ρ_b less than 1 g cm^{-3}. Six other samples have w_{pF0} around 0.4, which is larger than most samples. These come from the surface horizon of a grassland profile and the eluviated horizon (E) of a forest profile, and also have large carbon contents (> 1.3 %) compared to most samples (median carbon content: 0.29 %). The histogram of bulk density values, ρ_b, is shown at Figure 4.7c. Seven samples show ρ_b values smaller than 1. These are the same samples from Ah horizons of forest profiles as mentioned before. The remaining samples have bulk densities between 1.1 and 1.7. The narrow distribution of w_{pf0} as compared to the wider distribution of ρ_b demonstrates that differences between soil hydraulic properties mainly come from differences in soil structure.

Figure 4.8a shows boxplots of the relative loss of water content between pF 0 and pF 1, for each land cover and horizon position in the profile. Medians are not different between land covers nor between horizon depths. This would suggest that the loss of water content is comparable in all sampled Silt Loam soils, for any land cover and any horizon position. That would mean that the macroporosity is a specificity of the material. An analysis of the variance confirms this (p-values 0.56 (land cover) and 0.87 (horizon position)). The homoscedasticity is assessed using Levene's test. The p-values of 0.075 for the land cover and 0.049 for the horizon position suggest that the variances are equal between the different land covers, but are different between topsoil and subsoil.

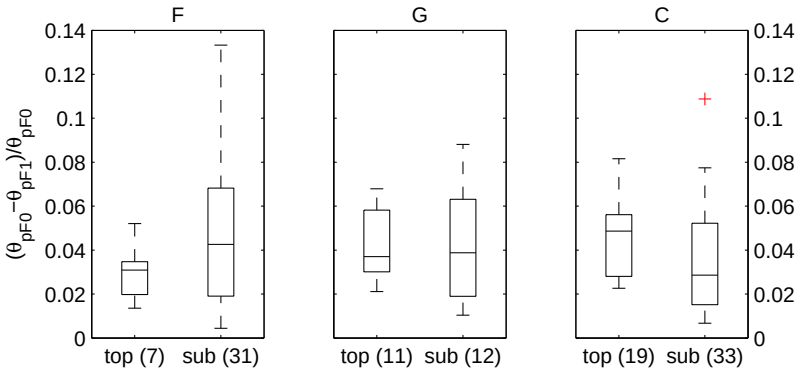

(a) Relative loss of water content between pF 0 and pF 1

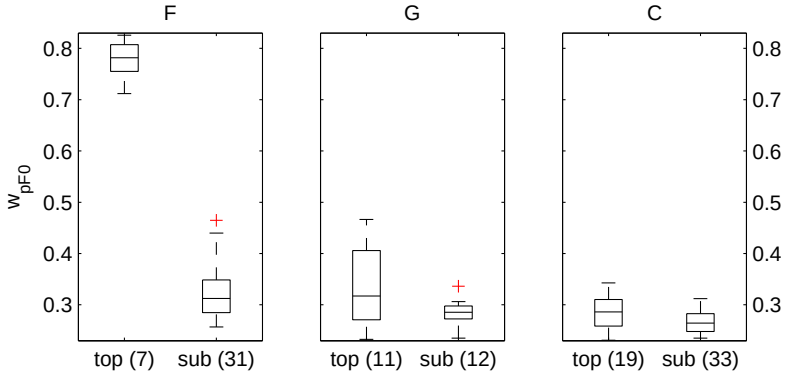

(b) Gravimetric water content at pF 0, w_{pF0}

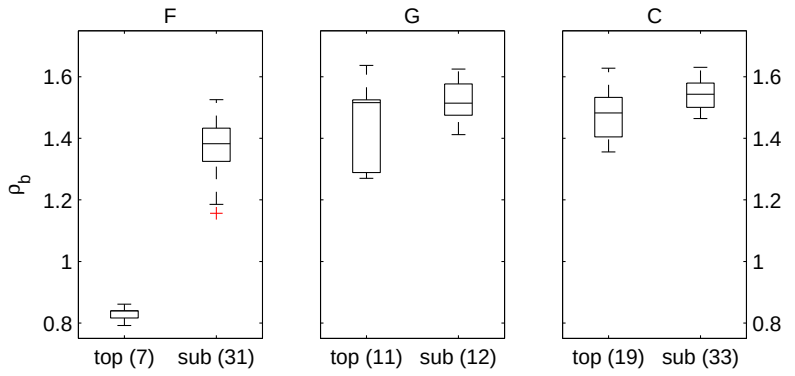

(c) Bulk density

Figure 4.8: Boxplots of the macroporosity indicators for the different land covers (F, G, C) and positions of the horizon in the profile (top, sub). The number of samples in each group is given in parentheses.

Figure 4.8b presents the distribution of the values of the gravimetric water content at pF 0, for the three land covers and the surface and sub-surface horizons. It shows that w_{pF0} in the cropland soils tends to be smaller than in the grassland and in the forest (p-value < 0.001). It also suggests that the subsoil tends to have smaller w_{pF0} than the topsoil (pvalue < 0.001). However, given the heterogeneity of the variances between the different groups, we should consider the results of the analysis of the variance with caution (p-value for Levene's test are < 0.001). The forest topsoil is different from all others (p-value < 0.001). We also observe that in the forest profiles, the vertical heterogeneity is the largest. The boxplots for the grassland suggest that, in these soils the horizontal heterogeneity is relatively large, mainly in the topsoil. We observe that in the cropland soils, w_{pF0} is relatively homogeneous, both vertically and horizontally.

The distributions of the third macroporosity indicator, ρ_b, stratified by land cover (F, G, C) and positions of the horizon in the profile (top, sub) are shown in Figure 4.8c. Results are consistent with those observed for w_{pF0}. The surface horizons of the forest profiles are distinct from all others. Variance in surface horizons of grassland is greater than in the subsoil. Subsoils of grassland and cropland show the same bulk densities.

Modelled MRC

We fitted several models describing the MRC on the moisture retention data measured with the sand-box apparatus and the pressure chambers. The 25, 50 and 75 percentiles of the adjusted RMSE distributions are presented in Table 4.3. Among the unimodal models, van Genuchten (1980) model (Eq. 3.1), with $m = 1$ (VG1) performs the best, closely followed by the model proposed by Kosugi (1996), KS. The good fitting of VG1 on silt loam soils has already been observed by other authors (Vereecken *et al.* (2010)). The two other forms of the VG model (fitted m and $m = 1 - 1/n$) produce comparable ARMSE values. The model of Vogel, rewritten by Ippisch *et al.* (2006), gives less good fits. The Brooks and Corey (1964) model, BC, is the least adapted to our data. We also present the adjusted RMSE values obtained with two bimodal models: DR (Durner, 1994) and DX (Dexter *et al.*, 2008a). The values are remarkably smaller than the ones obtained with all unimodal models, suggesting a bimodal model, with more flexibility, is preferable even if the number of parameters is larger. DR performs better than DX.

Table 4.3: Quartiles (percentiles 25, 50, 75) of adjusted RMSE [cm^3cm^{-3}] obtained by fitting different unimodal (VG0, VG1, VG2, BC, KS, IP) and bimodal (DR, DX) models on the MRC data

	VG0	VG1	VG2	BC	KS	IP	DR	DX
p25	0.011	0.008	0.011	0.019	0.009	0.012	0.001	0.002
p50	0.015	0.012	0.016	0.025	0.013	0.018	0.002	0.003
p75	0.022	0.019	0.023	0.034	0.021	0.026	0.003	0.006

Table 4.4: Distribution of suctions $|h_i|$ [cm] at which inflection points occur for models DR and DX. min and max are minimum and maximum values. px is the x percentile.

	$h_{2,DR}$	$h_{1,DR}$	$h_{2,DX}$	$h_{1,DX}$
min	0.67	102.15	23.21	1448.69
p25	1.59	916.20	195.47	2206.06
p50	4.56	1438.24	617.51	3180.77
p75	12.53	1716.60	981.13	4241.48
max	72.99	4362.69	1000.00	5872.18

When plotted as a function of $\log_{10}(h)$, bimodal models of the MRC have two inflection points corresponding in principle to maxima in the pore size distribution (see section 4.2.5). We can use the position of these inflection points, h_i, to assess the range of main pore diameter classes. We present the values of the suction at which this change in the slope of the MRC occurs for DR and DX at Table 4.4. Values of $|h_i|$ are very different for DR and DX. The inflection points occur at smaller $|h|$ values with model DR. However, given the better fits of DR compared to DX, we are more confident to use model DR

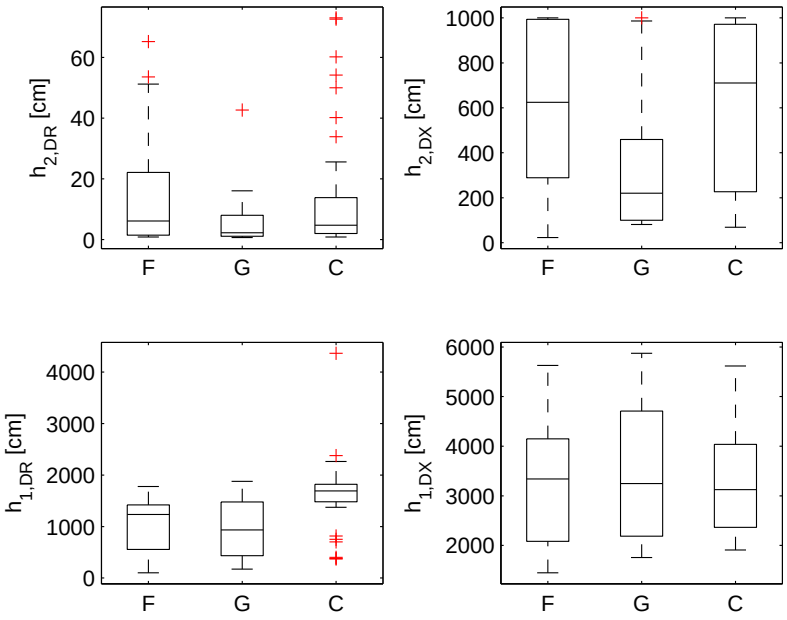

Figure 4.9: Boxplots of the suctions $|h_i|$ at which inflection points occur for DR and DX, for the three land covers (F: forest (38 samples); G: grassland (23 samples); C: cropland(52 samples))

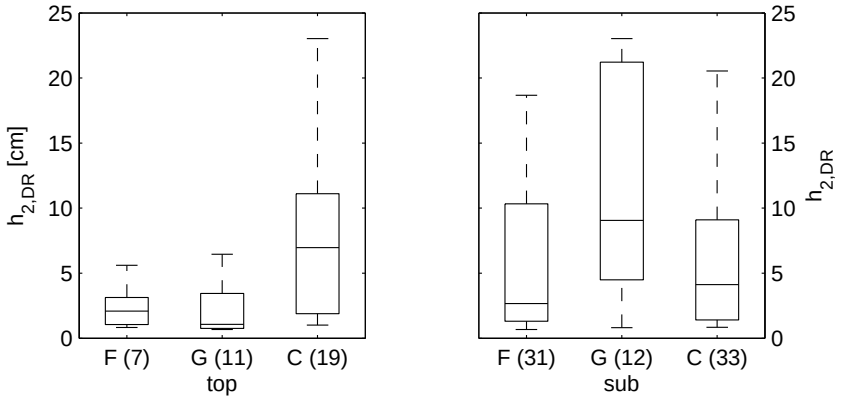

Figure 4.10: Boxplots of the suction $h_{2,\mathsf{DR}}$ at which the first inflection point of the MRC parametrized with DR model occurs, for surface and sub surface horizons (top, sub) and for the different land covers (F: forest, G: grassland, C: cropland). The number of samples in each group is given in parentheses.

to assess the shape of the MRC. The distribution of $h_{2,\mathsf{DR}}$ is asymmetric (see Table 4.4). However the variance is not very large, and only few samples have $h_{2,\mathsf{DR}}$ values larger than 20 cm. The first inflection point could be interpreted as the suction range above which macropores affect MRC. The median value of -4.6 cm is relatively close to the value of -6 cm proposed in Chapter 1 for the limit of validity of MV model. It involves pores larger than macropores as defined by Jarvis (2007), whose limit is comprised between -6 and -10 cm. Figure 4.9 shows the distributions of h_i values for different land covers. Means are not significantly different between land covers ($\alpha = 0.5$). A closer look at the values of $h_{2,\mathsf{DR}}$ (Fig. 4.10) shows us that variation in values of the first inflection point of MRC parametrised with DR seems larger in the subsoil. Levene's test reveals that the null hypothesis of equality of variances in the different land covers given the horizon depth cannot be rejected (p-values 0.06 (topsoil) and 0.34 (subsoil)). An interaction ANOVA model testing for both effects tells us that the means are not significantly different between groups (p-values 0.23 (land cover), 0.39 (horizon position) and 0.93 (interaction)).

These results suggest that the effect of macroporosity occurs in the same range in all sampled silt loam soils. This would indicate that structuring effect is a particularity of the material composing Belgian Silt Loam soils derived from eolian loess.

4.3.3 Multistep outflow and hydraulic conductivity

MSO results are analysed in two stages. First, we study the unprocessed data. We then look into hydraulic conductivity curves obtained from the inverse modelling of MSO experiments.

Unprocessed measurements

Data from MSO experiments are difficult to use as they are. Comparisons between experiments are possible only if the protocol is exactly the same. For example, soils could be compared in terms of final water content, total outflow at the end of each applied suction/pressure step or measured tension at different moments of the experiment. However, discrepancies in the duration and intensity of applied steps make these comparisons difficult. Still, protocols being quite comparable, we chose to use some of these directly available data, since they present the advantage of being free from any modelling assumption and associated fitting errors.

Figure 4.11a shows boxplots of saturated conductivities measured just before MSO experiments were run. We observe no significant differences between land covers or horizon positions. Variations in the observations extent to one order of magnitude. This suggest that the macroporosity is present in all groups and at the same extent, as was already suggested from the analysis of $h_{2,\mathsf{DR}}$.

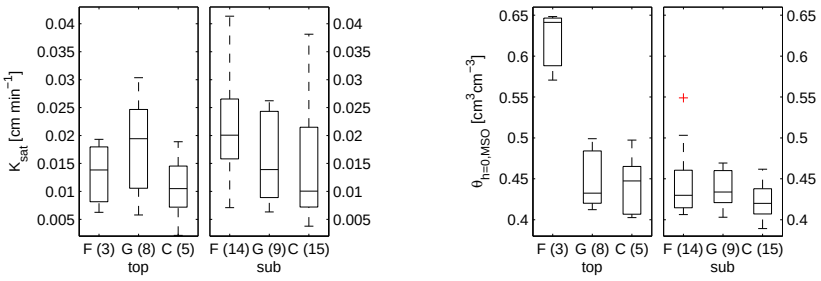

(a) K_{sat}

(b) $\theta_{h=0,\mathsf{MSO}}$

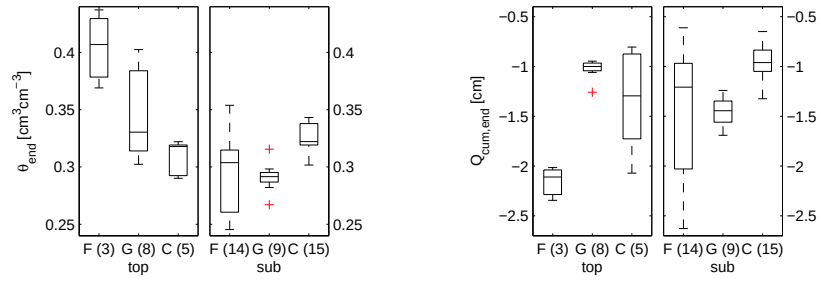

(c) $\theta_{t_{\mathsf{end}}}$

(d) $Q_{t_{\mathsf{end}}}$

Figure 4.11: Boxplots of measured MSO variables, stratified by horizon position (top/sub) and land cover (F,G,C). The number of samples in each group is given in parentheses. K_{sat}: measured saturated hydraulic conductivity (cm min^{-1}); $\theta_{h=0,\mathsf{MSO}}$: water content of samples undergoing MSO experiments with the water table at the bottom of the sample; $\theta_{t_{\mathsf{end}}}$: water content at the end of MSO experiments; $Q_{t_{\mathsf{end}}}$: total cumulative outflow at the end of MSO experiments.

Figure 4.11b shows boxplots of $\theta_{h=0,\mathsf{MSO}}$ according to the horizon position and the land cover. Values obtained for the forest topsoil horizons are larger than in the other groups, which is consistent with the previous observations on the MRC data (Fig. 4.5). Also, the inter-quartile is larger in the topsoil of grassland than in the subsoil.

Figure 4.11c shows boxplots of the water content at the end of MSO experiments: $\theta_{t_{\mathsf{end}}}$. Comparing it to Fig. 4.11b, showing $\theta_{h=0,\mathsf{MSO}}$, we observe that, in the subsoil, the reduction of variation in water content for the cropland and grassland soils is substantial. In the topsoil, this reduction is only seen in the cropland soils.

Figure 4.11d shows boxplots of the total cumulated outflow at the end of the MSO experiments, between $h = 0$ cm and $h = -960$ cm (bottom boundary condition). It is the difference between the two previous variables. The topsoil horizons from forest soils loose the most water during MSO experiments. This is consistent with the observations on the MRC.

For these four variables, we observed that surface and subsurface horizons have quite similar behaviours for cropsoils, more dissimilar for grasslands and very different for forest soils.

Inverse modelling results

MSO data, together with MRC, have been used to retrieve HCC and MRC functions using inverse modelling. Depending on the available data, we sometimes omitted the term relative to the suction head in the objective function (Eq. 4.3). As mentioned before, two different approaches were used to take the porous plate into account in the modelling of the MSO experiments. In a first attempt, it was modelled on one node and in a second attempt, it was modelled on two nodes. The first approach was indeed criticised for its lack of physically sound sense. However, the results obtained with the second approach were less conclusive. A number of experiments could not be inverted because the optimisation algorithm did not converge. Besides, as will be seen, some produced awkward hydraulic curves. The goodness of fit to the outflow and suction time series with both approaches was generally good, especially with DR. Usually fits to the moisture retention data were less good.

Figure 4.12 shows a scatter plot of optimised saturated conductivity with model MV and DR. With the first modelling approach (Fig. 4.12a), values obtained for parameter K_{sat} vary from one model to another. With model MV, the parameter often hits its upper limit of 1 cm min^{-1}. The model compensates for the rapid drop of conductivity close to saturation by setting $K_{sat,\mathsf{MV}}$ to unrealistic values. Values obtained with DR are much smaller and probably more realistic. However, when we compare $K_{sat,\mathsf{DR}}$ to the measured values, we see that they are uncorrelated. This means that even if DR is more flexible than MV, $K_{sat,\mathsf{DR}}$ is still an extrapolation parameter and cannot be linked to values observed at saturation. A dual-permeability model could perhaps be better but was not tested in this study. However, Laloy *et al.* (2010) showed that beyond pF 1, when macropores have no more effect, DR conductivity curves obtained from MSO data are reliable and representative of the matrix (see their Fig. 10b). The corresponding results obtained when modelling the porous plate on

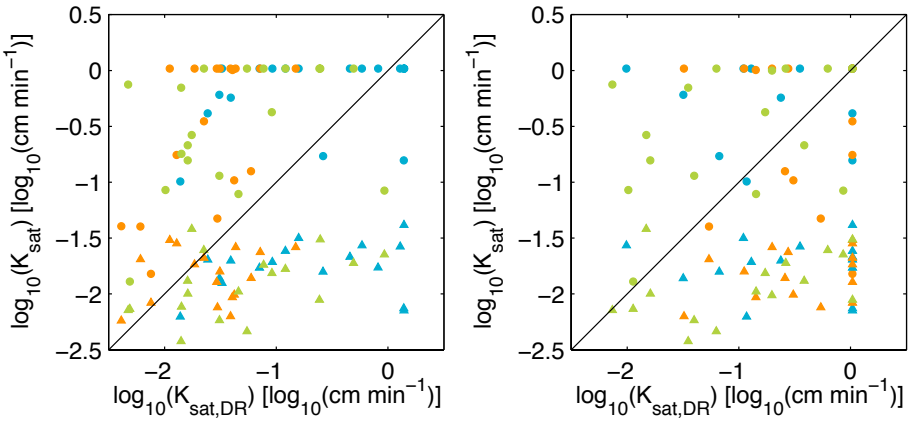

(a) Plate modelled on one node

(b) Plate modelled on two nodes

Figure 4.12: Scatter plot of the optimised values of parameters $K_{sat,\mathsf{DR}}$ and $K_{sat,\mathsf{MV}}$ (shown as circles), showing also measured saturated conductivity values, $K_{sat,obs}$(shown as triangles), for each land cover (F: blue, G: orange, C: green).

two nodes are shown in Figure 4.12b. First, the number of data is less than for the first approach since not all experiments could be inverted. Besides, a larger number of $K_{sat,\mathsf{DR}}$ hit the upper limit, even if this was set to an already large value. And this is not the only parameter for which the optimised value hit one the limits set for the optimisation process. This reduces the confidence in the results obtained with the second approach.

Moisture retention curves

Figures 4.13a to 4.13c show MRC obtained with MV from MSO inversions with the first approach (coloured lines) and with PTF from Chapter 1 (black lines). MRC are plotted in the range of suction observed with our MSO protocol, between $h = -1$ cm and $h = -300$ cm. Consistence between PTF predictions and inversions of MSO data differ between land covers. In forest topsoil (darker blue), PTF largely underestimate water content between pF 0 and pF 2. In the subsoil (brighter blue), PTF tend to overestimate water content derived from MSO. Curves from the topsoil evolve above all others. They have very large water retention close to saturation. Then two groups can be distinguished in the subsoil. Some curves have water content at pF 0 around 0.5. The others have water content at pF 0 between 0.35 and 0.45. All curves from the subsoil merge around pF 2. In grassland topsoil (darker orange), water content for three samples is underestimated by PTF. These samples have water content at pF0 larger than the others. Except for those samples, MRC for the grassland show little variation and there is a good agreement between the two methods presented. For the cropped soils (green), there is a good agreement between both methods. Variability observed for MRC derived from MSO inversion is nevertheless larger than for PTF.

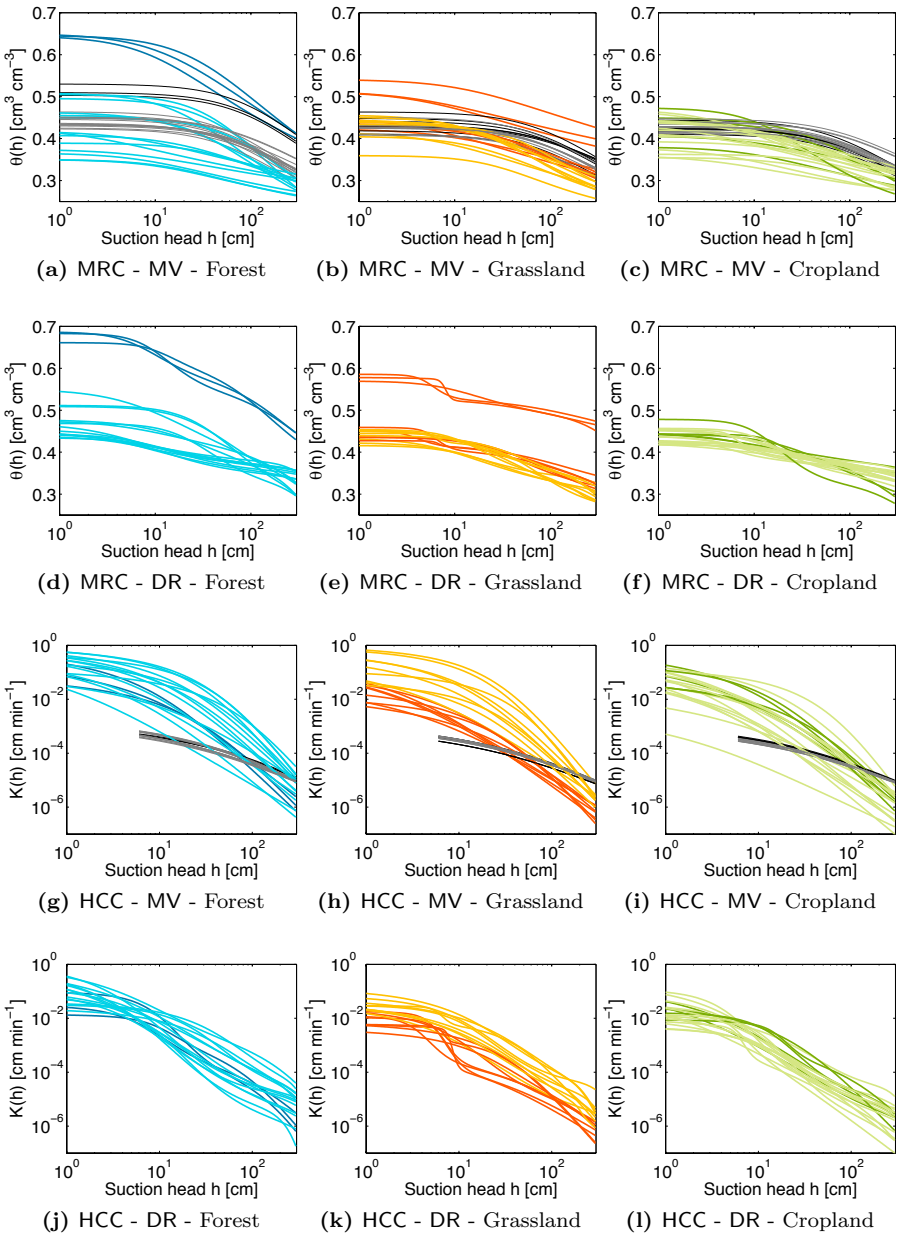

(a) MRC - MV - Forest **(b)** MRC - MV - Grassland **(c)** MRC - MV - Cropland

(d) MRC - DR - Forest **(e)** MRC - DR - Grassland **(f)** MRC - DR - Cropland

(g) HCC - MV - Forest **(h)** HCC - MV - Grassland **(i)** HCC - MV - Cropland

(j) HCC - DR - Forest **(k)** HCC - DR - Grassland **(l)** HCC - DR - Cropland

Figure 4.13: MRC and HCC obtained from MSO inversions with MV and DR, with the porous plate modelled on one node. Darker lines: topsoil; brighter lines: subsoil; blue: forest, orange: grassland, green: cropland, grey: predictions of PTF (Chapter 1).

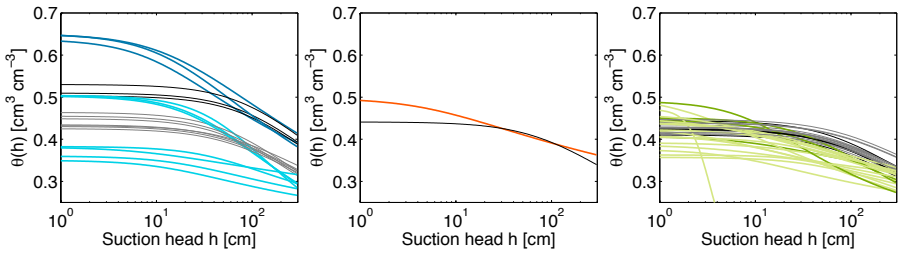

(a) MRC - MV - Forest (b) MRC - MV - Grassland (c) MRC - MV - Cropland

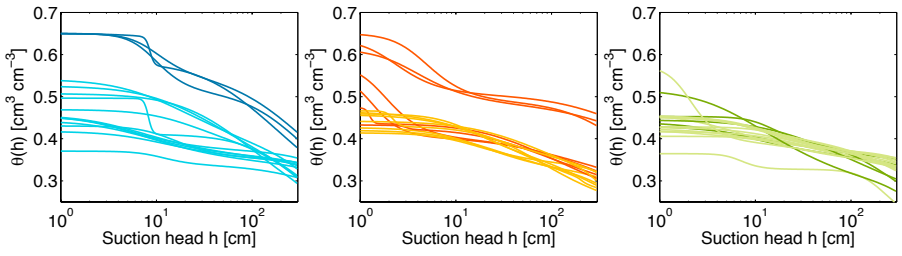

(d) MRC - DR - Forest (e) MRC - DR - Grassland (f) MRC - DR - Cropland

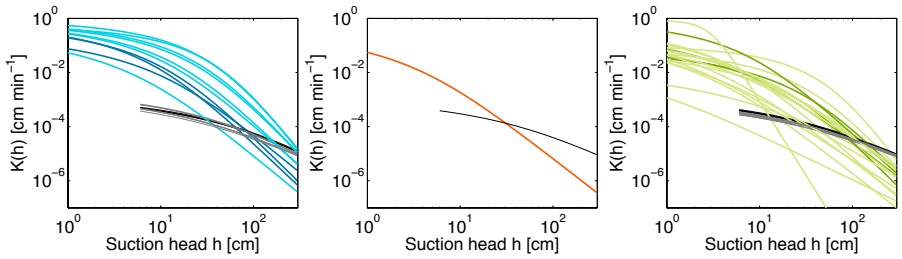

(g) HCC - MV - Forest (h) HCC - MV - Grassland (i) HCC - MV - Cropland

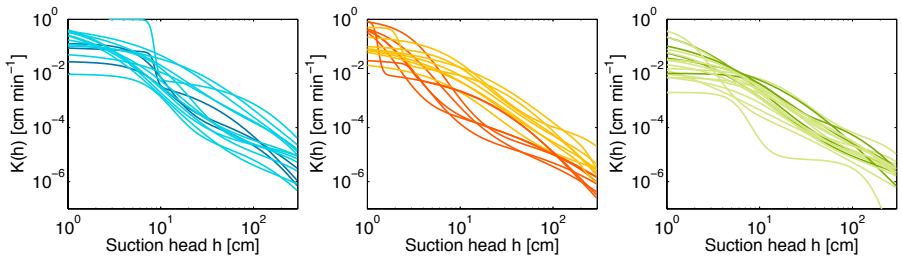

(j) HCC - DR - Forest (k) HCC - DR - Grassland (l) HCC - DR - Cropland

Figure 4.14: MRC and HCC obtained from MSO inversions with MV and DR, with the porous plate modelled on two nodes. Darker lines: topsoil; brighter lines: subsoil; blue: forest, orange: grassland, green: cropland, grey: predictions of PTF (Chapter 1).

Figures 4.13d to 4.13f show MRC obtained from the inversion of MSO experiments with DR using the first modelling approach for the porous plate. The first inflection points occur generally around pF 1, which is consistent with the values of $h_{2,\mathsf{DR}}$ obtained before (section 4.3.2). Contrasts discussed for MV are even more obvious with DR. In forest soil, topsoil (darker blue) is completely distinct from subsoil (brighter blue), in terms of value and shape. This is consistent with observations made above (section 4.3.2). In the subsoil, distinction between the two groups is still visible, with all curves merging around pF 2. In grassland soils, MRC from four topsoil (darker orange) samples have values larger than all others. This is consistent with previous observations: variation in water content in the topsoil is large. Curves from the subsoil (brighter orange) evolve in the same range as the other topsoil MRC. In cropped soils (green), MRC are much more homogeneous than in the other land covers.

The corresponding results obtained with the second approach are shown in Figures 4.14a to 4.14c for MV and 4.14d to 4.14f for DR. The observations made for the first approach still hold for the second approach for MV, except for one sample from one cropland subsurface horizon that shows an awkward curve. With DR, the number of curves with awkward shapes is larger. Even if the main tendencies can still be observed, too many samples show unrealistic curves, reducing one again the confidence we can have in these results.

Hydraulic conductivity curves

Figures 4.13g to 4.13i show HCC obtained from inversion of MSO experiments with MV. HCC are plotted between $h = -1$ cm and $h = -300$ cm, which is the range of pressure heads monitored during the experiments. Each subfigure relates to a land cover. Surface (dark coloured lines) and subsurface (bright coloured lines) are represented. Black lines show HCC obtained from PTF calibrated in Chapter 1. Curves from MSO and PTF systematically cross around pF 1.8. It is worth noting that PTF underestimate HCC variability much more than for MRC. It is expected since soil structure, by changing the connectivity and volume of the largest pores, will have much more impact on water flow (dependent on power 4 of pore diameter by Poiseuille law) than on water content (dependent on power 2 of pore diameter). This supports the hypothesis that classical predictors (%sand, %clay, %OC, ρ_b) cannot explain all the variability observed in soil hydraulic properties, and that this additional spatial variability arises from structural differences. HCC based on MSO are similar for topsoil horizons of a given land cover. In the subsoil, curves are more different.

Figures 4.13j to 4.13l show HCC obtained from the inversion of MSO data with DR. The three land covers are represented for both the surface and subsurface horizons. In forest soils, curves from the topsoil have a distinct shape, showing a clear first inflection point around pF 1.2. Curves from grassland topsoils evolve almost always below those of the subsoil. In four cases out of seven, there is a clear inflection point around pF 1. In the three other cases, the slope of the first part of the HCC is less steep. Cropped soils show more homogeneous behaviours whatever the depth and the sample.

The corresponding results obtained with the second modelling approach are shown in Figures 4.14g to 4.14i for MV and 4.14j to 4.14l for DR. Here again

a large number of curves show awkward behaviours, leading to a lack of confidence in these results. Observations made with the first modelling approach are confirmed for HCC obtained with MV in soils under forest. However, observations are different between the approaches for soils under grassland modelled with DR (Fig. 4.14k). The shapes of the HCC from surface horizons are still distinct from the subsurface horizons, but the hydraulic conductivity close to saturation is larger instead of smaller between pF 0 and pF 0.5.

Figure 4.15 shows the distributions of $K(h)$ values at $h = -1$, -6, -10, -50, -100 cm, given the land cover and the horizon position, with the first modelling approach. It is interesting to observe that the ranking of the land covers systematically remains between suction values. For surface horizons, the sequence F > C > G is observed and for the subsurface horizons, F $\geq$ G > C. Forest soils have the largest conductivities, whichever horizon or pressure head is considered. The variance in the subsoil increases when the soil gets drier. Subsurface horizons of grassland always have larger conductivities than the topsoil. This is however not observed with the second approach for modelling the porous plate (Fig. 4.14k), where the tendency is reverted at $h = -1$ cm. Surface horizons of grassland have the smallest conductivities. Hydraulic conductivities in cropsoils do not differ with depth. In the topsoil, values are generally between those of forest and grassland. In the subsoil, they tend to be lower than for the other land covers.

These observations show that hydraulic conductivity depends both on the land cover and the horizon position in the profile. Hydraulic conductivity in grassland surface horizon is smaller than in deeper horizons and smaller than in other land covers. Smaller conductivities of the surface horizons could be explained by compaction. Soil trampled by cattle would have less macropores in the surface. This would suggest that the effect of compaction has more impact than the soil aggregation associated to a larger organic matter content. Both effects compensate on bulk density (Fig. 4.8c). However this is not confirmed with the second modelling approach with which hydraulic conductivity between pF 0 and pF 0.5 is larger in surface horizons than in subsurface horizons. The spatial heterogeneity observed for the MRC (Fig. 4.13e and 4.14e) is not seen for the HCC in the range of validity of the MSO. It can be stated that the spatial heterogeneity therefore affects the meso- or micro-porosity: close to saturation, MRC shapes are similar and discrepancies between curves remain at least until pF 2.5. This explains why between pF 0 and 2.5, HCC are comparable. Under forest, large conductivities observed between -10 and -100 cm of pressure head, both in the surface and subsurface horizons, can be explained by the presence of a permanent root system and active soil fauna, building together a better connected network of pores in the macro- and meso-porosity. The structuring effect of organic matter is visible on the MRC, but not on the HCC. In croplands, the soil fauna is less active and tillage of the surface horizons periodically reorganises the pore network. Roots of crops are generally less deep than those of permanent grass or trees, leading to less well connected pores in the subsoil, as compared to grassland and forest.

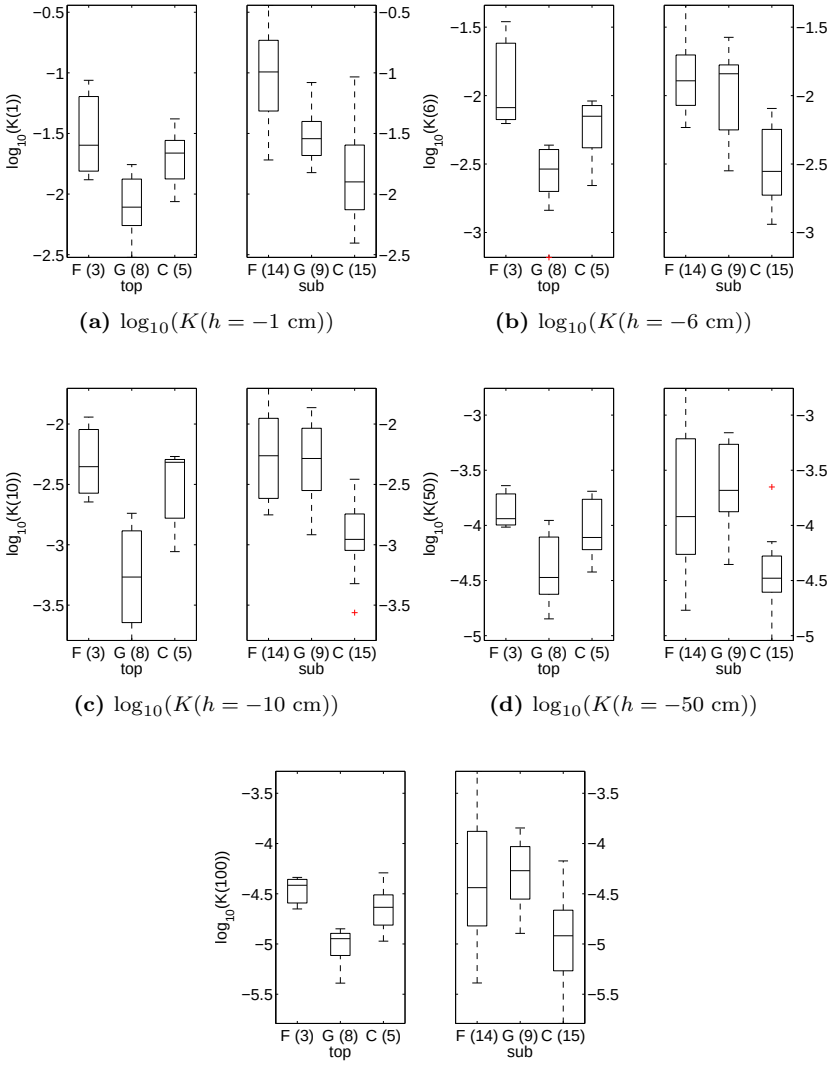

(a) $\log_{10}(K(h = -1 \text{ cm}))$ **(b)** $\log_{10}(K(h = -6 \text{ cm}))$

(c) $\log_{10}(K(h = -10 \text{ cm}))$ **(d)** $\log_{10}(K(h = -50 \text{ cm}))$

(e) $\log_{10}(K(h = -100 \text{ cm}))$

Figure 4.15: Boxplots of hydraulic conductivities [$\log_{10}(\text{cm min}^{-1})$] modelled with DR from MSO inversions at several h values, stratified by land cover (C, F, G) and horizon position (top/sub). The number of samples is given in parentheses.

4.4 Conclusion

In this study, we investigated the effects of land cover and horizon position in the profile as indicators of soil structure on hydraulic properties of soils of silt loam texture. We rely on the hypothesis that land cover influences the soil fauna, controls the root distribution, the type of carbon pool and is associated with certain mangement practices. It therefore could be a good indicator of soil structural development. We also use the horizon position in the profile as indicator, knowing that the structuring effect of biological features and management practices mainly affect the surface horizons.

We demonstrated that, although they have a similar texture, soils under different land covers show dissimilar hydraulic behaviours, in particular close to saturation. For moisture retention curves (MRC), data showed water content discrepancies until pF3 (-1000 cm of water column) for forest and grass soils. We also illustrated that pedotransfer functions (PTF) developed for cropland soils are not suited for other land covers, especially for forest soils.

Analysing MRC, we observed that (i) in forest soils, the vertical spatial heterogeneity is large, with clearly distinct surface horizons, (ii) grassland soils show a large horizontal spatial heterogeneity, mainly in the surface horizons, (iii) cropland soils are comparatively more homogeneous, both vertically and horizontally.

Macroporosity indicators showed us that pores larger than 0.3 mm (corresponding to pressure heads of -10 cm) were present in these silt-loam soils under all land covers at a comparable extent. They also confirmed that forest topsoil can contain much more water than the subsoil and than other land covers.

We also showed that bimodal models fitted the best to MRC data, and in particular Durner (1994) bimodal model (Eq. 3.3, 3.4) (DR). Examining the shape of DR curves, we observed that their first inflection point occurs around $h = -4.6$ cm, whatever the land cover. This suggests again that pores with diameter around 0.6 mm are present in all land covers and are a particularity of the studied loess derived soils.

We also analysed hydraulic conductivity curves (HCC) obtained from inversion of multistep outflow (MSO) experiments. Laloy *et al.* (2010) showed that structured soil cannot be modelled with MV or DR from MSO data. However, they showed that after pF 1, when macropores had no more effect, DR conductivity curve was reliable and representative of the matrix (see their Fig. 10b). The parameters obtained for those models have no physical meaning. We showed that DR saturated hydraulic conductivity was poorly correlated to observed values. It is an extrapolation parameter since we do not bring in the inversion information on the hydraulic behaviour in saturated conditions. However, fits provided by DR allow a flexibility necessary for fitting MRC. Hydraulic conductivities close to saturation ($-1 \geq h \geq 300$ cm) differ between land cover and according horizon position in the profile. Based on our hypothesis that land cover conditions soil structure, we explain these observations by the differences of rooting architectures, carbon pools and activity of soil micro-fauna under these three land covers. We tested the link between local morphological indices, obtained following the FAO (2006) guidelines, and hydraulic properties

at the sample scale but this did not give any satisfactorily results (not shown). This suggests that class PTF by land cover could be a good option for further developments, rather than including local morphological information directly in continuous functions. This is probably associated to the difficulty to get relevant and general morphological indicators with an objective value.

Limitations to the results of this study are twofold. First the MSO method provides no direct measurements of HCC and is constrained by soil hydrological models. Information on the soil hydraulic properties is present in the data, but inverse modelling is mandatory to have access to it. Besides the modelling approach influences the results. Second, even if already quite large, the number of available samples restrains the results to only eleven soil profiles.

As perspectives to this work, we propose to include land cover and horizon position in the profile in further developments of pedotransfer functions. Either as dummy variables or as first distinction for developing class PTF. We could also suggest the use of more elaborate models of the HCC specifically designed to deal with preferential flows such as Gerke and van Genuchten (1993a) dual porosity model (Eq. 3.5, 3.6) (DUAL) or MACRO (Larsbo and Jarvis, 2003) to better apprehend the soil functioning.

We also encourage other researchers to use fine suction-wise resolution when measuring MRC and HCC to highlight the soil hydraulic behaviour close to saturation. Another perspective could be to analyse the present data in relation to other structure indicators. Photographs of the soil profiles could be used to assess the macroporosity and the presence of biological features at the local scale.

Chapter 5

Hydraulic behaviour of volcanic soils linked to structure indicators*

5.1 Introduction

Basse-Terre (Guadeloupe) is an island in the Lesser Antilles archipelago, with limited water resources. It is affected by non-point pollution due to a very intensive banana cropping system. With a better knowledge of its soil hydraulic properties, the risks of contamination of the water bodies could be assessed and mitigated. Basse-Terre is one of the Leeward Islands, located amidst the island arc of the Lesser Antilles, at 16° 09 N, 61° 40 W. It covers an area of 847.82 km^2. It originates from volcanic eruptions, due to the subduction of oceanic crust of the North American Plate under the Caribbean Plate. Its highest volcano is the Soufrière, rising at 1467 m. As it is the case for other active or extinct volcanoes, the movement of the trade winds causes very great rainfall variations along the sides of the mountain and this within short distances (Colmet-Daage and Gautheyrou, 1974). The eastern coast of Basse-Terre Island, known as the Windward Coast (in French: Côte-au-vent), is exposed to the trade winds and receives a lot of rain, whereas the western coast of the island, known as the Leeward Coast (in French: Côte-sous-le-vent) is protected from the winds by the Soufrière volcano and is thus much drier. The rainfall also increases with the elevation whereas the temperature does not vary much along the year. This diversity in climates brings about different weathering rates and soil evolution processes in these relatively young and very permeable ash formations (Colmet-Daage and Gautheyrou, 1974).

Analysing soils developed in volcanic ashes from New Zealand, Parfitt and Childs (1988) showed that silicon concentration in soil solution decreased as rainfall increased, reflecting increasing leaching of the soils. In Basse-Terre, we observe a Andosol-Nitisol weathering sequence developed on dacitic-andesitic

*In collaboration with P. Cattan, CIRAD, Guadeloupe, France.

ash (Ndayiragije and Delvaux, 2004). The presence of allophane at higher altitudes also reflects the time sequence along the side of the volcano. Closer to the summit, the deposits are younger and contain fresh volcanic glasses that are unweathered and from which allophane can form. The typical sequence of soils encountered on the sides of the volcano La Soufrière is described below(Colmet-Daage and Lagache, 1965). An illustration of this can be found at Figure 5.1. The local nomenclature is finer than classes proposed by international systems. This is why we present the local classes.

- At high elevations, where the rainfall is large, the insolation low and the material young, allophanic soils are found.
  - Andosol (AN) has a humic-rich A horizon, a pseudo-silt texture (very soft to the touch), a high water retention capacity and is very permeable. It shows little difference between soil moisture in the field and at pF 3. It is also characterised by a low exchangeable-base content (2 mequ./100 g), and high contents in amorphous minerals.
  - Andosol perhydraté (AP) is found at higher elevations. It has a more greasy and soapy aspect and a bulk density as low as 0.3. Its profile is unsaturated in exchangeable bases. It is never dry but when exposed to air it forms small hard particles.
- Andic brown soil (sol brun andique) as defined by Colmet-Daage and Lagache (1965) (BA) is found at lower elevations in the allophane-halloysite transition. It has the apparent texture of a sandy pseudo-loam. The temporary dessication of its surface during less rainy periods lowers its gravimetric water content w around 40-50 %, but it still reaches 60-80 % at 1 m depth. Dessication of the surface horizon favours halloysite formation, whereas, in the deeper soil, allophane content is still large, giving it a creamy touch. The humic rich horizon is generally deep (50-60 cm). Its exchangeable-base content is higher than in allophanic soils.
- Rust-brown soil (sol brun rouille) as defined by Colmet-Daage and Lagache (1965) (BR) is found at even lower elevation, where there is less rainfall and more insolation. This leads to an increase in the proportion of halloysite, due to longer periods of dessication. It does not contain cristalline iron even if iron content may be high. The exchangeable bases content is larger than at higher elevations (> 12 mEq/100 g).

In the FAO system, AP, AN and BA are classified as Mollic Andosol and BR is classified as Halpic Nitisol.

We would like to determine which are the key factors controlling the soil hydraulic behaviour and whether they can be related to the soil classes or to pedological and morphological attributes. Dorel *et al.* (2000) already showed that the volumetric water content at high suctions (pF> 2.5), is positively and linearly related to allophane content, whereas at lower suctions, water content is explained by the combination of carbon and allophane contents. There is a decrease of total porosity and water retention, parallel to the decrease of andic features and altitude in the soil sequence (Dorel *et al.*, 2000). Other

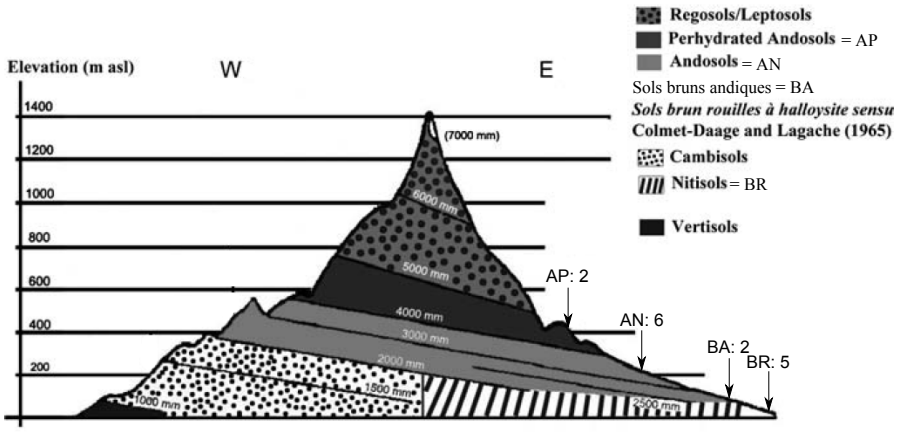

Figure 5.1: Sketch transects of Western (W) and Eastern (E) rainfall patterns as related to elevation (m asl) and major soil types in the island of Basse-Terre (Henriet *et al.*, 2008). Arrows indicate the localization and the number of experimental sites.

authors showed that water released at low suctions, associated with meso- and macropores, shows positive relationship with Alo content (Armas-Espinel *et al.*, 2003).

In order to develop pedotransfer functions (PTF) to help assess soil hydraulic properties, it is of interest to investigate how hydraulic properties can be linked to different indicators. In this chapter, two hypotheses were confronted (see Fig. 1): (i) soil pedogenesis (characterised by the soil type or its associated characteristic soil chemical properties) is the main driver for hydraulic properties or (ii) soil structure (characterised by morphological indicators) controls soil hydraulic properties. By measuring hydraulic conductivity and moisture retention curves together with chemical and structural indicators along a pedo-toposequence, our goal is to discriminate how structure and soil pedological properties impact hydraulic properties.

5.2 Material and methods

5.2.1 Selection of sites

Fifteen sites have been chosen along the topographical transect presented before (Figure 5.1). The selection of the exact sites was made according the following criteria:

- Soil classification: soils with decreasing andic properties have been selected to highlight the effect of pedogenesis on the soil hydraulic behaviour.
- Topography: the selected fields have a slope less than 5%, given the influence of steepness on the soil behaviour.

- Cropping system: given the influence of tillage on the soil behaviour (Dorel *et al.*, 2000), banana fields cultivated for at least four consecutive years were selected.
- Agricultural practices: to avoid the effect of a particular agricultural practice, priority was given to fields cultivated by different farmers.

The sites were sampled and *in situ* measurements were realised in 2008 and 2009. During the 2009 campaign, sampling at the exact same location than in 2008 was not possible when the agricultural practices had meanwhile changed. In such cases the closest field corresponding to the selection criteria was sampled instead.

5.2.2 Sampling and infiltrometer measurements

Disturbed soil samples were taken for chemical characterisation after 16 to 24 hours drying and 2 mm sieving. Two undisturbed samples of 100 cm^3 (Kopecki rings) were taken in each horizon for physical and retention characterisations. Besides, large samples (1 to 2 kg of soil) were collected for measurements of the moisture retention curves (MRC) on undisturbed clods. The samples were kept in hermetic plastic bags in an air-conditioned room awaiting the measurements. Undisturbed 1 L soil samples were collected at all sites at two depths (horizons A and B) for subsequent multistep outflow (MSO) experiments. Two suction infiltrometer measurements per site were realised at the soil surface with a 7.1 cm diameter disc. The disc was covered with a thin fabric holding the applied pressure thanks to an air-entry point around -30 cm. Prior to the measurements, the surface was levelled and a fine sand layer and a thin sponge were applied beneath the disc to ensure a good contact with the soil and to prevent the deterioration of the infiltrometer fabric. Suction steps of $-10, -6, -3, -1$ and 0 cm were applied and the water level in the reservoir of the infiltrometer was monitored until steady-state was reached. The cumulative infiltration is calculated from these measurements using equation 5.1:

$$I_{cum}(t_i) = (H(t_0) - H(t_i)) \left(\frac{D_R}{D_D}\right)^2 \tag{5.1}$$

where $I_{cum}(t_i)$ is the cumulative infiltration [L] at $t = t_i$ [T], $H(t)$ is the water level in the reservoir [L] at time t [T], t_0 is the initial time [T], D_R and D_D are the diameters [L] of the reservoir and of the infiltrometer disc, respectively. The infiltration rate at a certain suction head, $I(h)$ [LT^{-1}] is given by the slope of the cumulative infiltration as a function of time when steady state is reached.

The parameters of Gardner model (1958) of the hydraulic conductivity curve can be calculated with Wooding (1968) equation for infiltration through a circular source:

$$I(h) = \pi r^2 K_s \exp(\alpha^* h) \left[1 + \frac{4}{\pi r \alpha^*}\right] \tag{5.2}$$

where $I(h)$ [LT^{-1}] is the infiltration rate at suction h [L], r is the radius of the circular source [L], α^* and K_s are the parameters of Gardner model (see

Eq. 1.2). A local minimum search (Matlab lsqnonlin) is used to find a set of parameters that minimizes the errors between modelled and observed flow rates at the five measured suctions.

5.2.3 Structural indices

Descriptions of the soil profiles were realised in each site. Pits of 60 cm depth and 1.7 m wide were dug out perpendicular to the furrows, with a banana plant on the left and the inter-furrow on the right. An agricultural profile analysis (Gautronneau and Manichon, 1987) was realised on the 60 first cm of soil (maximum depth of mechanical soil work). A 60×100 cm grid composed of 10 cm wide squares was placed against the soil wall. The description consists in counting down and locating the roots and in identifying homogeneous units of soil according to the type of clods present. Four types are listed: fine earth (TF), easily discernible clod (SF), less easily discernible clod (SD) and continuous structure (SC). The fragmentation plane of the clods for types SF and SD can further be described as planar (δ) or rough (γ).

From the agricultural profile analysis, two indices were defined and associated to infiltrometer measurements. A vertical area was defined just below the infiltrometer disk 40 cm wide and 30 cm deep. On this surface the percentage of each type of clods was defined. The results are reported on a 5×5 cm grid and are processed using Microsoft Excel® pivot tables. An example is shown at Figure 5.2. root density (RD) was characterised on the same grid. In each square, the number of roots and their diameter are reported. RD is then determined as:

$$\mathsf{RD} = n \left[\pi \left(r + w \right)^2 - \pi r^2 \right] / S \tag{5.3}$$

where n is the mean number of roots per $(100\ \text{mm})^2$ area (S), r the average root radius [mm], w the average pore width between root and soil (assumed equal to 0.25 mm (Lin *et al.*, 1999 a)).

5.2.4 Chemical characterisation

Silicium, aluminium and iron were extracted with an ammonium oxalate solution ($(NH_4)_2C_2O_4$,0.2M, pH 3) during 4 hours in the dark, with a ratio soil:solution of 1:50. This operation allows the dissolution of the amorphous and hydric oxides (allophane and imogolite) and the Al-humic associations, but does not affect the crystalline minerals. The cations were measured out using plasma emission spectrophotometry to obtain Sio, Alo and Feo. The same cations were also extracted with a sodium pyrophosphate solution ($Na_4P_2O_7$, 0.1M) during 16 hours with a ratio soil:solution of 1:100. This operation extracts the iron and aluminium complexed with the organic matter without reacting with the mineral constituents. The amount of cations determined by atomic absorption consists in the cations present in the soil solution and those linked to the organic matter: Sip, Alp and Fep.
From these, the ferrihydrite and allophane contents are estimated using the relations 5.4 and 5.5:

$$\mathsf{Ferri} = \mathsf{Feo} \times 1.7 \tag{5.4}$$

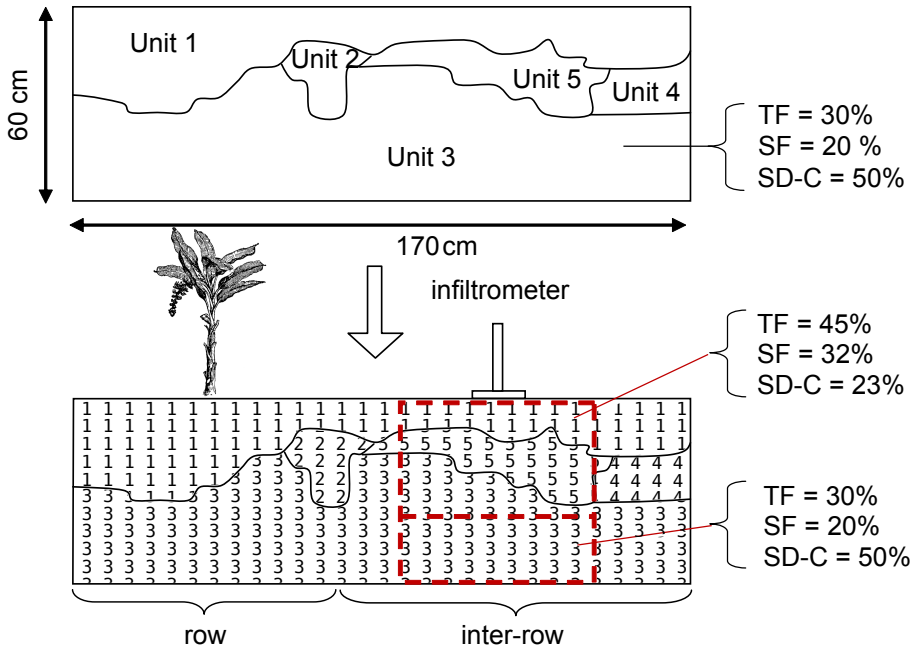

Figure 5.2: Example of soil structure description (Gautronneau and Manichon, 1987) and quantification. TF: fine earth; SF: easily discernible clod; SD-C: sorely discernible clod or continuous structure.

$$\mathsf{Allo} = f\left(\frac{\mathsf{Alo} - \mathsf{Alp}}{\mathsf{Sio}}\right) \times \mathsf{Sio} \tag{5.5}$$

Imogolite contribution to Alo and Sio is generally less than allophane (Parfitt and Kimble, 1989). Therefore $\frac{Al_o - Al_p}{Si_o}$ is assumed to be an estimation of the atomic ratio Al/Si in allophane. The value of $f\left(\frac{\mathsf{Alo}-\mathsf{Alp}}{\mathsf{Sio}}\right)$ is obtained from a look-up table (Parfitt, 1990). Alp/Alo ratio has been proposed by several authors (e.g. Parfitt and Kimble, 1989; Mizota and Van Reeuwijk, 1989) to characterise the dominant constituents of the exchange complex of andosols. It tends to 0 for purely allophanic soils and to 1 for non allophanic soils.

Total carbon (C) and nitrogen (N) contents were measured using a Thermo Finnigan NC soil analyzer (Milan, Italy). Given soil pH, the presence of carbonate is excluded and the total carbon content corresponds to the organic carbon content. The organic matter content is obtained by multiplying the carbon content by 1.724.

The exchangeable bases were determined by percolating a solution of ammonium acetate (CH_3COONH_4, 1M, pH 7) on a column containing a mixture of soil and washed sand. The cations Ca^{++}, Mg^{++}, K^+ and Na^+ were measured out with atomic absorption. Percolating the same column with ethanol eliminates the excess of NH_4^+. The cation exchange capacity (CEC) is deter-

mined with percolating the same column with a KCl solution (10%, pH 3) that moves the NH_4^+ measured out by distillation.

The acidity is measured with a pH-meter after one hour agitating a solution of soil:H_2O or soil:KCl (1M) in the ratio 1:5. The comparison of KCl pH with H2O pH provides an assessment of the nature of the net charge on the colloidal system. The numerical difference in the values of pH measured in KCl and H2O is referred to as the ΔpH ($\Delta\mathsf{pH} = \mathsf{pH_{KCl}} - \mathsf{pH_{H_20}}$). When this difference is negative, the colloid has a net negative charge, and when positive, it has a net positive charge.

The contents in exchangeable aluminium and hydrogen is measured out by percolating a KCl solution (1N) and titration with NaOH (total exchangeable acidity) and with HCl (0.1N) after addition of 10 ml of NaF (exchangeable Al).

5.2.5 Hydraulic characterisation

Undisturbed soil samples (100 cm^3) were used for measurements of the MRC. A sand-box apparatus was used at pF 0, 1, 1.5 and 1.8 ($-1, -10, -32$ and -63 cm). Pressure chambers were used for larger suctions. Undisturbed samples were used for measurements at pF 2.4 and 3 (-251 and -1000 cm). Smaller disturbed subsamples were used for measurements at pF 3.5, 4 and 4.2 ($-320, -10000$ and -15850 cm).

Thirty 1 L samples (10 cm high, 11.25 cm diameter) were used to determine hydraulic conductivity curves (HCC) by MSO and constant head methods. Samples were placed on a synthetic porous plate covered with a nylon membrane and saturated bottom-up during 48 hours. After saturation, the saturated hydraulic conductivity was measured by applying a constant head and measuring the outflow. Then, the MSO experiment itself took place: the bottom outflow and the tension were monitored while suction/pressure steps were applied at the bottom/top of the samples. The protocol used with these samples does not differ from the one used in previous chapters (2, 3 and 4). A combination of suction ($h \in [+10, -80]$ cm) and pressure ($h \in [-160, -960]$ cm) modes was used with tensiometers inserted in the middle of the samples. For details on the setup, see chapter 2. Parameters of Mualem-van Genuchten (van Genuchten, 1980) model (Eq. 3.1, 3.2) (MV) and Durner (1994) bimodal model (Eq. 3.3, 3.4) (DR) were optimised on the MSO data using AMALGAM-SO (Vrugt *et al.*, 2009). The objective function consisted in a weighted sum of three sub-objectives: the outflow at the bottom of the sample, the suction in the middle of the sample and the water content at the end of the experiment. The weights were set on the basis of the measurement errors for the first two sub-objectives and arbitrary at $(0.01)^{-2}$ for the third objective.

5.2.6 Statistical analysis

Data were analysed with Matlab® Statistical Toolbox. The stepwise regression tool was used to determine which potential predictors explained the larger part of the variation observed in the variables of interest. The explained variables were infiltration rates measured with the suction infiltrometer at several suction heads close to saturation. The potential predictors were the chemical

characteristics presented above, the quantified morphological indicators and their multiplicative combinations (Table 5.2).

5.3 Results and discussion

5.3.1 Data description

Chemical properties

The average values of some chemical properties are given in Table 5.1 for each soil type in surface and subsurface horizons. The content in ferrihydrite (ferri), decreases along the pedo-toposequence. This iron oxyde has an isoelectrical point between pH 7 and 9. It is hence positively charged in most soils and attracted to negatively charged particles, particularly to clay minerals (Dorel, 2001; West *et al.*, 2004). West *et al.* (2004) highlighted its particular attraction to halloysite. Allophane (Allo) is a clay mineral present in Andosols. Its content increases from BR through AN. Is is however smaller in AP surface horizons, since these soils have a higher organic matter content for which aluminium has a stronger attraction and because of the leaching of silica. Surface horizons have larger organic carbon contents (C) than subsurface horizons, since organic matter is not mobile. Along the pedo-toposequence, C increases because organic matter is linked to allophanes (in AN) and it creates complexes with Aluminium (in AP). At higher elevations, the soils always remains wet, also slowing the mineralisation process. Chadwick *et al.* (2003) proposed the sum of these first three chemical components and the imogolite content as a "non-crystallinity index". As expected, it increases along the pedo-toposequence, with the rainfall gradient. The ratio Alp/Alo is an indicator of the allophanic character of the soil. It increases when aluminium creates complexes with organic matter and when allophane content decreases. The ratio Sio/Alo is also an indicator of composition. These are the silicon and the aluminium contained in amorphous minerals and complexed with organic matter. Sio/Alo increases

Table 5.1: Average chemical properties of the four soil types (AP, AN, BA, BR) in surface (four first rows) and subsurface (four last rows) horizons.

	ferri*	allo*	C*	alloferric*	Alp/Alo	Sio/Alo	pHw	DpH
AP	22.8	75.5	89.8	188.1	0.41	0.42	5.7	0.7
AN	21.9	108.5	37.2	167.6	0.16	0.49	6.5	1.0
BA	18.3	54.7	32.1	105.1	0.29	0.35	6.2	1.1
BR	11.3	29.9	25.0	66.2	0.18	0.32	6.8	1.3
AP	25.4	147.9	41.7	215.0	0.09	0.47	5.4	0.2
AN	18.6	123.0	2.5	144.1	0.09	0.51	5.8	0.7
BA	13.4	71.2	10.1	94.7	0.26	0.41	5.2	1.0
BR	11.4	47.2	11.6	70.2	0.23	0.35	5.8	1.2

* Units in g kg^{-1}.

along the pedo-toposequence but decreases in the AP, where the content in Al-humus complexes is larger than in the other soil types. The soil pH can also be an indicator of the soil composition, since a larger organic matter content decreases the pH and the presence of iron oxides increases it. As expected, AP have lower pHw values than the surface horizons of the other soil types. In the subsurface horizons, all soil types have comparable pHw. The difference between the pH measured in water and in KCl solution (DpH) reflects the amount of H^+ ions fixed to the soil minerals. As such it gives indications on the soil cation exchange capacity (CEC). In the surface horizons, AP have lower values of DpH than the other soil types. In both surface and subsurface horizons, the value decreases along the pedo-toposequence, but the fall is stronger in the deeper horizons.

Moisture retention data

Figure 5.3 shows measured MRC averaged by soil type and horizon. All curves seem to cross around pF 3, unfortunately no data are available between pF 1.8 ($h = -80$ cm) and pF 3.5 ($h = -3000$ cm) to ascertain this observation. We observed that, close to saturation, the volumetric water content increases along the toposequence. When the soil gets drier, beyond pF 3, the tendency is reversed. In BA soils, the surface horizon has a behaviour close to BR soil, whereas the subsurface horizon MRC is more similar to AN. This is expected as soil classes are partly based on moisture content observations and can be explained by pedogenesis. BA soils are intermediate between AN and BR. Their surface horizon undergoes drier conditions than AN soils, meeting the conditions for secondary minerals formation. In the deeper horizons, this alteration cannot take place because the soil always remains wet. It is worth noting that, in the field, only BR soils and to a lesser extent surface horizons of BA soils

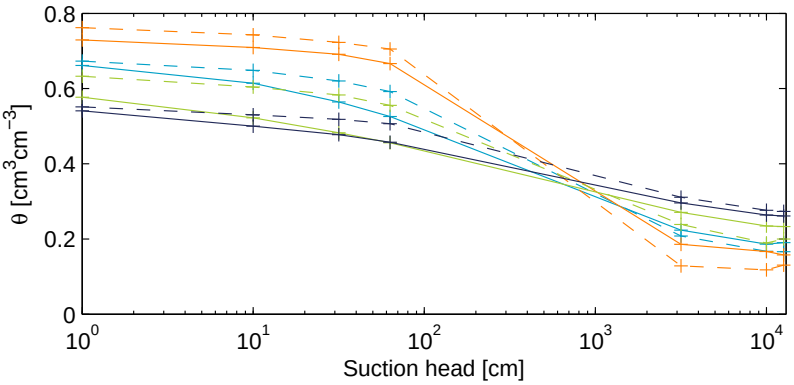

Figure 5.3: Average MRC by soil type and horizon. AP: orange, AN: light blue, BA: green, BR: dark blue. Surface horizon: continuous line, Subsurface horizon: dashed line. Number of samples in the different classes: in surface horizons: AP: 11; AN: 5; BA: 3; BR: 5; in subsurface horizons: AP: 2; AN: 5; BA: 3; BR: 5.

ever undergo suctions beyond pF 3. No measurements are available between $h = -1$ (pF 0) and $h = -10$ (pF 1) cm, where macroporosity occurs.

Hydraulic conductivity curves

Measurements of HCC were realised *in situ* with suction infiltrometer and in the laboratory thanks to MSO experiments and inverse modelling.

Suction infiltrometer measurements provide infiltration rates at several suction heads close to saturation. Their base ten logarithms, averaged by soil type, are given in Figure 5.4a. Given Wooding equation for infiltration under a circular source, we can retrieve parameters of Gardner equation by inverse modelling. The resulting HCC are presented at Figure 5.4b. Soil types cannot be discriminated based on HCC, on the opposite to MRC. The hydraulic conductivity values generally decrease very quickly.

Multistep outflow measurements were used to retrieve HCC by inverse modelling, parameterised with MV and DR. Fits of the outflow and suction time series are generally good, especially with DR. HCC obtained with DR for surface horizons plotted between pF 1 and pF 2.5 are presented at Figure 5.5. Samples from BR soil type (dark blue) show similar curves. HCC from AP (orange) also look alike, but only two samples are available. For AN and BA, curves are much less similar inside the soil type. Despite their important differences in terms of chemical properties and soil classifications, these soils do not discriminate in term of saturated hydraulic behaviours. These results lead us to postulate that hydraulic conductivity is more affected by local soil structure and that soil type

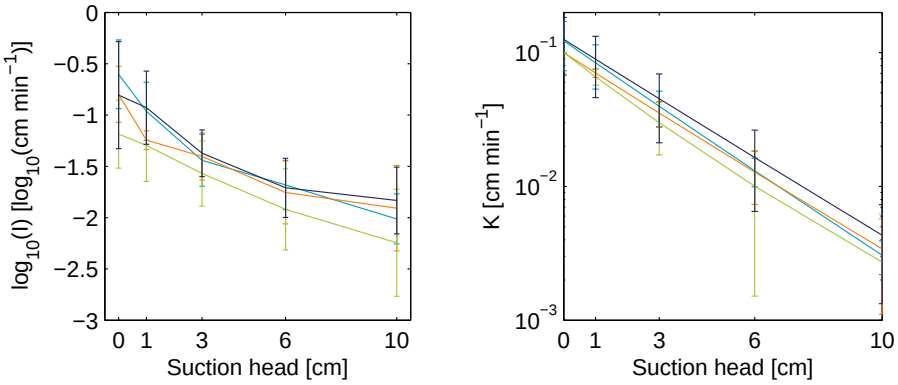

(a) Infiltration rates, I, at five suction heads

(b) Hydraulic conductivity, K.

Figure 5.4: Infiltration rates ($\log_{10}(I)$ averaged by soil type (left). HCC obtained with suction infiltrometer measurments and Wooding equation for surface horizons (right). AP: orange, AN: light blue, BA: green, BR: dark blue. Whiskers show one standard deviation in $\log_{10}(\text{cm min}^{-1})$

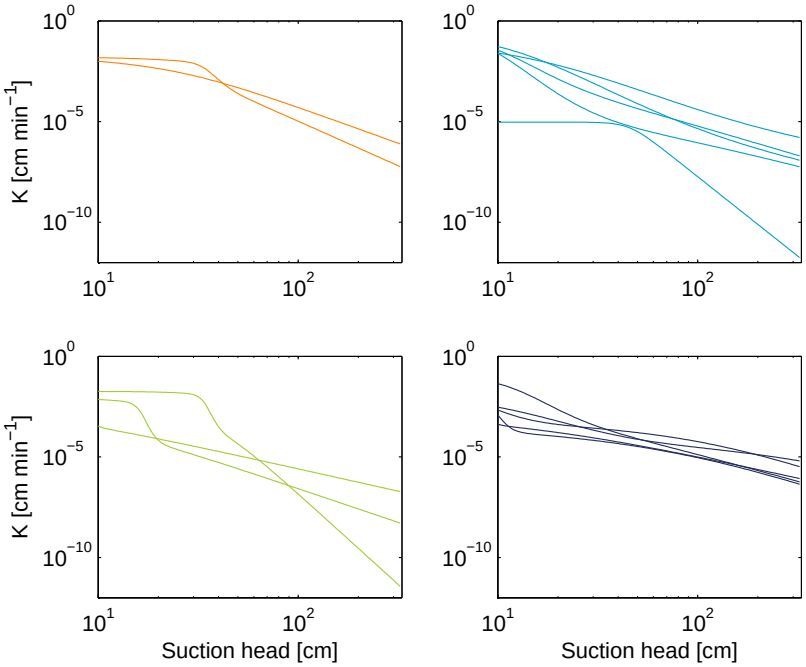

Figure 5.5: HCC obtained from inversion of MSO experiments for surface horizons. AP: orange, AN: light blue, BA: green, BR: dark blue.

does not suffice as structure indicator. Therefore, the potential relationships between soil hydrodynamics and local soil structure are further analysed.

5.3.2 Correlations between soil hydraulic properties and structure indicators

We analysed correlations between infiltration rates measured at several suction heads and variables from Table 5.2. With a stepwise regression tool, we selected the variables that significantly explain part of the observations variance. For the five measured suctions, RD was systematically selected and alone already explained a large part of the observed variance (Adj-R^2 between 0.1 and 0.59). Interestingly, the closer to saturation, the best the correlation is. Positive effect of RD on the infiltration rate can be explained by preferential flows along roots. RD was sometimes associated in the regressions with TF. The positive effect of TF on infiltration rates is consistent. The less compacted soils have larger pores, which facilitate water transfer. To improve the regressions, we tested the explicative power of combinations of variables from Table 5.2. The regressions obtained are plotted at Figure 5.6. And their coefficients are presented at Table 5.3. The variables have been transformed so that they are in the interval $[0, 1]$. The regression coefficients can therefore be compared.

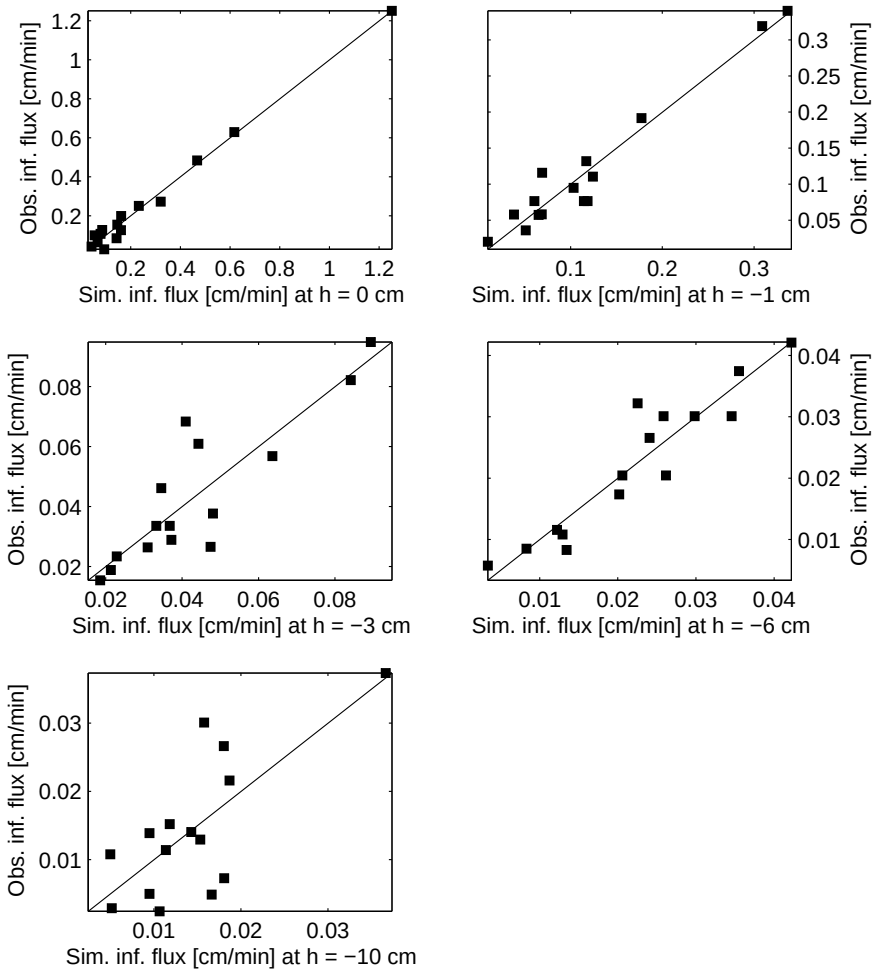

Figure 5.6: Regressions of the infiltration fluxes at several pressure steps on the predictors indicated in Table 5.3.

Table 5.2: Explaining variables included in the stepwise procedure

Acronym	Description
Alp	Aluminium extracted with $Na_4P_2O_7$ [g kg^{-1}]
Fep	Iron extracted with $Na_4P_2O_7$ [g kg^{-1}]
Sip	Silicon extracted with $Na_4P_2O_7$ [g kg^{-1}]
Alo	Aluminium extracted with $(NH_4)_2C_2O_4$ [g kg^{-1}]
Feo	Iron extracted with $(NH_4)_2C_2O_4$ [g kg^{-1}]
Sio	Silicon extracted with $(NH_4)_2C_2O_4$ [g kg^{-1}]
Alp/Alo	Ratio of Alp to Alo
Sio/Alo	Ratio of Sio to Alo
Allo	Allophane content [g kg^{-1}]
C	Carbon content [%]
DpH	pH_{H_2O} - pH_{KCl}
BD	soil bulk density [g cm^{-3}]
TF	Fine earth proportion (Gautronneau and Manichon, 1987)
SF	Easily discernible clods proportion (Gautronneau and Manichon, 1987)
SD	Less easily discernible clods and continuous structure proportion (Gautronneau and Manichon, 1987)
RD	Root density as defined at Eq. 5.3
topsoil	dummy variable for the horizon position (1: topsoil, 0: subsoil)

Table 5.3: Regression coefficients of variables explaining infiltration rates. Variables are between 0 and 1 so that coefficients weights are comparable.

	$h = 0$	$h = -1$	$h = -3$	$h = -6$	$h = -10$
TF	0	0.54	0	0	0
TFxTF	0	0	0.14	0	0
TFxRD	1.24	0.12	0	0.04	0.03
SFxSD	0	0	0.03	0	0.01
SDxSD	-0.24	0	0	0	0
BDxSD	0	0	0	0.02	0
AlpxSD	0.80	0	0	0	0
Alp/AloxTF	0	-0.47	-0.07	0	0
Sio/AloxBD	0	-0.30	0	0	0
FepxC	-0.72	0	0	0	0
DpH	0	0	0	-0.46	0
DpHxDpH	0	0	0	0.29	0
Adj-R^2	0.98	0.91	0.68	0.82	0.41

As observed with the more simple models, the determination coefficient Adj-R^2 decreases with increasing suctions (more negative h values). It is interesting to note that variable TFxRD stands out for all measured suctions except $h = -6$ cm. It does however not always have the same weight in the regression. Only at $h = 0$ cm, it has the largest coefficient. Its inclusion in the models is not unexpected since both TF and RD are intuitively facilitating infiltration, as already mentioned before. The only other variable to stand out more than once is SDxSD. It has positive coefficients at $h = -3$ and $h = -10$ cm. Its positve effect on infiltration rate is counter-intuitive since one would think that sorely discernible clods would impede infiltration rather than speed it up. However at the fringe of clods, preferential flow could occur. The other variables selected by the stepwise procedure are combinations of morphological and pedo-chemical variables.

5.4 Conclusion

We studied the hydraulic properties of tropical volcanic soils from a toposequence in Guadeloupe and their relationship with soil structure indicators. We first looked for the existence of a simple link between these properties and the local soil classification, which is based on the soil andic properties. We showed that MRC of different soil classes have distinct shapes. Differences between curves can be explained by the pedogenesis along the pedo-toposequence. This result could lead to the development of class PTF predicting of MRC based on soil type.

There is however no obvious link between soil classes and HCC. Close to saturation, hydrodynamic behaviour assessed with suction infiltrometer measurements could not be related to soil classes or soil chemical attributes only (not shown). No link could be established from HCC obtained from inversions of MSO experiments either. We postulate that water flow in near saturated conditions is more affected by local soil structure and that soil classes do not suffice to describe phenomena occurring at that scale. We therefore investigated more local structure indicators. We propose to derive structure indicators based on the proportion of soil units with different compaction levels assessed by an agricultural profile analysis. We showed that infiltration rates obtained from suction infiltrometer measurements are controlled by the root density and the fine earth content. We obtained yet better relationships with combinations of locally described soil morphology and pedo-chemical variables. Root density multiplied by fine earth content stands out at four suctions out of five. Multiplicative combinations of morphological and pedo-chemical variables bring valuable information for explaining infiltration rates.

This study illustrates that pedogenesis of tropical soils derived from volcanic ashes determines soil moisture retention and hydraulic conductivity. Very close to saturation, soil classes do not help explaining hydraulic conductivity values and local soil morphology indicators are necessary. Their combination to pedo-chemical information enhances the relationships.

These results are promising as they set a path for the combined use of quantified soil structure and physico-chemical properties to predict soil hy-

draulic behaviour close to saturation. Future studies could concentrate on the use of this type of combined variables to predict soil hydraulic properties and eventually to develop PTF suitable for tropical soils derived from volcanic ashes on the basis of a larger database.

Conclusion and perspectives

General conclusions

Knowledge of soil hydraulic properties is a prerequisite for modelling water flow in the vadose zone. Their spatial and temporal variability and their arduous measurement give ground for the development of pedotransfer functions (PTF). The predictive power of PTF can be improved by taking soil structure into account. In this thesis, we studied the hydraulic properties of soils from temperate and tropical regions in relation to soil structure indicators.
Our general objective was to improve the assessment of soil hydraulic properties based on soil structure indicators and auxiliary information. We therefore focused on (i) evaluating the sensitivity of measurement methods to soil structure effect on hydraulic properties; (ii) assessing the sources of uncertainty in measured soil hydraulic properties; (iii) identifying and quantifying relevant structure indicators for predicting soil hydraulic properties.

Measuring hydraulic properties: Sensitivity to soil structure

In chapter 2, we confirmed the ability of multistep outflow (MSO), combined with independently measured water retention data, to retrieve parameters of Mualem-van Genuchten (van Genuchten, 1980) model (Eq. 3.1, 3.2) (MV). However, chapter 3 showed the limits of the MSO device. Under saturated conditions, the set-up is prone to excessive experimental artefacts. Another limitation of this method is the mandatory use of inverse modelling thereby constraining the shape of the moisture retention curves (MRC) and hydraulic conductivity curves (HCC). The sensitivity of the measurements to the soil structure effects is further conditioned by the choice of the model used for the inversion. Durner (1994) bimodal model (Eq. 3.3, 3.4) (DR) gives a flexibility necessary for fitting MRC but does not consider macroporous flow. However the stability of Gerke and van Genuchten (1993a) dual porosity model (Eq. 3.5, 3.6) (DUAL) was not sufficient to produce robust results. The choice of one or the other should be conditioned by the requirements of the application. Perhaps, MACRO (Larsbo and Jarvis, 2003) could be considered as an alternative, since

it does not rely on the invalid use of Richards equation in the macropores but uses instead a "kinematic wave" approach.
In Chapter 5, we also exploited data obtained from a suction infiltrometer. Measurements were successfully related to soil structure indicators. Therefore the method can be considered as sensitive to the effects that structure has on hydraulic conductivity close to saturation. However the drawbacks of this field method (time-consuming, short range of suctions explored, unknown sampled volume) should not be undermined when applied to case studies.

Tackling the uncertainty of soil hydraulic properties

Throughout this thesis, various sources of uncertainty of soil hydraulic properties have been exposed. A first source of uncertainty is certainly macroporosity, especially when it is not taken into consideration by the measurement method. In chapter 1 we assumed that macropores influence the soil hydraulic behaviour between saturation, $h = 0$ cm, and pressure heads of $h = -6$ cm. We therefore developed PTF which are specifically not valid in this range, significantly improving their performance. In chapter 4, we showed that MRC of loess-derived soils of silt loam texture are indeed affected by macropores. In the studied soils, macropores are present at all depths to a comparable extent. As a consequence, the flexibility brought by bimodal models for describing the MRC was necessary. This seems to be a characteristic feature of all studied silt loam soils, whatever the land cover (forest, grassland or cropland). Second, the natural variability of the soil hydraulic properties is larger than what can be explained by soil texture, organic carbon content and bulk density. We already showed in Chapter 1 that these predictors cannot explain all the variability observed in hydraulic behaviour of cropland soils, especially not in close to saturation conditions. In Chapter 4, we showed that this was exacerbated for soils under forest and grassland. In other words, soil structure explains the variability that is unaccounted for by classical predictors. This should have an impact on stochastic modelling studies, which usually generate variability only based on the natural variability of texture. A third source of uncertainty are experimental errors that always affect hydraulic properties measurements. Particularly, MSO measurements may suffer from artefacts whose effects are difficult to quantify. Furthermore, the mathematical formalism applied to describe soil hydraulic functions also creates uncertainty. It is due to the structure of the model itself which may not be well adapted to the data if the assumptions on which it is based are too simple. It may generate a large uncertainty on the parameters calibrating the model, leading to a large predictive uncertainty. We confirmed in Chapter 3 that a good fitting of the data is not necessarily associated with small predictive uncertainty (Laloy *et al.*, 2010).

In spite of many efforts to characterise the soil hydraulic conductivity, it remains difficult to obtain reliable measurements, especially close to saturation. MSO may not be the most adapted tool and the models assumptions may not render the complexity of the soil hydraulic conductivity. We suggest the use of better adapted models. In the studied loess-derived silt loam textured soils, the flexibility of a bimodal model is necessary to render the shape of the MRC. It also helps simulating the very larges flows observed during the first steps of

MSO experiments. Indeed, 30 to 40% of the water is released between $h = 0$ cm and $h = -10$ cm of pressure head. The rate at which this release occurs is also very fast. Reducing the uncertainty of hydraulic properties predicted by PTF could be achieved using structure indicators.

Structure indicators

We tested the predictive power of several structure indicators. In the first chapter, we developed PTF based on commonly used information. Texture, organic carbon content and bulk density proved their value as predictors of MV parameters. But they also showed their limits: they are insufficient for explaining all the variability of hydraulic properties. We principally showed that they are unable to render the effects generated by the soil structure, close to saturation. Nevertheless, we provide a useful tool to predict MV parameters from sand, clay and organic matter contents together with soil bulk density.
In chapter 4, we studied soils of silt loam texture derived from loess deposits to highlight structure effects on hydraulic properties. Assuming that land cover defines the root architecture, the soil biological activity and land management practices, we proved its potential as a soil structure indicator. It could be used to develop class PTF. At a finer level, relating morphological indicators to measured soil hydraulic properties of silt loam soils did not come to any conclusive link. We hypothesise that it is either due to an inadequate description of the soil morphology or to the local influence of such structure indicators. In the former case, a new soil profile description could enhance the results. In the latter case, structure indicators should be described at the scale of the sample used for measuring the soil hydraulic functions.
In Chapter 5, we focused on tropical soils derived from volcanic ashes. Pedogenesis varies along the toposequence, due to age of material, rainfall and insolation gradients. We showed that MRC are related to the local soil classification, but that it does not suffice for explaining the variability observed in hydraulic conductivity close to saturation. We hypothesise that hydraulic conductivity is affected by local structure and that local soil morphology is necessary to describe it. We showed that root density and fine earth content characterised just beneath the infiltrometer provide valuable information. Better relationships are obtained when combining soil morphology indicators with pedo-chemical variables, confirming the intricate effects of pedogenesis and vegetation on soil structure.

Perspectives

By consolidating the understanding of the dynamics linking soil structure and hydraulic properties, this thesis makes a significant step towards shifting from a qualitative to a more quantitative use of pedological data. Such technological improvement can be of great use in a variety of application domains going from predicting polluant transfer to integrated hydrological modelling passing by crop growth modelling and soil moisture mapping. However, a series of

technical perspectives can be first discussed before getting back to the broader perspectives of this work.

Technical perspectives

Despite the conclusions obtained in this thesis, relationships between soil hydraulic properties and structure indicators still need to be better characterised. A first suggestion could be to ensure that soil morphology description is done at the same scale as the hydraulic characterisation, i.e. at the sample scale. Under these conditions, hydrological and morpho-pedological relationships are expected to be more robust and thereby more reliable. However, the research presented here should also be extended to other scales. In this thesis, soil hydraulic properties are generally studied at the sample scale and at best at the horizon scale. The validity of the hypotheses that have been tested should be verified in field conditions. Indeed, from an agronomic standpoint, soil functions at the level of the pedon. It is therefore important to consider the soil horizonation *in situ* as soil layering may induce unstable flow processes. Local artefacts can also occasion preferential flow, which can seriously affect the water transfer and solute transport through the vadose zone. Lysimeters experiments could be implemented, but their set-up is particularly cumbersome. Laboratory experiments using very large samples extending on several soil horizons and of a relatively large horizontal dimension could be carried out to further test the results obtained in this thesis.

Fine resolution of MRC measurements have revealed the presence of macropores in the silt loam samples studied in this thesis. Double porosity seems to be the rule rather than the exception in these soils. We therefore encourage researchers to use such an approach to better characterise MRC.

Large flows observed during the first steps of MSO experiments, when the water table has not reached the bottom of the sample, could not be reproduced by models based on Richards equation. Considering other flow mechanisms in the macropores could allow a better characterisation of the close to saturation hydraulic conductivity. Using models such as MACRO (Larsbo and Jarvis, 2003) could bring valuable input since these simulate the presence of macropores explicitly. Other models of the hydraulic functions could also be tested, such as free-form estimation (Iden and Durner, 2007).

The bigger picture

The benefit of incorporating soil structure in the assessment of water resources can bring valuable improvement to a number of applications, some of which are presented below.

Problems of groundwater contamination by various pollutants is an issue in intensive agricultural areas. The authorisation of new pesticides on the European market is controlled thanks to models that evaluate the time of transfer and decay in the unsaturated zone. These models use representative soil profiles to adjust the hydraulic properties to regional conditions. The use of PTF taking the soil structure into account could enhance the area of application of these tools. Class PTF based on the land cover could be used

as first approximation in fast response risk assessment for the dispersion of pollutants in the environment following accidents or in large scale evaluation of pollution risk.

Crop growth models can be valuable tools to estimate how crops transform agro-meteorological conditions into yield. These models have a soil component to calculate the soil moisture dynamics in interaction with the plants and the atmosphere. However, these modules are often overly-simplistic. Operational systems of along-the-season yield forecasting relying on this approach, such as the Crop Growth Monitoring System (CGMS) of the European Commission, could greatly benefit from improvements incorporating soil structure, especially when applied to areas were crops are grown in water limited conditions. Scenarios using different parametrisations of the soil component could be run and compared to evaluate whether adding information on the soil structure could improve the accuracy and precision of yield prediction at the European scale.

Water scarcity is already an issue and will worsen in the next decades. Irrigated land surfaces will increase and the water balance at the watershed scale will be affected. With climate change, regions such as the South of Europe will suffer from water scarcity and agriculture will need a very good management of water resources. Being able to model the soil water dynamics in those changing environments will help water stakeholders to manage water at the watershed scale and give ground to constructive discussions about the repartition of water between its different uses. Developing PTF based on land cover and soil classes could be very useful in integrated hydrological models since this information is easily available in maps and can therefore be used for large scale predictions.

Appendices

Appendix A

Sensitivity analysis

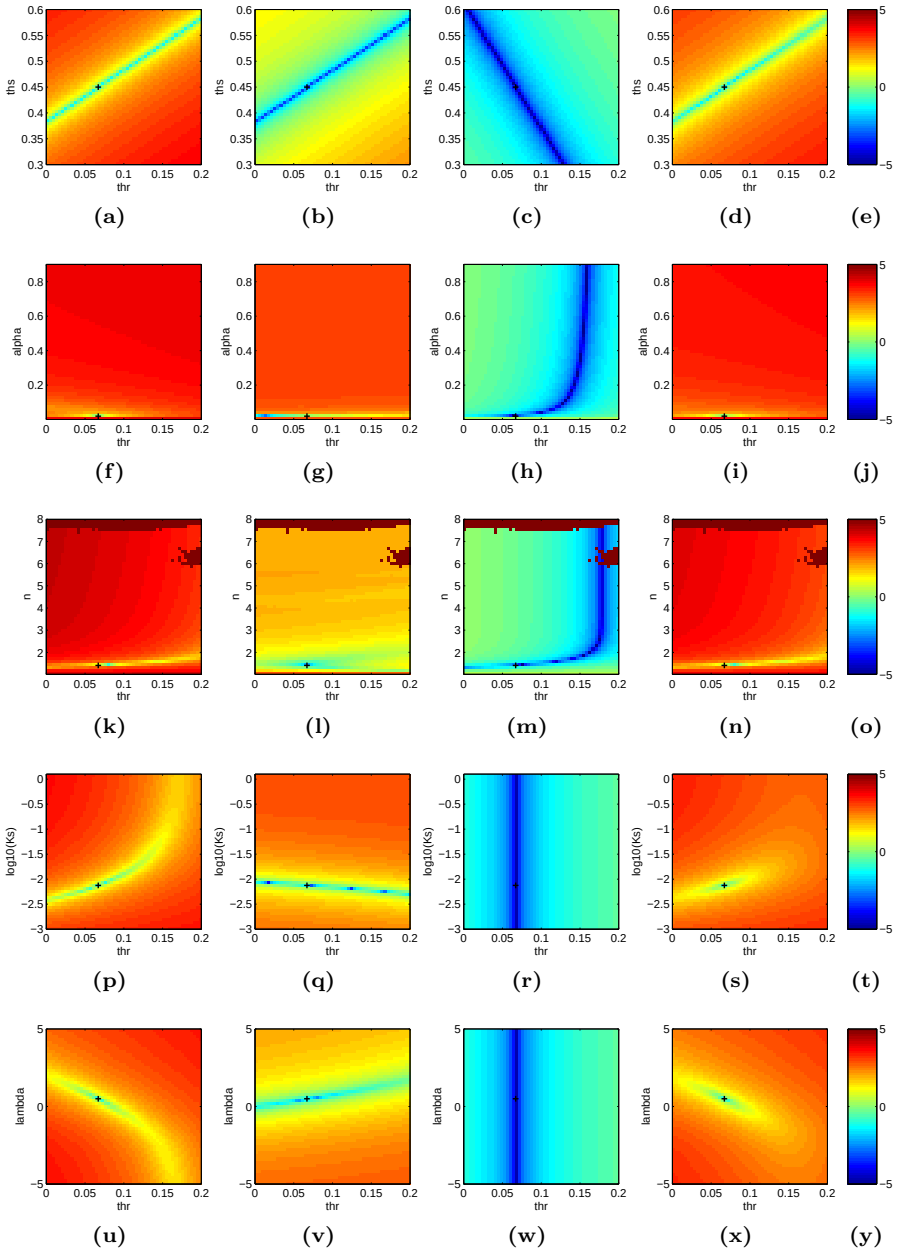

Figure A.1: Response surfaces of the different objectives of OF for couples of parameters of the MV model. For some combinations of parameters, the numerical solution does not converge ($\boldsymbol{\phi} \geq 10^5$).

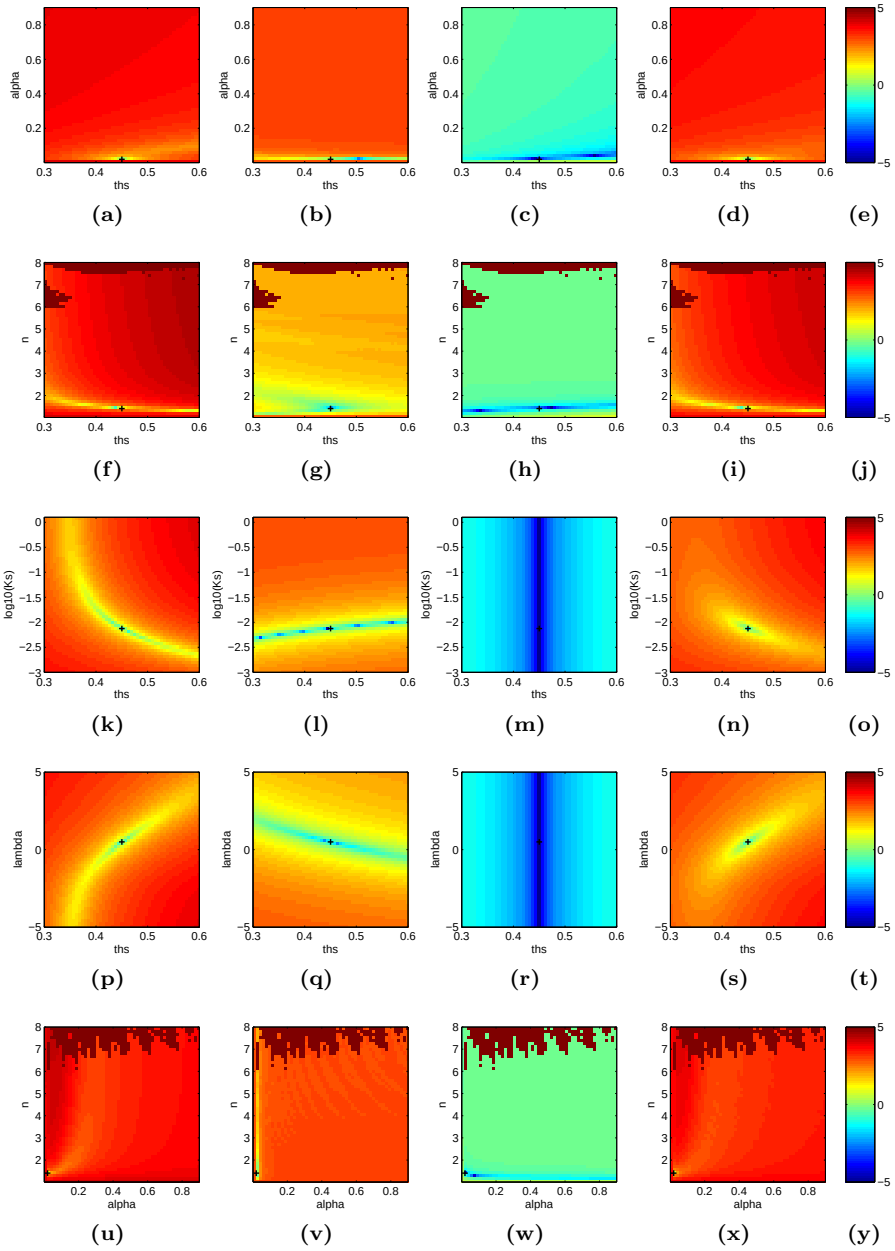

Figure A.2: Response surfaces of the different objectives of OF for couples of parameters of the MV model. For some combinations of parameters, the numerical solution does not converge ($\boldsymbol{\phi} \geq 10^5$).

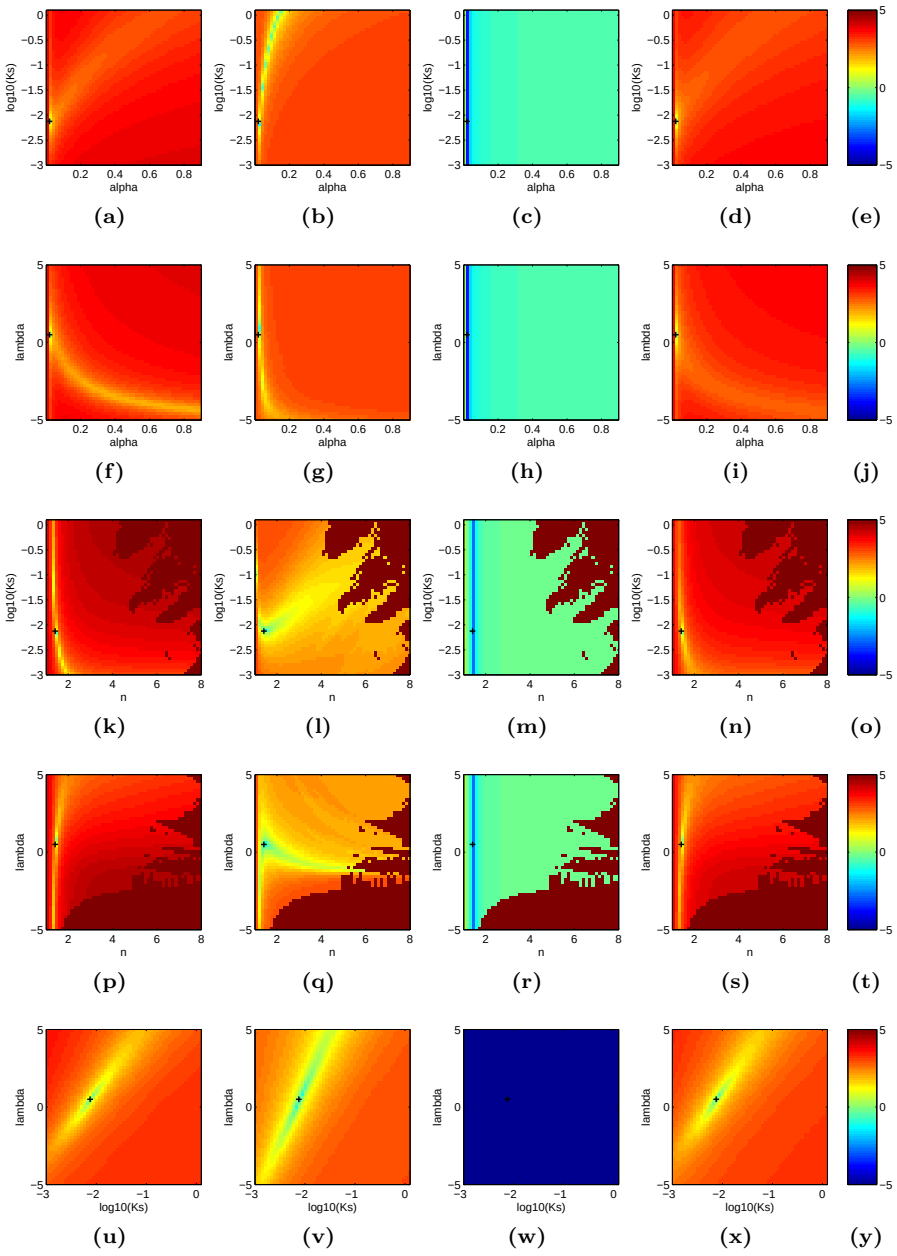

Figure A.3: Response surfaces of the different objectives of OF for couples of parameters of the MV model. For some combinations of parameters, the numerical solution does not converge ($\boldsymbol{\phi} \geq 10^5$).

Appendix B

Profile descriptions

The following pages consist of tables describing each of the eleven soil profiles referred to in Chapter 4.

General characteristics about the location of the soil profiles are first given. Each horizon is then described following the guidelines proposed by the FAO (2006). A picture of the soil profile is provided to help the reader visualise the described features.

Profile: LAU1	Date: 14/05/2008	Authors: Delvaux, B., Javaux, M., Poncelet, M.		
Weather conditions: sunny Land use (natural vegetation): beech forest, ferns History: once cropped (before 270 AC), exploited, classified 1994			Comments: Manganese, rust and white spots and withdrawal slits.	
Location: Bois de Lauzelle, Louvain-la-Neuve, Brabant Wallon, Belgium	GPS coord.: [m] x: 167.173 y:151.967 z: 166	Soil type: Aba(b)	Topography: class 1 - no slope	Drainage: class 3 - moderate
Geology: loess on Bruxellien Sand		Pierrosity: class 0 - none or very little		

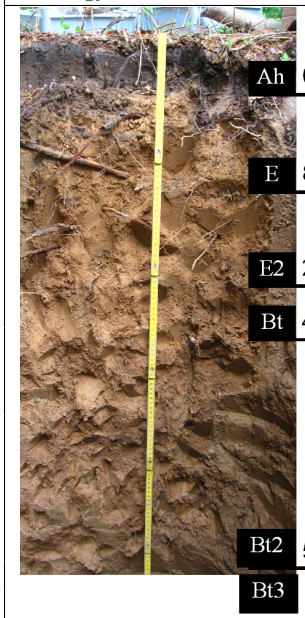

The Ah horizon's colours can be described as 10 YR 5/2, grayish yellow brown when dry and 10 YR 2/2, brown black when moist. It has a texture ratio of 29-50-21, and a coarse, weak, granular structure. It is very porous with a small bulk density, containing an important micro-fauna. The roots hold the grains together. The pH is 4.3.

The E horizon is vulnerable to compaction with dry and moist colors defined as 10 YR 7/4, dull yellowish orange - 10 YR 5/6, yellowish brown, with a texture ratio of 17-70-13, a fine and weak subangular blocky structure and more or less plane fractures. It is porous and has a high root density with a horizontal resistance of 3.0 +/- 0.1 kg/cm^2 and a pH of 4.5.

The dry and moist colors of the E2 horizon are 10 YR 7/4, dull yellowish orange - 10 YR 5/6, yellowish brown. The texture ratio is 17-70-13 with a medium and weak subangular blocky structure. A high root density and porosity gives it a horizontal resistance of 1.9 +/- 0.4 kg/cm^{2}and a pH of 4.4.

* The structure of the Bt horizon is described as very coarse, very strong and prismatic. It is not very porous with very little roots and a horizontal resistance of 4.8 +/- 0.4 kg/cm^2. This horizon is the most compact containing some black spots due to poor drainage.

The dry and moist colors of the Bt2 horizon are 10 YR 7/4, dull yellowish orange - 10 YR 5/6, yellowish brown with a texture ratio of 14-68-18 and a very coarse and strong angular blocky structure. It is porous and has few roots, with a horizontal resistance of 4.4 +/- kg/cm^2 and a pH of 4.3.

* Bt3 horizon's structure is prismatic that breaks up into coarse, weak angular blocks. It is highly porous with few roots and a resistance of 3.6 +/- 0.6 kg/cm^2.

Profile: LAU2	Date: 14/05/2008	Authors: Delvaux, B., Javaux, M., Poncelet, M.		
Weather conditions: sunny Land use (natural vegetation): beech forest History: never cropped, exploited, classified in 1994			Comments: No worm holes, high acidity and large humic horizon.	
Location: Bois de Lauzelle, Louvain-la-Neuve, Brabant Wallon, Belgium	GPS coord.: [m] x: 166383 y:151923 z: 130	Soil type: Aba(b)	Topography: class 4 - 3-25% slope	Drainage: class 3 - moderate
Geology: loess on Bruxellien Sand		Pierrosity: class 0 - none or very little		

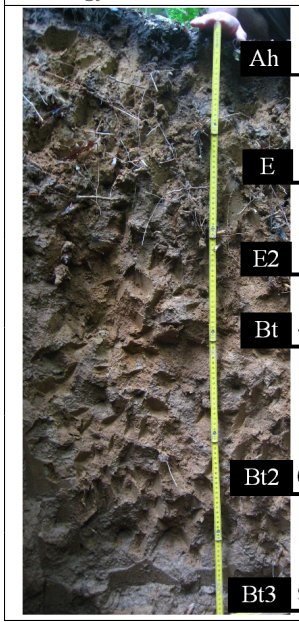

The Ah horizon has dry and moist colours as 10 YR 3/1, brown black - 10 YR 2/1, black, a texture ratio of 17-70-13 and mix of coarse, moderate, granular and medium, moderate subangular blocky structure with plane fractures. This horizon is not very porous but contains a lot of organic matter and has a pH of (4.1).

The E horizon, subject to compaction, is 10 YR 7/4, dull yellowish orange when dry and 10 YR 6/4, dull yellowish orange when moist. The texture ratio is 15-74-11 and the structure is defined as fine and weak subangular blocks with more or less plane fractures. The macroporosity is visible and it has a high root density with a pH of 4.4.

The E2 horizon has dry and moist colours as 10 YR 7/4, dull yellowish orange - 10 YR 6/4, dull yellowish orange with a texture ratio of 15-71-14 and a fine, very weak subangular blocky structure. It is porous, has a high root density and a pH of 4.4.

The Bt horizon has dry and moist colours as 10 YR 6/6, bright yellowish brown - 10 YR 5/6, yellowish brown with a texture ratio of 11-64-25 and a medium and moderate angular blocky structure. Few roots are to be found, in this porous horizon, characterized by a pH of 4.3.

The Bt2 horizon has colours as 10 YR 6/6, bright yellowish brown - 10 YR 5/6, yellowish brown and the texture is divided as 12-61-27. The structure is prismatic but the aggregates break up into coarse and strong blocks with plane fractures. This horizon is porous, with a low root density, flat fractures and has a pH of 4.3.

The Bt3 horizon is 10 YR 6/6, bright yellowish brown when dry and 10 YR 5/6, yellowish brown when moist. It is characterized by a texture ratio of 13-65-22 and a coarse , moderate and angular blocky structure. It is also porous with a few thin roots and a pH of 4.5.

<table>
<tr><td>Profile: MARP1</td><td>Date: 13/05/2008</td><td colspan="3">Authors: Delvaux, B., Javaux, M., Poncelet, M.</td></tr>
<tr><td colspan="3">Weather conditions: sunny
Land use (natural vegetation): pasture (Lolium perenne, Taraxacum officinale)
History: pasture since 1980, previously cropped</td><td colspan="3">Comments:
More horizontal than vertical dessication slits, old plough sole visible.</td></tr>
<tr><td>Location:

Centre A. de Marbais, Coroy, Brabant Wallon, Belgium</td><td>GPS coord.: [m]
x: 169 308
y:150 972
z: 176</td><td>Soil type:
Aba(b)</td><td>Topography:
class 2 - small slope</td><td>Drainage:
class 4 - normal</td></tr>
<tr><td colspan="2">Geology: loess on Bruxellien Sand</td><td colspan="3">Pierrosity: class 0 - none or very little; rocks at the Bt2/C interface</td></tr>
<tr><td> 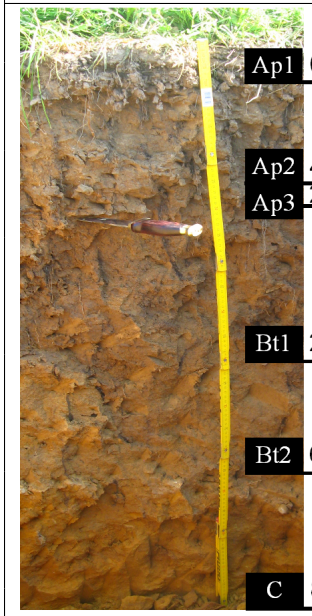
</td><td colspan="4">* The Ap1 horizon has a medium and weak granular structure. It is very porous in all directions and has a high root density, presenting rust spots and drainage problems.
The dry and moist colours of the Ap2 are 10 YR 6/4 dull yellowish orange - 10 YR 3/3 dull brown, with a texture ratio of 11-66-23 and a coarse and weak subangular blocky structure. This horizon is porous and has roots growing vertically and horizontally and has a pH of 6.4.
* The plough sole (Ap3) can be described as a fine and strong platy structure with clean fractures. There are no visible macropores but some vertical roots and worm channels. There are signs of poor drainage.
The dry and moist colours of the Bt1 horizon are 10 YR 6/6, bright yellowish brown - 10 YR 5/4, dull yellowish brown and the texture ratio is 9-60-31 and a structure described as a heterogenous, medium and weak prismatic with irregular fractures. This horizon is porous with some vertical roots and worm holes. It has a pH of 6.7 and is moist.
The dry and moist colours of the Bt2 horizon are 10 YR 6/6, bright yellowish brown - 10 YR 5/6, yellowish brown and the texture ratio is 10-66-24 with a very coarse and moderate angular blocky structure and irregular fractures. It is porous with some macropore diameters reaching 1cm. There are some vertical roots and stones. The pH is 7.1
The colours of the Bruxellien Sand are 10 YR 6/8, bright yellowish brown when dry and 10 YR 6/8, bright yellowish brown when moist. The texture ratio is 90-3-7 and the structure is characterised as very coarse, strong and angular blocky. There are few visible macropores but no roots and the pH is 7.2.</td></tr>
</table>

<table>
<tr><td>Profile: MARP2</td><td>Date: 16/03/2009</td><td colspan="3">Authors: Servais, M., Weynants, M.</td></tr>
<tr><td colspan="3">Weather conditions: dry and cloudy, 12 °C , weak wind; previous days dry
Land use (natural vegetation): pasture (Lolium perenne, bryophytes)
History: pasture since 1980, previously cropped</td><td colspan="2">Comments:</td></tr>
<tr><td>Location:

Centre A. de Marbais, Coroy, Brabant Wallon, Belgium</td><td>GPS coord.: [m]
x: 169 299
y:150 968
z: 182</td><td>Soil type:
Aba(b)</td><td>Topography:
class 2 - small slope</td><td>Drainage:
class 4 - normal</td></tr>
<tr><td colspan="2">Geology: loess on Bruxellien Sand</td><td colspan="3">Pierrosity: class 0 - none or very little; Pebbles at the Bt/D interface</td></tr>
<tr><td> 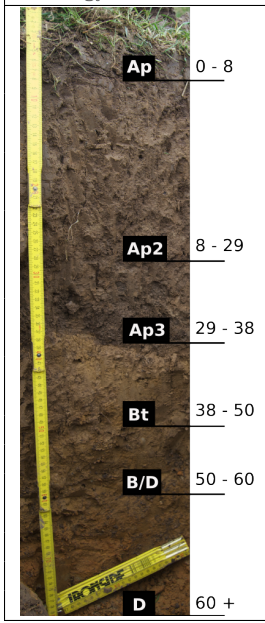
</td><td colspan="4">* The Ap1 horizon has a moderate fine blocky structure. Its consistence when dry is friable. It has few fine pores and many fine roots. It shows many earthworms channels. Its texture is 12-70-18 and it has a pH of 6.9.
* The Ap2 horizon has a moderate fine blocky structure and a firm consistence when moist. It has few fine pores and few to common fine roots. Its texture ratio is 13-68-19 and its pH is 7.3.
* The plough sole (Ap3) has the same structure as the horizons above, but is more resistent to penetration.
* The Bt horizon has a strong fine blocky structure and a firm consistence when moist. It has few very fine pores, common abundance of earthworm channels and few very fine roots. Its texture ratio is 11-68-21 and it has a pH of 7.9.
* The interface between the Bt horizon and the underlying clay-sand bedrock consists in rounded coarse gravels.
* The bedrock has a texture ratio of 52-15-33 and the structure is characterised as very coarse, strong and angular blocky. There are few visible pores and no roots.</td></tr>
</table>

Profile: MARC1	Date: 13/05/2008	Authors: Poncelet, M.		
Weather conditions: cloudy, dry Land use (natural vegetation): bare cropland History: barley, manure, mustard (intermixed), chicorey (april)			Comments: More horizontal than vertical dessication slits.	
Location: Centre A. de Marbais, Coroy, Brabant Wallon, Belgium	GPS coord.: [m] x: 168 870 y:151 163 z: 176	Soil type: Aba(b)	Topography: class 1 - no slope	Drainage: class 4 - normal
Geology: loess on Bruxellien Sand		Pierrosity: class 0 - none or very little; rocks at the Bt2/BC interface		
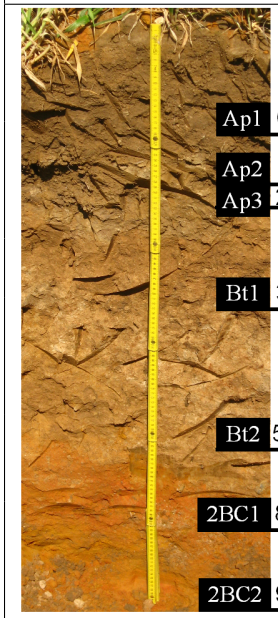	The dry and moist colours are 10 YR 5/3, dull yellow brown - 10 YR 4/4, brown, with a texture ratio of 15-64-21 and a mix of medium and weak subangular blocky and granular structure presenting irregular fractures. This horizon is highly porous with a high root density and some worm channels. It has a pH of 8.1 and is very heterogeneous horizontally due to soil tillage. The colours are defined as 10YR 6/4, dull yellow orange - 10 YR 4/3, dull yellowish brown with a texture ratio of 16-64-20 and a prismatic tendency that breaks up into a medium and strong subangluar blocky structure. It is porous with a fair amount of roots and some worm channels. It has a pH of 8.1 and is very heterogeneous with thatches intermixed. * This horizon represents the plough sole and is not continuous and presents a very coarse and strong platy structure. It is not porous and only a few roots penetrate it. This compact pedological horizon has dry and moist colours of 10YR 6/4, dull yellow orange - 10 YR 5/3, dull yellowish brown, with a texture ratio of 14-65-21 and a very coarse and strong angular blocky structure. The fractures are clear, internal pores are present and there are vertical roots and some worm channels. Its pH is 8.1. The colors are defined as 10 YR 7/3, dull yellow orange - 10 YR 5/4, dull yellowish brown with a texture ratio of 13-65-22 with a medium and moderate angular blocky structure. It has a vertical macroporosity with root and worm channels. Its pH is 8.1. The colours of this Bruxellian Sand are 10 YR 6/8, bright yellow brown - 7.5 YR 5/6, bright brown and its texture fraction is 57-25-18, presenting a massive structure that breaks up into very coarse and strong angular blocks with irregular fractures. It has very few macropores, no roots or worm holes and has a pH of 7.5. * The structure is defined as angular blocky, medium and weak. The texture is mainly coarse sand, presenting no roots or worm channels. The horizon is very moist.			

Profile: MARC2	Date: 25/03/2009	Authors: Servais, M., Weynants, M.		
Weather conditions: rainy, 10 °C ; past days rainy Land use (natural vegetation): cropland (*Zea mais*), tilled bare soil History: cropped			Comments: close to the motorway	
Location: Centre A. de Marbais, Coroy, Brabant Wallon, Belgium	GPS coord.: [m] 50°40'09.58" 4°38'10.73" E Elevation: 134 m	Soil type: Aba(b)	Topography: class 1 - no slope	Drainage:
Geology: loess on Bruxellien Sand		Pierrosity: class 0 - none or very little; some gravel at the bedrock interface		

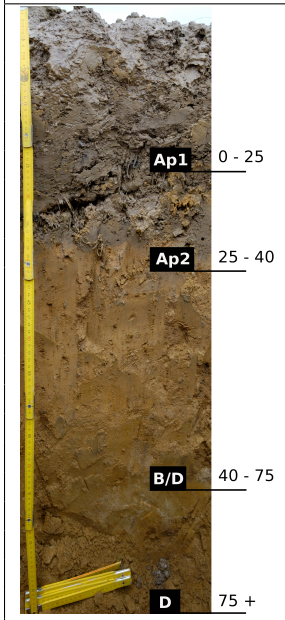

* The Ap1 horizon has a moderate fine to medium blocky structure. It contains some remaining vegetation. Its texture is 42-36-22 and it has a pH of 6.9.

* The Ap2 horizon has a moderate fine blocky structure. Its texture ratio is 42-45-13 and its pH is 7.3.

* The shallow bedrock has a weak blocky structure. There are few visible pores and very few very fine roots. There are very few biological features. It has a texture ratio of 70-22-8.

* The underlying bedrock has a texture ratio of 89-0-11.

<table>
<tr><td>Profile: MARC3</td><td>Date: 07/07/2009</td><td colspan="3">Authors: Beff, L., Pouglio, J., Weynants, M.</td></tr>
<tr><td colspan="3">Weather conditions: partially cloudy, 20 °C ; past days sunny and hot, with storms
Land use (natural vegetation): cropland (Zea mais)
History: cropped</td><td colspan="3">Comments:</td></tr>
<tr><td>Location:

Centre A. de Marbaix, Coroy, Brabant Wallon, Belgium</td><td>GPS coord.: [m]
x: 50°40’03.35” N
4°38’26.73” E
Elevation: 140 m</td><td>Soil type:
Aba(b)</td><td>Topography:
class 2 - 0.2-0.5%</td><td>Drainage:</td></tr>
<tr><td colspan="2">Geology: loess on Bruxellien Sand</td><td colspan="3">Pierrosity: class 0 - none or very little</td></tr>
<tr><td> 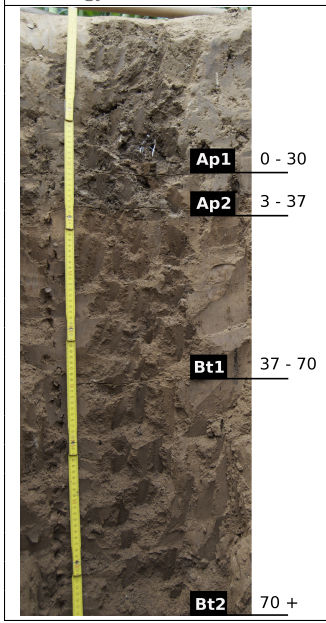
</td><td colspan="4">* The Ap1 horizon has a strong blocky angular structure. It has many roots. Its texture is 3-76-21 and it has a pH of 7.1.
* The Ap2 horizon is the plough sole. It is more resistent to penetration than the above horizon.
* The Bt1 horizon has a strong blocky angular structure. Its texture ratio is 1-67-32 and ihas a pH of 7.7.
* The Bt2 horizon has a weaker blocky structure. It has a texture ratio of 1-74-25 and a pH of 7.7.</td></tr>
</table>

Profile: GEN1	Date: 18/03/2009	Authors: Servais, M., Weynants, M.		
Weather conditions: sunny, 12 °C ; past days dry, with nightly frost Land use (natural vegetation): cropland (remains of *Zea mais*) History: cropped, recently turned to no tillage			Comments:	
Location: Gentinnes, Brabant Wallon, Belgium	GPS coord.: 50°34'19.79" N 4°35'46.75" E Elevation: 138 m	Soil type: Aba(b)	Topography: class 2 - 0.2-0.5%	Drainage:
Geology: loess on Bruxellien Sand		Pierrosity: class 0 - none or very little		
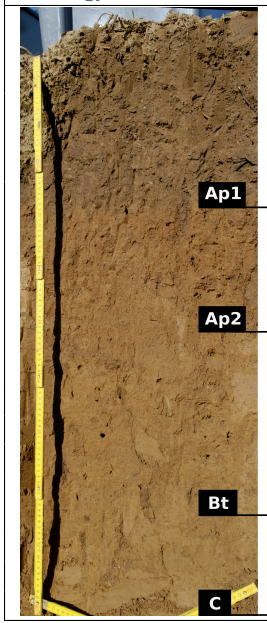	* The Ap horizon has a strong medium to coarse blocky angular structure. Its consistence whane moist is firm. It has few to common fine to medium pores and few medium roots. It has commonly abundant earthworm channels and some insects nests. Its texture is 10-71-19 and it has a pH of 7.8. * The Bt1 horizon has a moderate to strong medium prismatic structure. It is firm to friable when moist. It has common to many fine to very fine pores and very few fine roots. It has commonly abundant earthworm channels. Its texture ratio is 5-67-28 and its pH is 7.0. * The Bt2 horizon has a moderate to strong medium prismatic structure. It is friable when moist. It has many very fine pores and no roots, but earthworm channels. Its texture ratio is 9-67-24 and it has a pH of 7.8. * The Bt3 horizon has a prismatic to blocky angular structure. It has a firm consistence when moist. It has common very fine pores and no roots. It shows few to none biological features. It has a texture ratio of 9-67-2.			

<table>
<tr><td colspan="2">Profile: LLN1</td><td>Date: 127/02/2008</td><td colspan="2">Authors: Poncelet, M.</td></tr>
<tr><td colspan="3">Weather conditions: cloudy, dry
Land use (natural vegetation): bare cropland
History: barley, manure, mustard (intermixed), chicorey (april)</td><td colspan="2">Comments:</td></tr>
<tr><td>Location:

Louvain-la-Neuve, Brabant Wallon, Belgium</td><td>GPS coord.: [m]
x: 167 421

y:151 850
z: 178</td><td>Soil type:
Aba</td><td>Topography:
class 2 - slight slope (2-6%)</td><td>Drainage:
class 4 - normal</td></tr>
<tr><td colspan="2">Geology: loess on Bruxellien Sand</td><td colspan="3">Pierrosity: class 0 - none or very little</td></tr>
<tr><td colspan="2"> 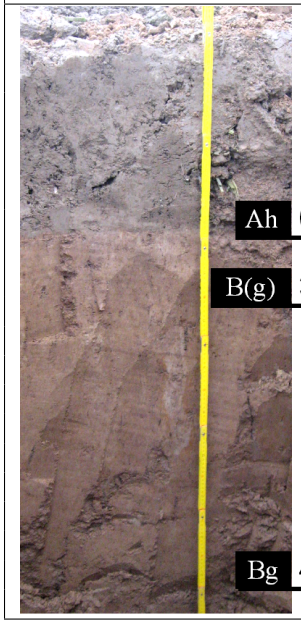
</td><td colspan="3">The Ap horizon has dry and moist colours as 10 YR 6/4, dull yellowish orange - 10 YR 4/4, brown. The texture ratio is 11-73-16 and subangular blocky structure. This porous horizon presents roots and worm channels with an average horizontal resistance of 3 +/- 0.3 kg/cm^2 and a pH of 6.9.
The dry and moist colours of horizon B(g) are 10 YR 6/4, dull yellowish orange - 10 YR 5/6, yellowish brown and the texture ratio is 5-70-25 with a subangular blocky strucutre. This horizon is highly porous containing roots and worm channels and an averagz resistance of 4.3 +/- 0.3 kg/cm^2 and a pH of 7.0.
The dry and moist colours of horizon Bg can be defined as 10 YR 6/6, bright yellowish brown - 10 YR 4/6, brown with a texture ratio of 10-67-23 and a subangular structure. It is also porous, containing roots and worm holes, a resistance of 3 +/- 0.5kg/cm^2 and a pH of 7.2.</td></tr>
</table>

<table>
<tr><td>Profile: MSG1</td><td>Date: 13/05/2008</td><td colspan="3">Authors: Delvaux, B., Javaux, M., Poncelet, M.</td></tr>
<tr><td colspan="3">Weather conditions: sunny
Land use (natural vegetation): old cropland (wheat and Lolium perenne)
History: last cropped in 2007, left untouched since</td><td colspan="2">Comments: The profile was not excavated properly and was facing north, which made the description difficult.</td></tr>
<tr><td>Location:

Mont-Saint-Guibert, Brabant Wallon, Belgium</td><td>GPS coord.: [m]
x: 168 811
y:149 100
z: 177</td><td>Soil type:
Aba</td><td>Topography:
class 1 - no slope</td><td>Drainage:
class 4 - normal</td></tr>
<tr><td colspan="2">Geology: loess on Bruxellien Sand</td><td colspan="3">Pierrosity: class 0 - none or very little</td></tr>
<tr><td> 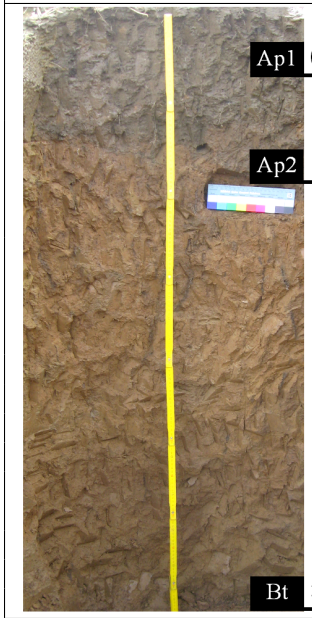
</td><td colspan="4">The Ap horizon's colour can be described as 10 YR 6/4, dull yellowish orange when dry and 10 YR 4/4, brown when moist, with a texture ratio of 11-70-18 and a fine, strong platy structure on the surface. This horizon is not very porous, has a high root density and some worm channels, with a pH of 8.1. There are signs of poor drainage at the surface.
This dry and moist colours of the Ap2 horizon are 10 YR 6/6, bright yellowish brown ? 10 YR 4/6, brown, with a texture ratio of 9-68-23 and a medium moderate blocky structure with a prismatic tendency. This horizon is slightly porous, with flat fractures and some root and worm holes with a pH of 7.9.
The Bt horizon has dry and moist colors as follows: 10 YR 6/6, bright yellowish brown ? 10 YR 5/6, yellowish brown, with a texture ratio of 5-73-22 and a very coarse, strong angular blocky structure with a prismatique tendency. It also presents large vertical macropores covered by worm excreta and has a pH of 7.7. There are also white spots at different areas on the horizon.</td></tr>
</table>

<table>
<tr><td>Profile: SMG1</td><td>Date: 13/05/2008</td><td colspan="3">Authors: Delvaux, B., Javaux, M., Poncelet, M.</td></tr>
<tr><td colspan="3">Weather conditions: sunny
Land use (natural vegetation): cropland (sugar beet)
History: sept. 2008: mustard + 7 tons chicken feces; sept. 2008: wheat, thatches intermixed</td><td colspan="3">Comments:
This field has not been tilled for at least 25 years, still a plough sole remains. It is also characterised by a very good drainage.</td></tr>
<tr><td>Location:

Mont-Saint-Guibert, Brabant Wallon, Belgium</td><td>GPS coord.: [m]
x: 168 811
y:149 100
z: 177</td><td>Soil type:
Aba(b)</td><td>Topography:
class 1 - no slope</td><td>Drainage:
class 4 - normal</td></tr>
<tr><td colspan="2">Geology: loess on Bruxellien Sand</td><td colspan="3">Pierrosity: class 0 - none or very little</td></tr>
<tr><td> 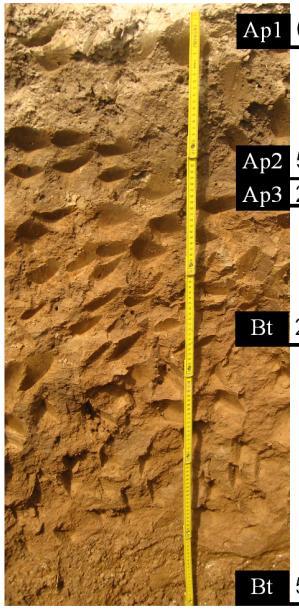
</td><td colspan="4">* The Ap1 horizon has very coarse, weak and granular structure, thus, very porous with many small roots and some worm holes.
The dry and moist colours of the Ap2 horizon can be described as 10 YR 5/4, dull yellow brown ? 10 YR 4/4, brown, with a texture ratio of 11-69-20. It has a mix of a medium, weak , granular and a coarse, weak subangular blocky structure. It has irregular fractures, is porous and has root and worm holes. The pH is 7.3. The horizon is somewhat heterogeneous due to past laboring.
* The structure of the old and discontinous plough sole is very coarse, moderate and platy. It is porous with root and worm holes disecting it vertically.
The colour of the Bt1 horizon can be defined as 10 YR 5/6, yellowish brown when dry and 10 YR 4/6, brown when moist. It hsa a texture ratio of 6-70-24 and a medium, moderate angular blocky strucutre with a prismatic tendency. The fractures are clean and smooth. It is porous with vertical root and worm holes. The pH is 7.6 and thee are traces of rust and manganese spots; a sign of poor drainage.
The Bt2 horizon is 10 YR 6/4, dull yellowish brown when dry and 10 YR 5/6, yellowish brown when moist and has a texutre ratio of 8-68-24 with a very coarse and strong prismatique strucutre with irregular fractures. There are large vertical macropores from roots and worms. The pH is 7.7 and there are rust spots scattered throughout the horizon.</td></tr>
</table>

References

Armas-Espinel, S., Hernández-Moreno, J. M., Muñoz-Carpena, R., and Regalado, C. M. 2003. Physical properties of "sorriba"-cultivated volcanic soils from Tenerife in relation to andic diagnostic parameters. Geoderma, 117(3-4):297–311.

Arya, L. M., Farrell, D. A., and Blake, G. R. 1975. A field study of soil water depletion patterns in presence of growing soy bean roots. I. Determination of hydraulic properties of the soil. Soil Science Society of America Journal, 39:424–430.

Assouline, S., Tessier, D., and Bruand, A. 1998. A Conceptual Model of the Soil Water Retention Curve. Water Resour. Res., 34:223–231.

Bagarello, V., Iovino, M., and Tusa, G. 2000. Factors affecting measurement of the near-saturated soil hydraulic conductivity. Soil Science Society Of America Journal, 64(4):1203–1210.

Botros, F. E., Harter, T., Onsoy, Y. S., Tuli, A., and Hopmans, J. W. 2009. Spatial variability of hydraulic properties and sediment characteristics in a deep alluvial unsaturated zone. Vadose Zone Journal, 8(2):276–289.

Bouma, J. 1989. Using soil survey data for quantitative land evaluation. Advances in Soil Science, 9:177–213.

Bouma, J., Belmans, C., Dekker, L. W., and Jeurissen, W. J. M. 1983. Assessing the suitability of soils with macropores for subsurface liquid waste disposal. Journal of Environmental Quality, 12(3):305–311.

Brooks, R. H. and Corey, A. T. 1964. Hydraulic properties of porous media. Hydrology Papers (Colorado State University), 3.

Chadwick, O. A., Gavenda, R. T., Kelly, E. F., Ziegler, K., Olson, C. G., Elliott, W. C., and Hendricks, D. M. 2003. The impact of climate on the biogeochemical functioning of volcanic soils. Chemical Geology, 202(3-4):195–223.

Colmet-Daage, F. and Gautheyrou, J. 1974. Soil associations on volcanic material in Tropical America with special reference to Martinique and Guadeloupe. Trop. Agric. (Trinidad), 51(2):121–128.

Colmet-Daage, F. and Lagache, F. 1965. Caractéristiques de quelques groupes de sols dérivés de roches volcanique aux Antilles Françaises. Cahiers de l'ORSTOM, Série Pédologie, 8(2):91–121.

Cornelis, W. M., Ronsyn, J., Van Meirvenne, M., and Hartmann, R. 2001. Evaluation of pedotransfer functions for predicting the soil moisture retention curve. Soil Science Society Of America Journal, 65(3):638–648.

Cornelis, W. M., Khlosi, M., Hartmann, R., Van Meirvenne, M., and De Vos, B. 2005. Comparison of Unimodal Analytical Expressions for the Soil-Water Retention Curve. Soil Science Society of America Journal, 69:1902–1911.

Dexter, A. R., Czyz, E. A., Richard, G., and Reszkowska, A. 2008a. A user-friendly water retention function that takes account of the textural and structural pore spaces in soil. Geoderma, 143:243–253.

Dorel, M. 2001. *Effet des pratiques culturales sur les propriétés physiques des sols volcaniques de Guadeloupe et influence sur l'enracinement du bananier*. Thèse présentée pour l'obtention du grade de docteur en sciences agronomiques et ingénierie biologique, Université catholique de Louvain, Belgique.

Dorel, M., Roger-Estrade, J., Manichon, H., and Delvaux, B. 2000. Porosity and soil water properties of Caribbean volcanic ash soils. Soil Use And Management, 16(2):133–140.

Durner, W. 1994. Hydraulic Conductivity Estimation For Soils With Heterogeneous Pore Structure. Water Resources Research, 30(2):211–223.

Durner, W., Schultze, B., and Zurmuhl, T. 1999. State-of-the-art in inverse modeling of inflow/outflow experiments. In van Genuchten et al., M., editor, *Proc. Int. Workshop on Characterizatin and Measurements of the Hydraulic Properties of Unsaturated Porous Media*, volume 1, pages 661–681. University of California, Riverside, CA.

Durner, W., Jansen, U., and Iden, S. C. 2008. Effective hydraulic properties of layered soils at the lysimeter scale determined by inverse modelling. European Journal Of Soil Science, 59:114–124.

Eching, S. O. and Hopmans, J. W. 1993. Optimization Of Hydraulic Functions From Transient Outflow And Soil-Water Pressure Data. Soil Science Society Of America Journal, 57(5):1167–1175.

FAO. 2006. *Guidelines for Soil Description*. World Soil Resources Reports. FAO, Rome, fourth edition.

Gardner, W. R. 1958. Some steady state solutions of the unsaturated moisture flow equation with application to evaporation from a water table. Soil Science, 85:228–232.

Gautronneau, Y. and Manichon, H. 1987. *Guide méthodique du profil cultural*. CEREF-ISARA/GEARA-INAPG.

Gerke, H. H. and van Genuchten, M. T. 1993a. A Dual-Porosity Model For Simulating The Preferential Movement Of Water And Solutes In Structured Porous-Media. Water Resources Research, 29(2):305–319.

Gerke, H. H. and van Genuchten, M. T. 1996. Macroscopic representation of structural geometry for simulating water and solute movement in dual-porosity media. Advances In Water Resources, 19(6):343–357.

Haase, D., Fink, J., Haase, G., Ruske, R., Pécsi, M., Richter, H., Altermann, M., and Jäger, K.-D. 2007. Loess in Europe–its spatial distribution based on a European Loess Map, scale 1:2,500,000. Quaternary Science Reviews, 26(9-10):1301 – 1312.

Henriet, C., Jaeger, N. D., Dorel, M., Opfergelt, S., and Delvaux, B. 2008. The reserve of weatherable primary silicates impacts the accumulation of biogenic silicon in volcanic ash soils. Biogeochemistry, 90:209–223.

Hollenbeck, K. J. and Jensen, K. H. 1998a. Experimental evidence of randomness and nonuniqueness in unsaturated outflow experiments designed for hydraulic parameter estimation. Water Resources Research, 34(4):595–602.

Hollenbeck, K. J. and Jensen, K. H. 1998b. Maximum-likelihood estimation of unsaturated hydraulic parameters. Journal of Hydrology, 210(1-4):192–205.

Hopmans, J. W., Simunek, J., Romano, N., and Durner, W. 2002. *Methods of Soil Analysis, Physical Methods*, volume 4, chapter Simultaneous determination of water transmission parameters and retention properties : Inverse methods. SSSA, Madison, WI.

Huyer, W. and Neumaier, A. 1999. Global optimization by multilevel coordinate search. Journal of Global Optilization, 14:331–355.

Iden, S. C. and Durner, W. 2007. Free-form estimation of the unsaturated soil hydraulic properties by inverse modeling using global optimization. Water Resources Research, 43(7):W07451.

Ippisch, O., Vogel, H.-J., and Bastian, P. 2006. Validity limits for the van Genuchten-Mualem model and implications for parameter estimation and numerical simulation. Advances in Water Resources, 29(12):1780–1789.

Jarvis, N. J. 2007. A review of non-equilibrium water flow and solute transport in soil macropores: principles, controlling factors and consequences for water quality. European Journal Of Soil Science, 58(3):523–546.

Javaux, M. and Vanclooster, M. 2006. Scale-dependency of the hydraulic properties of variably saturated heterogeneous sand subsoil. Journal of Hydrology, 327:376–388.

Kool, J. B. and Parker, J. C. 1988. Analysis of the Inverse Problem for Transient Unsaturated Flow. Water Resources Research, 24(6):817–830.

Kosugi, K. 1996. Lognormal Distribution Model for Unsaturated Soil Hydraulic Properties. Water Resources Research, 32:2697–2703.

Köhne, J. M., Köhne, S., and Simunek, J. 2009. A review of model applications for structured soils: a) Water flow and tracer transport. Journal of Contaminant Hydrology, 104(1-4):4 – 35. Preferential Flow.

Laloy, E., Weynants, M., Bielders, C., Vanclooster, M., and Javaux, M. 2010a. How efficient are one-dimensional models to reproduce the hydrodynamic behavior of structured soils subjected to multi-step outflow experiments ? Journal of Hydrology, 393:37–52.

Lambot, S., Javaux, M., Hupet, F., and Vanclooster, M. 2002. A global multilevel coordinate search procedure for estimating the unsaturated soil hydraulic properties. Water Resources Research, 38(11):1224–.

Larsbo, M. and Jarvis, N. 2003. MACRO5.0. A model of water flow and solute transport in macroporous soil. Technical description Studies in the Biogeophysical Environment, Emergo 2003:6, Department of Soil Sciences, SLU, Uppsala, Sweden.

Levene, H. 1960. *Contributions to probability and statistics: Essays in Honor of Harold Hotelling*, chapter Robust tests for equality of variances, pages 278–292. Stanford University Press, Palo Alto, CA.

Lilly, A. 2000. The relationship between field-saturated hydraulic conductivity and soil structure: development of class pedotransfer functions. Soil Use and Managment, 16(1):56–60.

Lilly, A. and Lin, H. 2004. Using soil morphological attributes and soil structure in pedotransfer functions. In Pachepsky, Y. and Rawls, W., editors, *Development of pedotransfer functions in soil hydrology*, volume 30 of *Developments in soil science*, pages 115–141. Elsevier, Amsterdam, The Netherlands.

Lin, H., Bouma, J., Wilding, L. P., Richardson, J. L., Kutilek, M., and Nielsen, D. R. 2005. Advances in hydropedology. Advances In Agronomy, Vol 85, 85:1–89.

Lin, H., Bouma, J., Pachepsky, Y., Western, A., Thompson, J., van Genuchten, R., Vogel, H.-J., and Lilly, A. 2006a. Hydropedology: Synergistic integration of pedology and hydrology. Water Resources Research, 42:W05301.

Lin, H., Bouma, J., and Pachepsky, Y. A. 2006b. Revitalizing pedology through hydrology and connecting hydrology to pedology. Geoderma, 131:255–256.

Lin, H. S., McInnes, K. J., Wilding, L. P., and Hallmark, C. T. 1999 a. Effects of soil morphology on hydraulic properties: I. Quantification of soil morphology. Soil Science Society of America Journal, 63:948–954.

Lin, H. S., McInnes, K. J., Wilding, L. P., and Hallmark, C. T. 1999 b. Effects of soil morphology on hydraulic properties: II.Hydraulic pedotransfer functions. Soil Science Society of America Journal, 63:955–961.

Mallants, D., Mohanty, B., Vervoort, A., and Feyen, J. 1997a. Spatial analysis of saturated hydraulic conductivity in a soil with macropores. Soil Technology, 10:115–131.

Mallants, D., Tseng, P.-H., Vanclooster, M., and Feyen, J. 1998. Predicted drainage for a sandy loam soil: sensitivity to hydraulic property description. Journal of Hydrology, 206(1-2):136–148.

McKeague, J. A., Wang, C., and Topp, G. C. 1982. Estimating saturated hydraulic conductivity from soil morphology. Soil Science Society of America Journal, 46:1239–1244.

Melebeck, B. 2009. *Multistep outflow*. Bsc thesis, Institut d'Etudes Suprérieures de Namur (I.E.S.N).

Mermoud, A. and Xu, D. 2006. Comparative analysis of three methods to generate soil hydraulic functions. Soil and Tillage Research, 87(1):89–100.

Mizota, C. and Van Reeuwijk, L. 1989. Clay mineralogy and chemistry of soils formed in volcanic material in diverse climatic regions.

Mualem, Y. 1976. A new model for predicting the hydraulic conductivity of unsaturated porous media. Water Resources Research, 12(3):513–522.

Ndayiragije, S. and Delvaux, B. 2004. Selective sorption of potassium in a weathering sequence of volcanic ash soils from Guadeloupe, French West Indies. CATENA, 56(1-3):185–198.

Nielsen, D. R., Biggar, J. W., and Erh, K. T. 1973. Spatial variability of field-measured soil-water properties. Hilgardia, 42(7):215–259.

Pachepsky, Y. and Schaap, M. 2004. Data mining and exploration techniques. In Pachepsky, Y. and Rawls, W. J., editors, *Development of pedotransfer functions in hydrology*, volume 30 of *Development in soil science*, pages 21–32. Elsevier, The Netherlands.

Pachepsky, Y. A. and Rawls, W. J. 2003. Soil structure and pedotransfer functions. European Journal of Soil Science, 54:443–451.

Pachepsky, Y. A., Rawls, W. J., and Lin, H. S. 2006b. Hydropedology and pedotransfer functions. Geoderma, 131:308–316.

Parfitt, R. and Childs, C. 1988. Estimation of forms of Fe and Al-a review, and analysis of contrasting soils by dissolution and Mossbauer methods. Australian Journal of Soil Research, 26(1):121–144.

Parfitt, R. and Kimble, J. 1989. Conditions for formation of allophane in soils. Soil Science Society of America journal (USA), 40(2):359–369.

Parfitt, R. L. 1990. Allophane in New Zealand - A review. Australian Journal Of Soil Research, 28:343–360.

Peters, A. and Durner, W. 2006. Improved estimation of soil water retention characteristics from hydrostatic column experiments. Water Resources Research, 42:W11401.

Priesack, E. and Durner, W. 2006. Closed-form expression for the multi-modal unsaturated conductivity function. Vadose Zone Journal, 5(1):121–124.

Puhlmann, H., Von Wilpert, K., Lukes, M., and Droge, W. 2009. Multistep outflow experiments to derive a soil hydraulic database for forest soils. European Journal of Soil Science, 60(5):792–806.

Reid, I. 1973. The choice of assumed particle density values in soil tests. Area, 5(1):10–12.

Richards, L. 1931. Capillary conduction of liquids through porous mediums. Physics, 1:318–333.

Richter, D. D. and Mobley, M. L. 2009. Monitoring Earth's Critical Zone. Science, 326(5956):1067–1068.

Romano, N. and Santini, A. 1997. Effectiveness of using pedo-transfer functions to quantify the spatial variability of soil water retention characteristics. Journal Of Hydrology, 202(1-4):137–157.

Schaap, M. G. and Leij, F. J. 2000a. Improved prediction of unsaturated hydraulic conductivity with the Mualem-van Genuchten model. Soil Science Society of America Journal, 65(3):843–851.

Schaap, M. G., Leij, F. J., and van Genuchten, M. T. 2001. ROSETTA: a computer program for estimating soil hydraulic parameters with hierarchical pedotransfer functions. Journal Of Hydrology, 251(3-4):163–176.

Scheffe, H. 1952. An analysis of variance for paired comparisons. Journal of the American Statistical Association, pages 381–400.

Scheinost, A. C., Sinowski, W., and Auerswald, K. 1997. Regionalization of soil water retention curves in a highly variable soilscape .1. Developing a new pedotransfer function. Geoderma, 78(3-4):129–143.

Simunek, J., Sejna, M., and van Genuchten, M. T. 2005. HYDRUS-1D. Computer Software.

Smalley, I. J., Jefferson, I. F., Dijkstra, T. A., and Derbyshire, E. 2001. Some major events in the development of the scientific study of loess. Earth-Science Reviews, 54(1-3):5 – 18.

St. Clair, S. and Lynch, J. 2010. The opening of Pandora's Box: climate change impacts on soil fertility and crop nutrition in developing countries. Plant and Soil, 335(1-2):1–15.

Tietje, O. and Tapkenhinrichs, M. 1993. Evaluation of pedo-transfer functions. Soil Science Society of America Journal, 57:1088–1095.

Tukey, J. 1953. Some selected quick and easy methods of statistical analysis. Transactions of the New York Academy of Sciences, 16(2):88.

United Nations, Department of Economic and Social Affairs, Population Division. 2009. World Population Prospects: The 2008 Revision, Highligths.

van Genuchten, M. T. 1980. A closed-form equation for predicting the hydraulic conductivity of unsaturated soils. Soil Science Society of America Journal, 44:892–898.

VanDam, J. C., Stricker, J. N. M., and Droogsters, P. 1994. Inverse Method To Determine Soil Hydraulic Functions From Multistep Outflow Experiments. Soil Science Society Of America Journal, 58(3):647–652.

Vanwalleghem, T., Poesen, J., McBratney, A., and Deckers, J. 2010. Spatial variability of soil horizon depth in natural loess-derived soils. Geoderma, 157(1-2):37–45.

Vereecken, H. 1988. *Pedotransfer functions for the generation of hydraulic properties for Belgian soils*. Ph.D. thesis, Katholieke Universiteit Leuven, Belgium.

Vereecken, H., Maes, J., Feyen, J., and Darius, P. 1989a. Estimating the soil moisture retention characteristic from texture, bulk density, and carbon content. Soil Science, 148(6):1–12.

Vereecken, H., Maes, J., and Feyen, J. 1990. Estimating unsaturated hydraulic conductivity from easily measured soil properties. Soil Science, 149(1):389–403.

Vereecken, H., Weynants, M., Javaux, M., Pachepsky, Y., Schaap, M. G., and van Genuchten, M. 2010. Using Pedotransfer Functions to Estimate the van Genuchten-Mualem Soil Hydraulic Properties: A Review. Vadose Zone Journal, 9:1–26.

Vogel, H. J. and Roth, K. 1998. A new approach for determining effective soil hydraulic functions. European Journal Of Soil Science, 49(4):547–556.

Vogel, H.-J. and Roth, K. 2003. Moving through scales of flow and transport in soil. Journal of Hydrology, 272:95–106.

Vogel, H. J., Samouelian, A., and Ippisch, O. 2008. Multi-step and two-step experiments in heterogeneous porous media to evaluate the relevance of dynamic effects. Advances In Water Resources, 31(1):181–188.

Vogel, T., van Genuchten, M. T., and Cislerova, M. 2001. Effect of the shape of the soil hydraulic functions near saturation on variably-saturated flow predictions. Advances in Water Resources, 24:133–144.

Vrugt, J. A., ter Braak, C. J. F., Clark, M. P., Hyman, J., and Robinson, B. A. 2008b. Treatment of input uncertainty in hydrologic modeling: Doing hydrology backward with Markov chain Monte Carlo simulation. Water Resources Research, 44:W00B09.

Vrugt, J. A., Robinson, B. A., and Hyman, J. 2009. Self-Adaptive Multimethod Search for Global Optimization in Real-Parameter Spaces. IEEE Transactions on Evolutionary Computation, 13(2):243–259.

Walkley, A. and Black, I. 1934. An examination of the Degtjareff method for determining soil organic matter and a proposed modification of the chromic acid titration method. Soil Science, 37:29–38.

West, S. L., White, G. N., Deng, Y., Mc Innes, K. J., Juo, A. S., and Dixon, J. B. 2004. Kaolinite,Halloysite, and Iron Oxide Influence on Physical Behavior of Formulated Soils. Soil Science Society of America Journal, 68:452–1460.

Weynants, M., Vereecken, H., and Javaux, M. 2009. Revisiting Vereecken Pedotransfer Functions: Introducing a Closed-Form Hydraulic Model. Vadose Zone Journal, 8(1):86–95.

Wildenschild, D., Hopmans, J. W., and Simunek, J. 2001. Flow Rate Dependence of Soil Hydraulic Characteristics. Soil Science Society of America Journal, 65:35–48.

Wooding, R. A. 1968. Steady infiltration from a shallow circular pond. Water Resour. Res., 4:1259–1273.

Wösten, J. H. M., Lilly, A., Nemes, A., and Le Bas, C. 1999. Development and use of a database of hydraulic properties of European soils. Geoderma, 90(3-4):169–185.

Wösten, J. H. M., Pachepsky, Y. A., and Rawls, W. J. 2001. Pedotransfer functions: bridging the gap between available basic soil data and missing soil hydraulic characteristics. Journal of Hydrology, 251(3-4):123–150.

Zacharias, S. and Wessolek, G. 2007. Excluding Organic Matter Content from Pedotransfer Predictors of Soil Water Retention. Soil Science Society of America Journal, 71:43–50.

Zhou, X., Lin, H. S., and White, E. A. 2008. Surface soil hydraulic properties in four soil series under different land uses and their temporal changes. Catena, 73:180–188.

Zurmuhl, T. and Durner, W. 1998. Determination of parameters for bimodal hydraulic functions by inverse modeling. Soil Science Society Of America Journal, 62(4):874–880.

List of publications

Publications in peer-reviewed journals

Weynants, M., Vereecken, H., and Javaux, M. 2009. Revisiting Vereecken Pedotransfer Functions: Introducing a Closed-Form Hydraulic Model. Vadose Zone Journal, 8(1):86–95.

Vereecken, H., **Weynants, M.**, Javaux, M., Pachepsky, Y., Schaap, M. G., and van Genuchten, M. 2010. Using Pedotransfer Functions to Estimate the van Genuchten-Mualem Soil Hydraulic Properties: A Review. Vadose Zone Journal, 9:1–26.

Laloy, E., **Weynants, M.**, Bielders, C., Vanclooster, M., and Javaux, M. 2010. How efficient are one-dimensional models to reproduce the hydrodynamic behavior of structured soils subjected to multi-step outflow experiments ? Journal of Hydrology, 393:37–52.

Weynants, M., Laloy, E., and Javaux, M. (in preparation). Soil hydraulic properties obtained from multistep outflow: impact of model choice, protocol and spatial variability on the uncertainty at the horizon scale. To be submitted to Journal of Hydrology.

Weynants, M. and Javaux, M. (in preparation). Impact of land cover and horizon depth on close to saturation hydraulic properties of silt loam soils. To be submitted to European Journal of Soil Science.

Publications at international meetings

Fully published in proceedings

Weynants, M., Vereecken, H., Vanclooster, M., and Javaux, M. 2007. Improving pedotransfert function by adding structure-related parameters. In Candela, L., Vadillo, I., Aagaard, P., Bedbur, E., Trevisan, M., Vanclooster, M., Viotti, P., and Lopez-Geta, J., editors, *WAter POllution in natural POrous media at different scales. Assessment of fate, impact and indicators (WAPO2)*, Hidrogeologia y aguas subterraneas n°22.

Weynants, M. and Javaux, M. 2008. Impact de l'occupation du sol sur les propriétés hydrodinamiques des sols estimées par des fonctions de pédotransfert. In *33èmes journées du GFHN*.

Published as abstracts

Weynants, M. and Javaux, M. 2007. Using Belgian soil series classification to predict soil hydraulic properties. In *EGU General Assembly, Geophysical Research Abstracts*, volume 9, page 09318.

Weynants, M. and Javaux, M. 2008. Improving pedotransfer functions predictions by adding pedological information. In *Eurosoil 2008, 25-28 August 2008, Vienna, Austria*.

Weynants, M., Javaux, M., and Laloy, E. 2010. What are the respective effects of the protocol, the model and the spatial variability on uncertainty in MSO experiments. In *EGU General Assembly, Geophysical Research Abstracts*, volume 12, page 12494.

Germeau, M., **Weynants, M.**, P., C., Dorel, M., and Javaux, M. 2010. Investigating hydropedological relations using quantified morphological data under banana plants on a transect in Guadeloupe. In *EGU General Assembly, Geophysical Research Abstracts*, volume 12, page 12647.

Laloy, E., **Weynants, M.**, Bielders, C., Vanclooster, M., and Javaux, M. 2010. Using multi-step outflow experiments to characterize structured soils: which model to choose? In *EGU General Assembly, Geophysical Research Abstracts*, page 9808.